Astronomy & Astrophysics manuscript no. Coronal˙Atlas˙Preprint November 24, 2004
(DOI: will be inserted by hand later)

The SUMER Spectral Atlas of Solar Coronal Features

W. Curdt[1], E. Landi[2,3] and U. Feldman[2,3]

[1] Max-Planck-Institut für Sonnensystemforschung, 37191 Katlenburg-Lindau, Germany
[2] Artep Inc., 2922 Excelsior Springs, Ellicott City, MD 21042, USA
[3] E.O. Hulburt Center for Space Research, Naval Research Laboratory, Washington DC 20375-5320, USA

Preprint of A&A 427, 1045

Abstract. We present a spectral atlas of the solar corona in the far-ultraviolet (FUV) and extreme ultraviolet (EUV) wavelength range. The atlas is based on observations obtained between 670 Å and 1609 Å in first order of diffraction and between 465 and 670 Å in second order with the SUMER (Solar Ultraviolet Measurements of Emitted Radiation) spectrograph on *SOHO (Solar and Heliospheric Observatory)*. This paper complements the SUMER Spectral Atlas of Solar Disk Features, also published in A&A. The atlas contains off-limb spectra of the corona above a coronal hole, a quiet region, the active corona, and a flare. We provide wavelengths of all detected lines and identification, if available; 311 out of 507 coronal emission lines could be identified or reconfirmed, including several new identifications. Brief descriptions of the data reduction and calibration procedures are given. The spectral radiances are determined with a relative uncertainty of 0.15 to 0.40 (1σ) and the wavelength scale is accurate to typically $\simeq$30 mÅ. The atlas is also available in a machine readable format.

Key words. Sun: UV radiation, Sun: corona, Sun: flare, line: identification, atlases

1. Introduction

The solar corona cannot be seen when observed in the visible because of the enormous brightness of the solar disk. However, the existence of the corona has been known since prehistoric times from rare eclipse observations, when it becomes visible to the naked eye for several minutes. The nature of the corona remained unexplained, despite the many attempts to determine it, which began around the middle of the 19th century. Spectroscopic observations in the visible had shown that the coronal light is composed of discrete emission lines of which the most prominent are the "red" (6374 Å) and the "green" (5303 Å) lines. For a long time, all attempts to identify the coronal lines as known laboratory spectral lines failed, in spite of the enormous progress in atomic physics and the systematic research in laboratories all over the world. In desperation some scientists postulated the presence in the solar corona of an element "coronium" lighter than hydrogen to which they attributed the coronal emission.

The first major breakthrough in coronal research occurred in 1939, when Grotrian (1939) suggested that the coronal line emission is due to forbidden transitions in highly ionized atoms. By studying energy levels of Cl-like iron (Fe^{+9}) that were derived by Edlén from laboratory-generated spectra, he noticed a coincidence between the difference of levels within the ground configuration and one of the unidentified coronal lines. Motivated by Grotrian's suggestion, Edlén succeeded identifying additional lines as transitions within the ground configuration of several other highly ionized atoms (Edlén 1943). Confident in the identifications he concluded that the coronal emission must emerge from million-degree plasmas. The identification of the most prominent coronal emission lines with forbidden transitions of highly ionized species was the starting point of modern coronal physics. It took, however, another decade until the full dimension of Edlén's discovery became apparent.

The bright resonance lines emitted by ions abundant in 1-2 million degree coronal plasmas appear at wavelengths shorter than 500 Å. Nevertheless, a substantial number of lines, and in particular those resulting from forbidden transitions within levels of the ground configuration, spin forbidden transitions between the ground configuration and the first excited configuration, or from transitions associated with levels of excited configurations, are expected to fall at wavelengths of 500 Å $\leq \lambda \leq$ 2000 Å. These ranges are not accessible from the ground and could not be observed until the 1950s, when rockets became available to lift spectroscopic instruments into space.

During the first three decades of the space era spectrometers aboard rockets and satellites recorded solar spectra in the wavelength range from 500 Å to 2000 Å that included numerous emission lines. A substantial number

Send offprint requests to: W.Curdt
(curdt@mps.mpg.de)

of the newly recorded lines were identified with transitions in highly ionized atoms abundant in the solar upper atmosphere (Burton & Ridgeley 1970, Jordan 1971, Doschek *et al.* 1976, Feldman & Doschek 1977, Sandlin *et al.* 1977, 1986 and Feldman & Doschek 1991). With the launch of the *Solar and Heliospheric Observatory (SOHO)* that included the Solar Ultraviolet Measurements of Emitted Radiation (SUMER) and the Coronal Diagnostic Spectrometer (CDS), two advanced high-resolution spectrometers, a renewed interest in solar spectroscopy occurred. Based on SUMER recorded spectra Feldman *et al.* (1997) published the most comprehensive list, to date, of lines in the 500 to 1600 Å wavelength range that were emitted by a quiet coronal streamer. The introduction to that paper provides a detailed overview of the spectroscopic measurements and identifications prior to the launch of *SOHO*. A list of high temperature ($T_e \geq 2\times10^6$ K) lines emitted by active region and flare plasmas but not by the quiescent corona also recorded by SUMER were published by Feldman *et al.* (1998, 2000) and by Curdt *et al.* (2001a).

Prior to the launch of the *SOHO*, the most comprehensive list of absolute intensities of solar emission lines emitted by plasmas ranging in temperature between 1×10^4 K and 3×10^6 K and accessible to normal incidence spectrometers was published by Vernazza and Reeves (1978). The published list was generated from spectra acquired by the S055 Extreme Ultraviolet spectrometer on the *Skylab* mission, which had a spectral resolution of 1.6 Å (FWHM) and a spatial resolution of $5''\times5''$. The intensities of the brightest lines spanning the 277 to 1335 Å wavelength range were measured from spectra recorded against the solar disk and above the limb and emitted by active region, quiet region and coronal hole plasmas. Due to the fairly low spectral resolution of the instrument many of the moderately intense lines were blended with each other or with nearby brighter lines while most of the fainter ones were lost in the background. Using spectra recorded by the S082 B normal incidence spectrograph on *Skylab*, Doschek *et al.* (1976) published absolute intensities of bright lines in the wavelength range from 1150 to 2000 Å which were emitted by quiet region plasmas at temperatures of $T_e \leq 2.5\times10^5$ K.

Intensities of lines emitted by stellar upper atmospheres have been observed by the *EUV Explorer (EUVE)*, the *International Ultraviolet Explorer (IUE)*, the *Far Ultraviolet Spectroscopic Explorer (FUSE)*, and the *Hubble Space Telescope (HST)* Goddard High-Resolution Spectrograph (*HST*-GHRS) and Space Telescope Imaging Spectrograph (*HST*-STIS). In a recent communication, Ayres *et al.* (2003) present a survey of high temperature forbidden lines identified in high-resolution *HST*-STIS FUV spectra of late-type stars. Redfield *et al.* (2003) published a similar survey from spectra recorded by FUSE. The solar corona is of special interest for stellar applications, since its emission can be separated from the disk emission (which significantly helps to reveal blending) and it can be spatially resolved and observed with much higher photon statistic than stellar coronae. It also can be considered an exceptional good standard of a cool G2 V star corona.

Curdt *et al.* (2001b) published a detailed SUMER disk atlas (to be referred to as the disk atlas). Although the disk atlas consists primarily of lines and continua emitted by the chromosphere and transition region plasma, it also contains several coronal emission lines, which are bright enough to be discerned against the intense emission from the cooler regions.

In this paper we present an atlas consisting of spectral profiles and a line list representing the quiescent corona, the corona above coronal holes, and the active and flaring corona, as observed by SUMER above the solar limb. The off-limb atlas contains lines typical of plasmas at temperatures of $T_e \geq 7\times10^5$ K and has to be understood as a companion paper to the disk atlas. The line list contains all observed lines with measured wavelengths, measured radiances, and identification along with atomic transitions when available. For the sake of conciseness, in this paper we will restrict the repetition of details and general information, which has already been presented in the disk atlas, to an absolute minimum.

2. The SUMER instrument

SUMER is part of the *SOHO* mission of ESA and NASA. *SOHO* was launched in 1995 and injected into a halo orbit around the first Lagrangian point, L1, on 14 February 1996 where, in continuous view of the Sun, it orbits the Sun at a distance of 1.5×10^6 km sunward from the Earth.

SUMER is a high-resolution telescope and spectrograph designed to obtain stigmatic slit images with spatial and spectral resolution elements of $1''$ and $\simeq$40 mÅ (in first order) as well as high temporal resolution over the wavelength range from 465 Å to 1610 Å. The accessible range depends on which of two detectors is used. While detector 'A' can in principle record spectra from 780 Å to 1610 Å in first order of diffraction, the range of detector 'B' reaches from 660 Å to 1500 Å. The lower wavelength limit for second order lines results from the steep fall-off of the reflectivity of the silicon carbide optics below 500 Å; the shortest-wavelength identified line falls at 465.2 Å. The dispersion of the instrument is slightly wavelength dependent. For detector 'A', it varies from 45.2 to 41.9 mÅ/pixel (first order) and 22.6 to 20.9 mÅ/pixel (second order) from one end to the other of the SUMER wavelength range; for detector 'B', it varies from 44.7 to 41.2 mÅ/pixel (first order) and from 22.3 to 20.6 mÅ/pixel (second order). Each detector has 1024 spectral and 360 spatial pixels.

First order lines and second order lines appear superimposed in the spectrum. A few lines could also be observed in third order (Feldman *et al.* 1997). The central area of the detector is coated with KBr (potassium bromide). This coating increases the detection quantum efficiency (DQE) mainly in the range from 900 Å to 1500 Å. Intensities of lines on both sections of the photocathode can be used to discriminate second order lines from first

order lines, since the photocathode responsivity changes differently for lines in different orders.

Off-disk observations of previously unobserved faint intersystem lines are only possible because of the high surface quality of the primary mirror, which results in relatively low scattered light levels, and because of its more efficient low-noise detectors compared to previous instruments that used photographic plates, as discussed by Feldman *et al.* (1997) and Curdt *et al.* (1997). Few (if any) spectral lines were recorded by earlier space instruments from regions that extended more than 20″ above the limb. In comparison, SUMER has recorded line intensities extending out to 600″ (Feldman *et al.* 1999).

Many more instrumental details can be found in the disk atlas. A comprehensive description of the instrument is given by Wilhelm *et al.* (1995), and first results and inflight performance characteristics are given by Wilhelm *et al.* (1997a) and Lemaire *et al.* (1997).

3. Observations

Since the present atlas aims to cover the off-limb solar spectrum emitted by coronal holes, quiet Sun, active regions and flares, many datasets observed at different times and at different locations were necessary. Table 1 provides the basic characteristics of the observations used to create the plots and to derive the radiances given in the line list.

Both detectors have been considered in the present work. Detector 'A' was designated the prime source for both first and second order lines, but the 660 to 780 Å section of detector 'B' also was used, so that many lines that detector 'A' observes as second order lines also could be identified in detector 'B' in first order. This helped to discriminate between first and second order lines in detector 'A', to observe several first order lines that were too faint or blended to be identified in detector 'A', and to slightly improve wavelength measurements.

3.1. Coronal hole

The two coronal hole spectra used in the present work were both taken in the early stages of the *SOHO* mission above the north and south coronal holes during solar minimum. The field of view was selected in order to minimize any contribution from overarching quiet Sun material.

Both datasets consist of "REFSPEC" spectral scans, encompassing the whole SUMER wavelength range with a long exposure time (300 s and 1200 s for detectors 'A' and 'B', respectively). The use of the 4″×300″ slit in the detector 'A' dataset and of the 1″×300″ slit in the detector 'B' dataset ensures that the same level of signal to noise was achieved.

Both the detector 'A' and 'B' wavelength ranges have been divided into a number of sub-ranges, each shifted from the adjacent one by a fixed amount: detector 'A' range was divided in 44 sections with ≃18 Å shift; the detector 'B' wavelength range was observed in 61 sections with a ≃13 Å shift. The entire wavelength ranges of both detectors have been used for identification purposes.

In both datasets, we have selected for the analysis a fixed number of pixels located in the brightest regions along the slit, corresponding to the heights above the limb (in $R_\odot$ and 10^3 km) reported in Table 1.

3.2. Quiet Sun

The detector 'A' quiet Sun observation is unique in its kind, and it consists of the longest exposure time ever achieved in the UV wavelength range on the Sun. It is described in detail in Parenti *et al.* (2003). The dataset was obtained observing a quiescent streamer in the southeast quadrant of the Sun. It consists of a modified REFSPEC sequence where the entire detector 'A' wavelength range was divided in 38 sections each shifted by ≃20 Å from the previous one. The basic observing sequence consisted of several consecutive observations of each of the wavelength sections with an exposure time of 300s and the wide slit (4″×300″). This sequence was then repeated five times at three different heights above the solar limb, in order to cover a large distance from the limb. The entire observation lasted approximately a week. In order to maximize the signal-to-noise ratio, and at the same time avoid any transition region material, we have selected the series of observations that was pointed at (-600″,-941″); in this dataset, each wavelength section was observed three consecutive times during each sequence. Therefore, for each wavelength range we have 5×3=15 observations of 300 s, for a total observing time of 75 minutes.

The detector 'B' quiet Sun observation was taken in 1997, in a region in the southwest quadrant of the Sun devoid of any activity. The dataset consisted of a REFSPEC sequence with a long exposure time (1500s), that compensated the use of the narrow 1″×300″ slit. The wavelength range was divided into 61 sections with a shift of ≃13 Å; however, only the first 10 sections have been considered in the present work, corresponding to the lowest wavelength range up to 830 Å, unavailable to detector 'A' in first order.

In both datasets, we have selected the brightest region along the slit, corresponding to the heights above the limb reported in Table 1.

3.3. Active region

The two active region REFSPECS that we have considered in the present work have been observed during solar maximum close to the solar equator. The detector 'A' dataset has been observed over a large active region complex which gave rise to several strong flares during the prolonged SUMER campaign that aimed at monitoring active region behaviour at the limb. However, no flare activity was recorded during the spectral scan considered in the present work. The dataset consists of a standard REFSPEC sequence, composed of 38 sections each shifted

Table 1. *Details of the observing sequence used in the present work*

Region	Det.	Date	Slit center	Height (Mm)	Height ($R_\odot$)	Slit	t_{exp} (s)
Coronal Hole	'A'	13 March 1996	(0″,-1180″)	39-54	1.056-1.077	4″×300″	300
Coronal Hole	'B'	11 November 1996	(0″,1149″)	17-40	1.024-1.057	1″×300″	1200
Quiet Sun	'A'	13-19 June 2000	(-600″,-941″)	25-44	1.036-1.063	4″×300″	4500
Quiet Sun	'B'	20 June 20 1997	(600″,-900″)	14-26	1.020-1.038	1″×300″	1500
Active region	'A'	4 April 2001	(954″,500″)	34-49	1.049-1.070	1″×300″	300
Active region	'B'	6 December 2000	(-1000″,-320″)	50-59	1.072-1.084	4″×300″	4200
				59-70	1.084-1.100	4″×300″	4200
Flare	'A'	9 May 1999	(968″,395″)	21-68	1.030-1.097	4″×300″	300

by ≃20 Å from the previous one and observed with 300 s exposure time.

The detector 'B' dataset was taken during the December 2000 campaign, over a medium-size active region. The dataset consisted of a modified REFSPEC, where only the 660 to 860 Å range was observed in 10 sections each shifted by ≃13 Å. However, each section was consecutively observed 14 times, for a total effective observing time of 70 minutes, yielding the longest observing time achieved in the UV on a solar active region.

In the active region observed with detector 'A', we have selected the brightest pixels in the dataset, corresponding to the height above the limb reported in Table 1. In the detector 'B' active region, cool material was present in the brightest section of the slit. In order not to include any spectral lines emitted by this cool material, and at the same time to select the brightest areas along the slit, the pixels selected for the present study are not the same for all exposures, and they come from two different sections of the slit, whose corresponding height above the limb is reported in Table 1.

3.4. Flare

A comprehensive flare spectral atlas in the SUMER wavelength range has been published by Feldman *et al.* (2000). The dataset analysed in this work was the first complete flare spectrum observed by SUMER. Since then, several flare campaigns have been carried out, but few if any complete flare spectral scans across the SUMER wavelength range have been obtained. Since the aim of the present paper is to present the spectrum of the solar corona above the limb at all solar conditions, for the sake of completeness we have included the dataset already published by Feldman *et al.* (2000). The description of the observing sequence can be found in Feldman *et al.* (2000). Basic details of the flare observations are given in Table 1.

4. Data Reduction

4.1. Flatfield and geometrical distortion correction

After decompression, the data set has been flat-field corrected. The flat field exposures closest in time to each of the datasets have been used for the correction. After the flat-field correction, data have been corrected for the geometrical distortion present in SUMER spectra. We have used for both operations the standard SUMER software.

In the case of the quiet Sun detector 'A' dataset, observations were taken at different heights but with the same position along the solar E-W direction. Slit positions were chosen so that there was 10″ overlapping between observations at different heights (see Parenti *et al.* 2003 for more details). Inspection of these overlapping spectra has revealed a residual distortion in the last 1-5 pixels near the bottom edge of the detector. To investigate this effect, we have analysed the centroids of the chromospheric lines: above the limb, these lines are composed of instrument-scattered light and are expected to appear as straight lines along the slit because all solar signatures are smeared. We have analysed the centroid positions along the slit for several positions along the wavelength direction of the detector and have determined an interpolated residual correction function that allows to correct for this effect at any position in the detector, and applied it to the data.

4.2. Spectral averaging

To improve the signal-to-noise ratio of the observed spectra, we have averaged the emission of the selected pixels along the slit in each spectral section of each dataset.

However, some more comments are required for the quiet Sun detector 'A' and active region detector 'B' datasets. The active region detector 'B' dataset was composed of 14 subsequent exposures of each spectral section. To improve the signal-to-noise ratio, we have first averaged all the 14 exposures, and then we have averaged on the selected pixels along the slit. Since the 14 exposures repeated one after the other, without changing the instru-

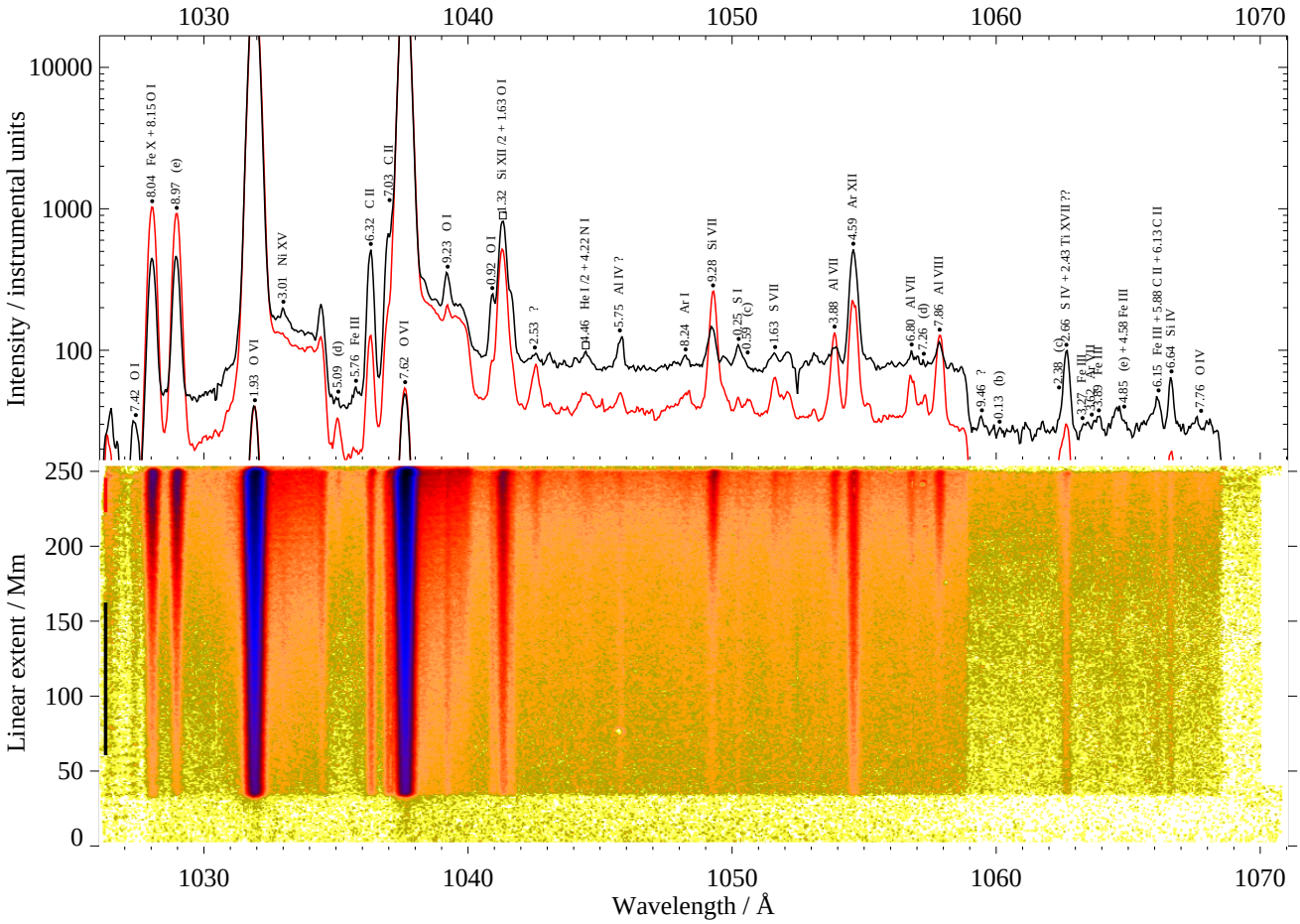

Fig. 1. The SUMER spectral window around 1050 Å after application of basic data reduction steps. 15 frames of 5 minute integration time have been added for this deep exposure. The slit is positioned in the South-East quadrant of the field of view. North is up and closer to the limb than the bottom pixels. We have also added the line identification and two profiles, the red one averaged in the near-limb section of the slit, the black one further out

ment pointing, wavelength range and configuration, the averaging was straightforward.

The quiet Sun detector 'A' dataset required additional care. In fact, this dataset is composed of five identical sequences, and within each sequence each spectral section was observed three times before changing to the next spectral section. So, each spectral section has been observed 15 times. The three subsequent exposures within each sequence have been averaged together as for the active region, detector 'B', leaving us with 5 averaged exposures for each spectral section. However, since the five subsequent sequences were run at different times, after instrument repointing and changes in the wavelength sections, instrumental effects like the thermoelastic oscillation (cf., Rybàk *et al.* 1999 for more details) introduced shifts along the wavelength direction between each sequence. In order to avoid artificial line broadening and blending due to these shifts, the five averaged spectra for each section have been first coaligned, and then averaged together. The coalignment shift to each of the five spectra has been obtained by cross-correlation of all the strongest and unblended spectral lines in each of the spectral scans. An example of such a processed primary data product is shown in Fig.1, where we display a data array recorded with detector 'A' in the wavelength range around 1050 Å. Fig.1 also illustrates the subsequent data reduction steps.

4.3. Gaussian line fitting

Gaussian spectral line profiles have been fitted to all possible spectral features in all datasets, using a multigaussian program that permits decomposition of partially blended lines.

In each dataset, more than one measurement of line intensity and wavelength were possible, because each line could be measured in different spectral sections, several lines were observed in both detectors, and short wavelength lines can be observed in first and second order. Final wavelengths were obtained by averaging all the measurements for each line.

4.4. Wavelength Calibration

To determine the wavelength scale, fitted line centroids and spectral pixels need to be converted to angstrøm. Since there is no absolute wavelength reference available in the spectrometer, a wavelength scale can only be derived using solar chromospheric lines, that in off-disk spectra are seen as instrument-scattered light.

The dispersion changes as a function of wavelength, and so each exposure needs an individual calibration. The wavelength calibration is based on identifying the position of chromospheric lines on the detector: the fact that scattered light is practically free of Doppler shifts due to plasma velocity variations along the slit makes these lines very useful for establishing an absolute wavelength scale. Emission lines from neutrals and singly ionized species, which are fairly strong and unblended in the solar disk spectrum and for which the absolute wavelengths are known with high accuracy, have been used as reference lines.

By fitting a gaussian line profile and measuring the line centroid in pixels, the pixel-to-wavelength relation in each spectral scan can in principle be performed with a precision of 5 mÅ and better if sufficient lines are available for this purpose. The pixel-to-wavelength relation has been determined by a correlation of the line centroids for all the reference lines in each 43 Å window with their known literature wavelengths. Since the non-linear dispersion is known very accurately from the optical design, this correlation leads to a constant offset for each spectral scan. A by-product of this process has been the elimination of some mis-identifications and the identification of problems with the literature values of the wavelengths of some of the reference lines.

The identification of reference lines is sometimes difficult due to blending and to the presence of prominent lines both in first and second order in the SUMER spectrum. Except for a few close blends, the line centroids could be determined by multi-Gauss fits with estimated uncertainties of the order of 0.2 pixel ($\approx$ 10 mÅ in first order) or better. The accuracy of the laboratory wavelengths of atomic lines is often better than 2 mÅ. Most of the laboratory wavelengths used for the wavelength calibration were taken from Kelly (1987).

After the spectra have been wavelength-calibrated, the wavelengths should be accurate to typically 30 mÅ relative to quiet-Sun chromospheric layers. This value can easily reach 40 mÅ for faint lines or in cases with blend problems. In contrast to the disk atlas, no net Doppler flows are expected, neither for the measured lines nor for the reference lines, which with few exceptions are purely seen as scattered light from the entire disk. A few exceptions might occur in flare and active-region spectra.

4.5. Radiometric calibration

The intensity has been converted from counts into physical units. Given the radiometric calibration of SUMER before and during the mission (Hollandt *et al.* 1996; Wilhelm *et al.* 1997b; Schühle *et al.* 1998, 2000), we give the absolute spectral radiances of all observed coronal features in the wavelength range from 660 Å to 1609 Å in first order of diffraction. The radiance of the profiles is scaled to mW sr^{-1} m^{-2} Å^{-1}, while in the line list spectral pixels have been integrated scaling the line emission to photon arcsec^{-2} cm^{-2} s^{-1}. The overall uncertainty of the radiometric calibration before the *SOHO* accident in 1998 is estimated to 15 % below 1250 Å, and increases at longer wavelengths to 30 %. After the *SOHO* recovery these values have changed to 30 % and 40 %, respectively.

We have corrected the spectra for local-gain depression effects of the detector channel plates and dead-time effects of the electronics (Wilhelm *et al.* 2000). However, the large majority of the lines are sufficiently weak not to be significantly affected by this correction. A few bright spectral lines, e.g. the 977 Å C III, sometimes exceed the detector capabilities and produce a ghost in the right shoulder of such a line. We have taken out sections affected by this instrumental artefact.

The intensities in the present atlas have been chosen among all the measurements available for each line from detector 'A', when available. Detector 'B' measurements were used in the wavelength range between 660 and 792 Å, where no first-order detector 'A' spectra are available. Therefore, intensities of lines reported in the same solar feature (i.e. quiet Sun, or coronal hole) may actually be emitted by different regions, so that they cannot be directly compared. Also, the instrument required considerable time to cover the entire spectral range. Since the morphology of the structures observed in the active corona may have changed while the spectral range was scanned, the intensities of lines may become less comparable with increasing difference in wavelength.

Flare intensities are intrinsically variable with time, so we felt that it was meaningless to report measured intensities, since the spectra were not simultaneous and physical conditions of the emitting plasmas were very different from one end to the other of the SUMER range. In the line list, flare intensities are theoretical, calculated per unit emission measure using the CHIANTI database (Dere *et al.* 1997, Young *et al.* 2003) at the temperature of maximum abundance for each ion. Observed flare lines which have no emissivity value available in CHIANTI or are unidentified, are marked by 'x' in the line list.

5. Selection of coronal lines

Once wavelengths and intensities were measured, it was necessary to discriminate between lines emitted by the local coronal plasma and lines observed as instrumental scattered light from disk chromospheric and transition region features.

This crucial task has been carried out by investigating the distribution of the line intensity along the SUMER slit in each of the datasets. In principle, this method allows to carry out an effective discrimination between the

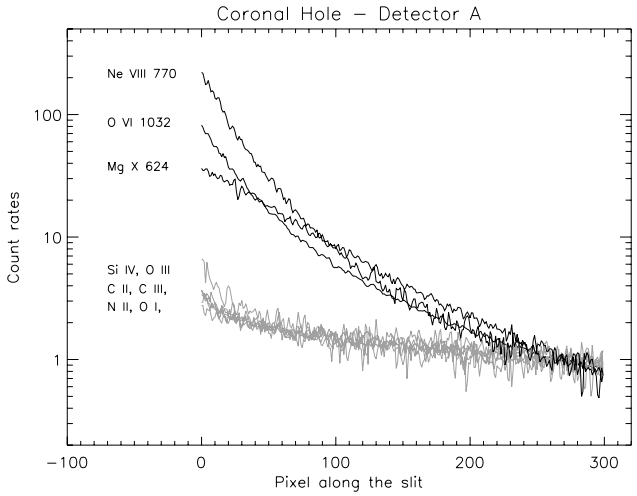

Fig. 2. Intensity distributions of a few strong coronal lines (black line) and several instrument-scattered light lines (grey lines), as a function of the position along the slit. Intensities are in counts.

two types of lines because the intensity of lines emitted by local plasma decreases with distance from the limb much faster than the intensity of the instrument-scattered lines. While the latter show a decrease of at maximum a factor between 2 and 4 from one end to the other of the SUMER slit, the intensity of the locally emitted lines can decrease, depending of the ionization stage, by more than an order of magnitude. In the present work, we have measured the "typical" intensity distribution along the slit for coronal and instrumental scattered light from the strongest lines in the SUMER wavelength range. This "typical" intensity distribution has been used as a benchmark to discriminate between coronal and scattered light lines. Examples of "typical" intensity distributions for the coronal hole, detector 'A' dataset are displayed in Fig. 2. Coronal lines are characterized by variations of about two orders of magnitude in the intensity at the two edges of the slit; their distributions are slightly different due to different reaction of each emitting ion to changes in the physical properties of the emitting plasma along the slit. All scattered light lines in Fig. 2 have an identical intensity profile, determined by instrumental effects only and not by the local plasma, and they vary by a factor 2 to 3. These low-temperature lines are indicated by 'F' in the line list.

However, there are two problems to consider. The first problem is given by the fact that while instrument-scattered light is independent of the local conditions of the plasma in the field of view, its intensity depends on the conditions of the solar-disk plasma, so in principle observations carried out at different times and dates can have different intensity profiles of the scattered light. To avoid this problem, we have calculated scattered lines intensity profiles like those displayed in Fig.2 for each of the datasets we have used.

The second problem is given by weak coronal lines, whose intensity rapidly decreases to levels where it becomes negligible relative to background noise or the instrument-scattered intensity either of its own emission from the disk, or of the emission of a blending chromospheric or transition region line at similar wavelength. The intensity profiles of these lines exhibit "mixed" behaviour: a profile typical of a true coronal line, in pixels close to the brightest pixels along the slit and selected for this atlas; away from them, the profile changes towards an instrument-scattered one. In this case, it is difficult to discriminate between a true coronal or a scattered light emission, especially when a line is so weak that scattered light or noise are big contributors also in the brightest pixels. This problem determines the lower intensity limit at which a coronal line can be safely identified; in the present work, we have rejected all lines whose origin could not be unambiguously identified. These lines are indicated by 'I' in the line list.

It is important to note that in each observation the SUMER slit was placed at sufficiently high solar latitudes to allow the SUMER field of view to include plasma at very different heights above the limb. In such a case the coronal line intensities varied from one end to the other of the slit much more than the scattered line intensities. The only exception is the active region, detector 'B' dataset, where the inclination of the slit was such that plasma in the field of view was confined within 0.1 $R_{\odot}$ above the limb. In this case, the difference in behaviour between the scattered and the coronal line was more limited and thus a fraction of the observed lines that may have had a coronal origin was rejected due to their ambiguous intensity profiles. Subtraction of the scattered light background is possible for individual lines and individual exposures, if the fall-off curve can be determined. There is, however, no general procedure available to quantify the scattered-light contribution. Therefore we have added the average quiet-Sun radiance profile from the disk atlas for comparison, which may allow an estimate of the scattered-light contribution.

The identification of flare lines was more straightforward, due to their strong confinement to a small portion of the SUMER slit, even if in that observation the SUMER field of view had similar problems to the active region, detector 'B' dataset. SUMER has not yet observed a flare spectrum recorded on detector 'B'.

6. The SUMER spectral atlas of off-disk features

6.1. Physical properties of the emitting plasmas

The measurement of the physical properties of the emitting plasmas is beyond the scope of the present paper, but a brief review of diagnostics results obtained from spectra emitted by similar regions can be of help to the reader in understanding which physical conditions can be expected.

The quiet Sun, detector 'A' spectrum has been thoroughly analysed by Parenti *et al.* (2003), who have determined the physical parameters (emission measure, electron density and temperature, elemental abundance) of

Table 2. *Ions contributing lines to the atlas.*

Element	V	VI	VII	VIII	IX	X	XI	XII	XIII	XIV	XV	XVI	XVII	XVIII	XIX	XX	XXI	XXII	XXIII
N	X																		
O		X																	
F																			
Ne		X	X	X															
Na			X	X	X	X													
Mg		X	X	X	X	X	X												
Al			X	X	X	X	X												
Si		X	X	X	X	X	X	X	X										
P					X														
S		X	X	X	X	X	X	X	X										
Cl			X				X	X											
Ar			X	X	X		X	X	X										
K					X		X	X	X										
Ca			X	X	X	X		X	X	X	X								
Sc																			
Ti											X	X							
V																			
Cr						X	X					X	X	X		X			
Mn													X	X		X	X		
Fe			X	X		X	X	X					X	X	X	X	X	X	X
Co								X	X						X				
Ni										X	X				X		X		X

the emitting plasma as a function of time along the whole week encompassing the observations, and as a function of the position along the slit. Parenti *et al.* (2003) demonstrated that the plasma emitting the spectrum observed by SUMER can be approximated with an isothermal plasma whose characteristics remained constant throughout the week of observation. At the position along the slit considered in the present work, the plasma properties were $T \simeq 1.2\times10^6$ K, $N_e \simeq 2\times10^8$ cm^{-3}, EM $\simeq 3\times10^{43}$ cm^{-3}. The element abundances show a normal dependence on the First Ionization Potential (FIP effect), with the low-FIP/high-FIP abundance ratio higher by a factor $\simeq 4$ than in the photosphere (low-FIP elements have a FIP$\leq$ 10 eV, high-FIP elements have FIP$\geq$ 10 eV). Since similar results have been found in other works studying the off-disk quiet Sun (i.e. Landi & Feldman 2003 and references therein), it is reasonable to assume that the electron temperature of the quiet Sun plasma recorded by detector 'B' is very similar, however, being recorded closer to the solar surface the electron density will be higher.

Several studies on off-disk coronal hole plasmas have been carried out with the SUMER experiment, all yielding similar results even though the observations were carried out years apart. In all cases, the emitting plasma was found to be nearly isothermal, although the temperatures were lower than in the quiet Sun and ranged from 5 to 8×10^5 K (Wilhelm *et al.* 1998, Wilhelm 1999). Electron densities have been found to lie in the range from 2 to 10×10^7 cm^{-3} (Wilhelm *et al.* 1998, Wilhelm 1999, Doyle *et al.* 1999, Doschek *et al.* 1997, 2001), significantly lower than in the quiet Sun. Interestingly, the spectra recorded above a coronal hole show some similarity to the on-disk sunspot spectrum with enhanced emission in Fe VII, Fe VIII or Mg VIII lines.

Active regions plasmas are not isothermal, due to the presence of multi-temperature magnetic structures along the line of sight. Plasma conditions in different off-disk active regions may be very different, according to the age and size of the region, to the solar cycle phase when the observations are carried, to their activity and even to the position within each region (as demonstrated in Fig.3 at the separation line at 792 Å). Therefore the analysis of spectra emitted by active features is more complex than in coronal holes and quiet Sun, and no simple range of density, temperature, emission measure and abundances can be given.

The flare considered in the present work has been extensively studied by Landi *et al.* (2003), who carried out plasma diagnostics as a function of time for all the duration of the observations. Temperatures in the flare peaked at slightly less than 10 MK, and then steadily decreased; the surrounding, non-flaring plasmas remained quiescent at temperatures of $\simeq 4$ MK. The evolution of the emission measure of the emitting plasma was also determined. The reader is referred to that paper for further details.

6.2. Line Identification

The identifications presented in the Feldman *et al.* (1997) paper were used as the starting point for identifying the quiet Sun coronal lines in the present paper. The spectra on which the 1997 identification were based were emitted by quiet Sun streamer plasma at a height of 21000 km above the equatorial limb. Since during the observations part of the SUMER slit intersected a prominence, the recorded spectra consisted not only of coronal lines ($T_e \geq 6\times10^5$ K) but also of lines emitted by cooler plasmas. In addition, a number of lines appear which are very bright in disk spectra and were scattered into the spectrometer by surface imperfections of the SUMER front mirror. Although the 1997 spectra contained some 900 lines, 375 were judged to be coronal lines, and only 200 of them were identified. Since the original publication appeared in press 40 additional lines were identified as high excitation transitions in Si VII (Kink *et al.* 1997, 1999), Fe VII (Ekberg & Feldman 2003a) and Fe VIII (Ekberg & Feldman 2003b). In addition few more lines were identified as ground configuration forbidden transitions of K XIII, Cl X, Cl XI and Cl XII

(Feldman *et al.* 2004). The identifications of Dwivedi *et al.* (1999) in their study of the coronal emission in the spectral ranges from 980 Å to 1020 Å and from 1174 Å to 1214 Å also have been scrutinized for this work.

On May 9, 1999 SUMER succeeded in recording spectra from a M7.6 flare and the active region surrounding it. Using the recorded spectra Curdt *et al.* (2000) and Feldman *et al.* (2000) identified some 70 lines associated with the active region and flaring plasmas. The lines in these papers were the basis for the identifications of the high temperature lines ($T_e \geq 3 \times 10^6$K) presented here. The current paper contains 496 isolated lines (plus 11 cases of contributing emission which can not be decomposed) emitted by coronal plasmas at temperatures of $6 \times 10^5 \leq T_e \leq 2 \times 10^7$ K; 362 of them were present in the quiet Sun coronal spectra and the rest in the coronal hole, active region or flaring plasma. Of the 507 contributing lines in the spectra 311 lines (≈61%) are identified, belonging to 90 different ions from all elements between N and Ni, with the exception of F, Sc and V (see Table 2). We believe that the vast majority of the unidentified lines belong to transitions within or between levels of excited configurations.

In flaring plasmas the temperatures can surpass 2×10^7K resulting in resonance transitions that appear in the extreme ultraviolet (EUV) and soft X-ray (SXR) spectral regions that for the most part are devoid of lines typical of much cooler plasmas. Many of the transitions within the ground configuration ($2s^2 2p^k$; k=1,5) of highly ionized atoms that are most abundant in flaring plasmas fall in the SUMER range. Additionally transitions of the type $1s2s\ ^3S_1$-$1s2p\ ^3P_{0,2}$ in elements with Z≤20 also fall in this range. Since those lines are intermixed with much lower excitation lines, they provide diagnostic capabilities not possible for measurements in the EUV and SXR ranges. While black-body and recombination continua are normally not present in solar coronal spectra, SUMER often has observed bremsstrahlung during flares as a strong enhancement of the continuum emission emerging from the same confined plasma as the flare lines. Magnetic dipole transitions in highly ionized species, e.g., the Fe XIX 1118 Å line, are a by-product of the physical processes generating emission in the SXR range and can be taken as SXR proxy, thus allowing spectroscopy of such plasmas, particularly Doppler shift measurements, which currently are not possible in the EUV and SXR bands below 100 Å.

6.3. Description of the Atlas

The spectra in this atlas are displayed as composite profiles of different exposures. Except for small sections around Lyman-α and near the limits of the SUMER spectral range we have selected data recorded on the KBr photocathode. The bare-MCP sections have been treated separately throughout the radiometric calibration process to compensate for the differences in responsivity, thus enhancing lines recorded in second order of diffraction.

Similar to the disk atlas, spectra are displayed as profiles in different colours. In Fig.3 the spectra of the corona above a quiet region, an active region, a coronal hole, and in a flare appear as black line, as red line, as blue line, and as green line, respectively. The spectra are presented in portions of 42 Å with 2 Å of overlap. For details of the heights above the limb at which each of the spectra shown in the figure were recorded see Table 1. Notice that the spectral plots at wavelengths shorter than 792 Å were recorded by detector 'B' while those plotted above 792 Å were recorded by detector 'A'. Different from the line list, where we for practical reasons give the line radiance in units of photon arcsec^{-2} 2 cm^{-2} s^{-}1, in the plot spectral radiances are given in units of mW sr^{-1} m^{-2} Å^{-1} for both orders of diffraction.

Each resolved emission line is indicated by a coded mark, the measured wavelength in angstrøm (Å), and the identification. If available, unidentified lines are characterized by the temperature classification of Feldman *et al.* (1997). The wavelength values are restricted to three digits, one digit before and two rounded digits after the decimal point. In the plot we have indicated some of the ambiguous lines rejected for the line list. For a better orientation, we also have included the average quiet-Sun profile and the identification of the most important lines from the disk atlas (dotted grey line). The marks are coded according to the temperature classification 'chromospheric' (circles), 'transition region' (squares), 'coronal' (triangles), or 'flare' (diamond). Generally, the identifications are placed on top of the profile with the highest emission. Flare line identifications were treated separately and always appear at the flare profile. Open symbols represent lines which are observed in second or third order.

7. Summary

The spatially resolved solar spectra studied in this atlas cover the 670 Å to 1609 Å wavelength range. Additional lines were identified in second or third order of diffraction down to 465 Å. This atlas, which also is available in machine readable form, combines better spectral and spatial resolution, superior signal to noise ratios as well as wider wavelength coverage than any previously published atlas of a similar kind. It represents our most up-to-date knowledge about the emission of solar coronal features in the SUMER spectral range and includes 507 lines of which ≈61% are identified. It illustrates absolute intensities of the most common solar upper atmosphere coronal structures throughout most of the range with an accuracy of 15%. The lines listed in the atlas belong to the 90 ions listed in Table 2.

The published line intensities - restricted to co-spatial and co-temporal observations - provide a rich resource for probing electron densities, electron temperatures, opacities and elemental abundances of the basic solar upper atmosphere structures. Due to the higher spatial resolution of the SUMER spectrograph the plasma parameters of small solar features also can be investigated. The present

atlas represents a powerful tool for the planning of future observations, i.e., to determine adequate integration times, to identify possible blends, and to select proper data extraction windows in upcoming solar experiments. It can also be used as a proxy when investigating stellar spectra. The absolute intensities of lines emitted by the diverse set of ions when combined with the properties of the emitting plasmas can - with the same restrictions mentioned above - be used as a check on the accuracies of atomic physics code calculations.

8. Acknowledgements

The SUMER project is financially supported by DLR, CNES, NASA and the ESA PRODEX Programme (Swiss contribution). SUMER is part of *SOHO*, the Solar and Heliospheric Observatory, of ESA and NASA. U.F. acknowledges financial support from NRL/ONR 6.1 basic research programs and NASA grants. The work of E.L. is supported by the NNH04AA12I and W10,232 NASA grants. We appreciate valuable comments of the referee which have helped to improve this communication.

References

Ayres, T.R., Brown, A., Harper, G.M. *et al.* 2003, ApJ 583, 963
Burton, W.M., & Ridgeley, A. 1970, Solar Phys. 14, 3
Curdt, W., Feldman, U., Laming, J.M. *et al.* 1997, A&AS 126, 281
Curdt, W., Landi, E., Wilhelm, K., Feldman, U. 2000, Phys.Rev.A 62, 022502
Curdt, W., Landi, E., & Feldman, U. 2001a, in P. Brekke, B. Fleck, J.B. Gurman (ed.) *Recent Insights into the Physics of the Sun and Heliospere*, Proc. IAU Symp. 203, Manchester, 2000, PASP 203, 260
Curdt, W., Brekke, P., Feldman, U. *et al.* 2001b, A&A 375, 591
Dere, K.P., Landi, E., Mason, H.E. *et al.* 1997, A&AS 125, 149
Doyle, J.G., Teriaca, L., & Banerjee, D. 1999, A&A 349, 956
Doschek, G.A., Feldman, U., VanHoosier, M.E., & Bartoe, J.-D.F. 1976, ApJS 31, 417
Doschek, G.A., Warren, H.P., Laming, J.M. *et al.* 1997, ApJ 482, L109
Doschek, G.A., Feldman, U., Laming, J.M., Schühle, U., & Wilhelm, K. 2001, ApJ 546, 559
Dwivedi, B.N., Curdt, W., Wilhelm, K., 1999, ApJ 517, 516
Edlén, B., 1943, Zeitschr. f. Astrophys. 22, 30
Ekberg, J.O., & Feldman, U. 2003a, ApJ 595, 517
Ekberg, J.O., & Feldman, U. 2003b, ApJS 148, 567
Feldman, U., Doschek, G.A. 1977, J. Opt. Soc. Am. 67, 726
Feldman, U. & Doschek, G.A. 1991, ApJS 75 925
Feldman, U., Behring, W.E., Curdt, W. *et al.* 1997, ApJS 113, 195
Feldman, U., Curdt, W., Doschek, G.A. *et al.* 1998, ApJ 503, 467
Feldman, U., Doschek, G.A., Schühle, U., & Wilhelm, K. 1999, ApJ 518, 500
Feldman, U., Curdt, W., Landi. E., & Wilhelm, K. 2000, ApJ 544, 508
Feldman, U., Landi, E., Curdt, W., 2004, ApJ 607, 1039
Grotrian, W. 1939, Naturwissenschaften 27, 214
Hollandt, J., Schühle, U., Paustian, W. *et al.* 1996, Appl. Opt. 35, 5125
Jordan, C. 1971, Sol. Phys. 21, 381
Kelly, R.L. 1987, J. Phys. Chem. Ref. Data 16, 1
Kink, I., Jupen, C., Engström, L. *et al.* 1997, ApJ 487, 956
Kink, I., Engström, L., & Feldman, U. 1999, ApJ 512, 496
Landi, E., Feldman, U., Innes, D.E., & Curdt, W. 2003, ApJ 582, 506
Landi, E., & Feldman, U. 2003, ApJ 592, 607
Lemaire, P., Wilhelm, K., Curdt, W. *et al.* 1997, Sol. Phys. 170, 105
Parenti, S., Landi, E., & Bromage, B.J.I 2003, ApJ 590, 519
Redfield, S., Ayres, T.R., Linsky, J.L. *et al.* 2003, ApJ 585, 993
Rybàk, J., Kučera, A., Schühle, U. & Wöhl, H. 1999 in A. Wilson (ed.) *Magnetic Fields and Solar Processes*, Proc. 9^{th} EPS meeting, Florence, 1999, ESA-SP-448, 361
Sandlin, G.D., Brueckner, G.E. & Tousey, R. 1977, ApJ 214, 898
Sandlin, G.D., Bartoe, J.-D.F., Brueckner, G.E. *et al.* 1986, ApJS 61, 801
Schühle, U., Brekke, P., Curdt, W. *et al.* 1998, Appl. Opt. 37, 2646
Schühle, U., Curdt, W., Hollandt, J. *et al.* 2000, Appl. Opt. 39, 418
Vernazza, J.E. & Reeves, E.M. 1978, ApJS 37, 485
Young, P.R., Del Zanna, G., Landi, E. *et al.* 2003, ApJS 144, 135
Wilhelm, K., Curdt, W., Marsch, E. *et al.* 1995, Sol. Phys. 162, 189
Wilhelm, K., Lemaire, P., Curdt, W. *et al.* 1997a, Sol. Phys. 170, 75
Wilhelm, K., Lemaire, P., Feldman, U. *et al.* 1997b, Appl. Opt. 36, 6416
Wilhelm, K., Marsch, E., Dwivedi, B.N. *et al.* 1998, ApJ 500, 1023
Wilhelm, K. 1999, Astroph. & Sp. Sci. 264, 43
Wilhelm, K., Schühle, U., Curdt, W. *et al.* 2000, Metrologia 37(5), 393

Explanations to Table 3:

o	3^{rd} order lines for which no calibration is available
*	taken with a different slit at a different height above the limb
#	lines measured from spectra recorded by detector 'B'
1^{st} or 2^{nd}	it was not possible to determine the order of diffraction
x	flare line where calculated radiance was not available or unidentified line (flare intensities are from calculations – for details see text)
[	blend
F	cold line
I	intermediate temperature line
1^{st}	1^{st} order line

Table 3. Line list of the SUMER spectral atlas

λ_{obs} Å	Line	Transition	QS	CH	AR	flare	Notes
			line radiance L/ phot cm^{-2} s^{-1} arcsec^{-2}				
465.22	Ne VII	$2s^2\ ^1S_0 - 1s2s\ ^1P_1$	o	o			3^{rd} order
466.24	Ca IX	$3s^2\ ^1S_0 - 3s3p\ ^1P_1$	o		o		3^{rd} order
491.39	S XIII	$2s^2\ ^1S_0 - 2s2p\ ^3P_1$	o		6.2		3^{rd} order
499.40	Si XII	$2s\ ^2S_{1/2} - 2p\ ^2P_{3/2}$	23.3		166.4		
520.66	Si XII	$2s\ ^2S_{1/2} - 2p\ ^2P_{1/2}$	13.3		100.9		
538.93	S XII	$2s^2 2p\ ^2P_{3/2} - 2s2p^2\ ^4P_{3/2}$	0.49		0.81		
539.44	Ca VII	$3s^2 3p^2\ ^3P_0 - 3s3p^3\ ^3P_1$	0.045				
544.28	Ca VII	$3s^2 3p^2\ ^3P_1 - 3s3p^3\ ^3P$	0.12		0.64		
545.23	Ca XIV	$2s^2 2p^3\ ^4S_{3/2} - 2s^2 2p^3\ ^2P_{3/2}$			0.43	358	
550.04	Al XI	$2s\ ^2S_{1/2} - 2p\ ^2P_{3/2}$	7.9		48.5		
[551.45	S VII	$2p^5 3s\ ^3P_1 - 2p^5 3p\ ^3S_1$	0.12	0.18	0.35		1^{st} in QS and AR
[551.45	Ca VII	$3s^2 3p^2\ ^3P_2 - 3s3p^3\ ^3P_2$					
552.09	S XI	$2s^2 2p^2\ ^3P_1 - 2s2p^3\ ^5S_2$	0.31		0.54		
555.38	Ca XV	$2s^2 2p^2\ ^3P_1 - 2s^2 2p^2\ ^1S_0$				101	
557.76	Ca X	$3s\ ^2S_{1/2} - 3p\ ^2P_{3/2}$	9.0	5.2	19.7		
558.59	Ne VI	$2s^2 2p\ ^2P_{1/2} - 2s2p^2\ ^2D_{3/2}$		0.36			
559.96	Ne VII	$2s2p\ ^3P_0 - 2p^2\ ^3P_1$	0.069	0.25#			
560.40	Ne VII	$2s2p\ ^3P_1 - 2p^2\ ^3P_1$	0.090		0.85		
561.76	Ne VII	$2s2p\ ^3P_2 - 2p^2\ ^3P_2$	0.32	0.65			
562.80	Ne VI	$2s^2 2p\ ^2P_{3/2} - 2s2p^2\ ^2D_{5/2}$		0.70			F in QS and AR
564.00	Si XI	$2s^2\ ^1S_0 - 2s2p\ ^3P_2$	1.63		2.6		F in CH
567.83	Fe XX	$2s^2 2p^3\ ^4S_{5/2} - 2s^2 2p^3\ ^2D_{3/2}$				5210	
568.16	Al XI	$2s\ ^2S_{1/2} - 2p\ ^2P_{1/2}$	5.3		23.5		F in CH
569.25	(e)		0.41		0.59		F in CH
574.01	Ca X	$3s\ ^2S_{1/2} - 3p\ ^2P_{1/2}$	6.0	3.2	12.2		
574.88	S XI	$2s^2 2p^2\ ^3P_2 - 2s2p^3\ ^5S_2$	0.66		1.2		F in CH
577.68	Ca X ?		0.14				
579.85	Ca XIV	$2s^2 2p^3\ ^4S_{3/2} - 2s^2 2p^3\ ^2P_{1/2}$			1.2	167	
580.91	Si XI	$2s^2\ ^1S_0 - 2s2p\ ^3P_1$	15.8		33.9		F, 1^{st} in CH
581.34	(c)		0.059	0.19	0.20		
581.60	(c)		0.21	0.21	0.44		
582.86	Ca VIII	$3s^2 3p\ ^2P_{1/2} - 3s3p^2\ ^2D_{3/2}$		0.20			F in QS and AR
585.75	Ar VII	$3s^2\ ^1S_0 - 3s3p\ ^1P_1$	0.15	0.13			
585.77	Fe XXI	$2s^2 2p^2\ ^3P_1 - 2s^2 2p^2\ ^1D_2$				1460	
586.08	(e)		0.20	0.13	0.25		
591.63					0.32		
592.23	Fe XIX	$2s^2 2p^4\ ^3P_2 - 2s^2 2p^4\ ^1D_2$			0.85	4960	
[592.68	(f)		6.4	0.14	7.5		
[592.80						0.52	
593.08	(f)		0.66		0.73		
596.99	Ca VIII	$3s^2 3p\ ^2P_{3/2} - 3s3p^2\ ^2D_{5/2}$		0.35			
604.15	Si XI	$2s2p\ ^1P_1 - 2p^2\ ^1D_2$	2.5		4.1*		
604.88	Cl VII	$2p^6 3p\ ^2P_{3/2} - 2p^6 3d^2 D_{5/2}$					
609.80	Mg X	$2s\ ^2S_{1/2} - 2p\ ^2P_{3/2}$	213.0	25.7	341.2*		
611.61	Si X	$2s^2 2p\ ^2P_{1/2} - 2s2p^2\ ^4P_{3/2}$	0.77		0.76*		F in CH
613.17	Al IX	$2s2p^2\ ^2P_{3/2} - 2p^3\ ^2D_{5/2}$	0.34		0.22*		F in CH
[621.11	Si X	$2s^2 2p\ ^2P_{1/2} - 2s2p^2\ ^4P_{1/2}$					cf., 1242.0 Å

Table 3—Continued

λ_{obs} Å	Line	Transition	QS	CH	AR	flare	Notes
			line radiance L/ phot cm^{-2} s^{-1} arcsec^{-2}				
622.47	K XIII	$2s^2\,2p^3\ ^4S_{3/2} - 2s^2\,2p^3\ ^2P_{1/2}$			1.0		
623.33	Al X	$2s^2\ ^1S_0 - 2s2p\ ^3P_2$	0.44		0.63		
624.71	Si X	$2s^2\,2p\ ^2P_{3/2} - 2s2p^2\ ^4P_{5/2}$	8.4	0.72	9.9		
624.97	Mg X	$2s\ ^2S_{1/2} - 2p\ ^2P_{1/2}$	118.2	16.0	345.6		
626.41	(f)		0.68		1.73		
627.48	(d)		0.13		0.12		F in CH
630.50	Ca VII	$3s^2\,3p^2\ ^3P_1 - 3s\,3p^3\ ^3D_2$			0.80		
631.00	(e)		0.30	0.082	0.11		
631.43	(d)		0.10				F in CH, AR
632.72	(e)		0.24		0.71		F in CH
633.54			0.072				
634.74			0.085				
635.62			0.080				
636.34	K IX	$3s\ ^2S_{1/2} - 3p\ ^2P_{1/2}$	0.23	0.19	0.63		
637.48	Ar VII	$3s\,3p\ ^3P_1 - 3p^2\ ^3P_1$	0.11	0.058			
637.75	Al X	$2s^2\ ^1S_0 - 2s2p\ ^3P_1$	3.0	0.18	4.9		
638.13	(e)		0.26		0.48		F in CH
638.92	Si X	$2s^2\,2p\ ^2P_{3/2} - 2s2p^2\ ^4P_{3/2}$	6.6	0.40	8.0		
639.14	Ca VII	$3s^2\,3p^2\ ^3P_2 - 3s\,3p^3\ ^3D_3$	0.36		0.64		F in CH
639.89	(e)		0.18		0.087		F in CH
640.14			0.55		0.44		
641.18			0.018		0.26		
641.27	Ar VII	$3s\,3p\ ^3P_1 - 3p^2\ ^3P_0$	0.054		0.076		F in CH
642.31			0.039				
642.53	Ar IX	$2p^5\,3s\ ^3P_2 - 2p^5\,3p\ ^1D_2$	0.026	0.035	0.040		
642.97	(e)		0.23		0.40		F in CH
644.47	Ar VII	$3s\,3p\ ^3P_2 - 3p^2\ ^3P_1$	0.23		0.36		
648.25			0.076		0.26		
648.68	Ca XIII	$2s^2\,2p^4\ ^3P_1 - 2s^2\,2p^4\ ^1S_0$			1.1	65.0	I in QS
648.70	S VI	$3d\ ^2D_{5/2} - 4p\ ^2P_{3/2}$					I in QS
649.09	Ar XII	$2s^2\,2p^3\ ^4S_{3/2} - 2s^2\,2p^3\ ^2P_{3/2}$				281	
649.21	Si X	$2s^2\,2p\ \ ^2P_{3/2} - 2s2p^2\ ^4P_{1/2}$	1.9	0.15	2.8		
650.41	S VI	$3d\ ^2D_{3/2} - 4p\ ^2P_{1/2}$	0.11				I in QS
654.07						x	
654.32			0.038				
654.88						x	
655.81			0.043				
656.69	Ar XIII	$2s^2\,2p^2\ ^3P_1 - 2s^2\,2p^2\ ^1S_0$			0.37	43.5	I in QS
657.33						x	
658.27			0.15		0.26		F in CH
660.19					0.64	x	F in QS
662.39	(d)		0.21	0.064	0.41		
662.95	Cr XVIII	$2s^2\,2p^3\ ^4S_{3/2} - 2s^2\,2p^3\ ^2D_{5/2}$				3.8	
662.95	Mn XVIII	$2s^2\,2p^4\ ^3P_2 - 2s^2\,2p^4\ ^1D_2$				27.3	
668.52	S VIII	$2p^4\,3p\ ^4P_{5/2} - 2p^4\,3d\ ^4D_{5/2}$	0.037				
669.02	(d)		0.16	0.077			
670.02	Al X	$2s2p\ ^1P_1 - 2p^2\ ^1D_2$	0.38	0.071	0.61		

Table 3—Continued

λ_{obs} Å	Line	Transition	QS	CH	AR	flare	Notes
			line radiance L/ phot cm^{-2} s^{-1} arcsec^{-2}				
670.31	Ar XII	$2s^2\,2p^3\ ^4S_{3/2} - 2s^2\,2p^3\ ^2P_{1/2}$			0.35	116	I in QS
672.03	S VIII	$2p^4\,3p\ ^4P_{5/2} - 2p^4\,3d\ ^4D_{7/2}$	0.078				F in CH, I in AR
675.34	S VIII	$2p^4\,3p\ ^4D_{5/2} - 2p^4\,3d\ ^4F_{7/2}$	0.068				F in CH, I in AR
676.29	Ca IX	$3s^2\ ^1S_0 - 3s3p\ ^3P_2$	0.069	0.11			
676.29	S VIII	$2p^4\,3p\ ^4D_{7/2} - 2p^4\,3d\ ^4F_{9/2}$					
676.51	Si IX	$2s^2\,2p^2\ ^3P_1 - 2s2p^3\ ^5S_2$	2.0	0.63	2.1		
676.81	(e)		1.0	0.29	1.5		
677.72				0.087			
679.27	Fe XX	$2s^2\,2p^3\ ^2D_{5/2} - 2s^2\,2p^3\ ^2P_{3/2}$				274	
679.79	Mg VIII	$2s2p^2\ ^2P_{1/2} - 2p^3\ ^2D_{3/2}$	0.33	0.066	0.43		
680.39	Al IX	$2s^2\,2p\ ^2P_{1/2} - 2s2p^2\ ^4P_{3/2}$	4.3	0.33	4.4		
680.67	S VII	$2p^5\,3p\ ^3D_3 - 2p^5\,3d\ ^3F_4$		0.045			
681.70	Na IX	$2s\ ^2S_{1/2} - 2p\ ^2P_{3/2}$	7.6	4.9	34.6		
682.93			0.036				
683.20	S VIII	$2p^4\,3p\ ^4P_{1/2} - 2p^4\,3d\ ^4D_{3/2}$	0.056		0.077		I in QS
684.04	(c)		0.12	0.14	0.28		
686.44	Fe VIII	$3p^5\,3d^2\ ^2P_{3/2} - 3p^6\,4p\ ^2D_{5/2}$	0.14	0.30			F in AR
686.44	S VIII	$2p^4\,3s\ ^2D_{5/2} - 2p^4\,3p\ ^2P_{3/2}$					F in AR
686.82	S VII	$2p^5\,3p\ ^1D_2 - 2p^5\,3d\ ^1D_2$	0.055				
686.82	S VIII	$2p^4\,3p\ ^2D_{5/2} - 2p^4\,3d\ ^2F_{7/2}$					
687.68	S VII	$2p^5\,3p\ ^3P_2 - 2p^5\,3d\ ^1F_3$	0.013				
687.68	S VIII	$2p^4\,3p\ ^2D_{3/2} - 2p^4\,3d\ ^2F_{5/2}$					
688.24	Al IX	$2s^2\,2p\ ^2P_{1/2} - 2s2p^2\ ^4P_{1/2}$	0.11	0.044	0.33		
688.68	Fe VIII	$3p^5\,3d^2\ ^2P_{3/2} - 3p^6\,4d\ ^2D_{3/2}$	0.022				
689.63	Mg VIII	$2s2p^2\ ^2P_{3/2} - 2p^3\ ^2D_{5/2}$	0.31	0.33	0.76		
691.42	Ca IX	$3s^2\ ^1S_0 - 3s3p\ ^3P_1$	0.32	0.84			
691.54	Al IX	$2s^2\,2p\ ^2P_{3/2} - 2s2p^2\ ^4P_{5/2}$	0.44	0.15	0.92		
692.69	S VIII	$2p^4\,3p\ ^2F_{7/2} - 2p^4\,3d\ ^2G_{9/2}$	0.027				
692.69	Ar IX	$2p^5\ \ 3s^3P_2 - 2p^5\,3p\ ^3D_2$					
693.33			0.079	0.085			
693.61			0.040				
693.96	Mg IX	$2s^2\ ^1S_0 - 2s2p\ ^3P_2$	0.88	0.99	3.3		
694.13	Na IX	$2s^2\ ^2S_{1/2} - 2p\ ^2P_{1/2}$	3.5	2.6	18.4		
694.69	Si IX	$2s^2\ \ 2p^2\ ^3P_2 - 2s2p^3\ ^5S_2$	4.1	1.5	6.7		
695.06	(c)		0.33	0.34	0.81		
697.17	Fe VIII	$3p^6\ \ 4p\ ^2P_{1/2} - 3p^6\,4d\ ^2D_{3/2}$	0.24	0.62			
697.40	Ar IX	$2p^5\ \ 3s^3P_2 - 2p^5\,3p\ ^3D_3$	0.051		0.031#		
700.24	Ar VIII	$3s\ ^2S_{1/2} - 3p\ ^2P_{3/2}$	1.0	0.87	1.3		
701.00					0.13		
703.64	Al IX	$2s^2\,2p\ ^2P_{3/2} - 2s2p^2\ ^4P_{3/2}$	0.34	0.20	0.63		
706.04	Mg IX	$2s^{2\,1}S_0 - 2s2p\ ^3P_1$	10.2	9.2	21.5		
706.46	S VI	$3p^2P_{1/2} - 3d\ ^2D_{3/2}$	0.044				F in CH
706.80	(c)		0.033		0.087		
707.65	(c)		0.058		0.12		
708.49	(c)		0.053				
708.89	S IX	$2p^3\,3p\ ^5P_2 - 2p^3\,3d\ ^5D_3$	0.12		0.15		
709.81					0.12		

Table 3—Continued

λ_{obs} Å	Line	Transition		QS	CH	AR	flare	Notes
				line radiance L/ phot cm^{-2} s^{-1} arcsec^{-2}				
711.39				0.038#				
712.22	Al IX	$2s^2 2p\ ^2P_{3/2}$	$- 2s2p^2\ ^4P_{1/2}$	0.051	0.17			
712.22	S IX	$2p^3 3p\ ^3D_2$	$- 2p^3 3d\ ^3F_3$					
712.67	S VI	$3p\ ^2P_{3/2}$	$- 3d\ ^2D_{5/2}$		0.12			F in QS, AR
713.49						0.20		
713.82	Ar VIII	$3s\ ^2S_{1/2}$	$- 3p\ ^2P_{1/2}$	0.45	0.51	0.85		
714.79	S IX	$2p^3 3p\ ^5P_3$	$- 2p^3 3d\ ^5D_4$	0.17		0.19		
715.12	S IX	$2p^3 3p\ ^3F_3$	$- 2p^3 3d\ ^3G_4$	0.059				
717.05				0.12#				
717.69	Fe VIII ?	$3p^6 4p\ ^2P_{3/2}$	$- 3p^6 4d\ ^2D_{5/2}$					
717.85	Ar XI	$2p^3 3s\ ^5S_2$	$- 2p^3 3p\ ^5P_3$	0.12	0.12	0.22	x	
718.29	(e)			0.33	0.11	0.42		
719.40	S IX	$2p^3 3p\ ^3F_4$	$- 2p^3 3d\ ^3G_5$	0.079	0.045	0.17		
721.26	Fe VIII	$3p^6 4p\ ^4P_{3/2}$	$- 3p^6 4d\ ^2D_{5/2}$	0.37	1.2	1.1		
721.55	Fe XX	$2s^2 2p^3\ ^4S_{3/2}$	$- 2s^2 2p^3\ ^2D_{3/2}$				8140	
723.75	Fe VIII	$3p^6 4p\ ^2P_{3/2}$	$- 3p^6 4d\ ^2D_{3/2}$	0.077	0.12	0.15		
724.69	Cl XI	$2s^2 2p^3\ ^4S_{3/2}$	$- 2s^2 2p^3\ ^2P_{1/2}$			0.30		
725.84	Ar IX	$2p^5\ 3s^3P_1$	$- 2p^5 3p\ ^3D_2$	0.077#		0.053		
730.41	Ar XI	$2p^3 3s\ ^5S_2$	$- 2p^3 3p\ ^5P_2$	0.037		0.14		F in CH
732.20						0.12		
732.68	(d)			0.098#		0.073		
733.83	(f)			0.063		0.051#		
735.11						0.054#		
735.26	(c)			0.024				
736.18						0.11		
736.42	Ar XI	$2p^3 3s\ ^5S_2$	$- 2p^3 3p\ ^5P_1$	0.081		0.28		F in CH
737.61				0.016				
738.87	Fe VII	$3d4p\ ^3P_2$	$- 3d4d\ ^3P_2$			0.15#		F in CH
740.04	Fe VII	$3d4p\ ^1F_3$	$- 3d4d\ ^1G_4$	0.057	0.11			
740.11	Ar VIII	$2p^6 4d\ ^2D_{5/2}$	$- 2p^6 5p\ ^2P_{3/2}$					
740.74	Cr XVII	$2s^2 2p^4\ ^3P_2$	$- 2s^2 2p^4\ ^1D_2$			0.39	20.1	
741.67				0.020	0.097			
743.98						0.13		
745.49	Fe VII	$3d4p\ ^3F_2$	$- 3d4d\ ^3F_2$	0.031		0.22		
745.80	Ar XI	$2s^2 2p^4\ ^3P_1$	$- 2s^2 2p^4\ ^1S_0$	0.047		0.20		
749.56	Mg IX	$2s2p\ ^1P_1$	$- 2p^2\ ^1D_2$	1.6	1.6	4.4		
752.51	Fe VIII	$3p^5 3d^2\ ^2P_{1/2}$	$- 3p^6 4d\ ^2D_{3/2}$	0.011	0.036			
754.98	Ar VI ?	$3s^2 3p\ ^2P_{3/2}$	$- 3s3p^2\ ^2D_{3/2}$	0.020				
755.40	(d)			0.025				
756.72	Al VIII	$2s^2 2p^2\ ^3P_1$	$- 2s2p^3\ ^5S_2$	0.052	0.11	0.17		
758.59	Mn XIX	$2s^2 2p^3\ ^4S_{3/2}$	$- 2s^2 2p^3\ ^2D_{3/2}$				32.8	
762.65	Mg VIII	$2s^2 2p\ ^2P_{1/2}$	$- 2s2p^2\ ^4P_{3/2}$	0.099	0.33	0.35		
769.38	Mg VIII	$2s^2 2p\ ^2P_{1/2}$	$- 2s2p^2\ ^4P_{1/2}$	0.24	0.97	0.97		
770.42	Ne VIII	$2s^2 S_{1/2}$	$- 2p\ ^2P_{3/2}$	39.5	41.4	177.9		
772.29	Mg VIII	$2s^2 2p\ ^2P_{3/2}$	$- 2s2p^2\ ^4P_{5/2}$	1.3	4.1	4.8		
772.53	Al VIII	$2s^2 2p^2\ ^3P_2$	$- 2s2p^3\ ^5S_2$	0.11	0.45	0.72		
776.25	S X	$2s^2 2p^3\ ^4S_{3/2}$	$- 2s^2 2p^3\ ^2P_{3/2}$	2.3	0.14	4.1		I in CH

Table 3—Continued

λ_{obs} Å	Line	Transition	QS	CH	AR	flare	Notes
			line radiance L/ phot cm^{-2} s^{-1} arcsec^{-2}				
777.18	(e)		0.11		0.26		
778.38			0.11				
779.45	Ni XXI	$2s^2\,2p^4\ ^3P_2 - 2s^2\,2p^4\ ^3P_1$				152	
780.34	Ne VIII	$2s\ ^2S_{1/2} - 2p\ ^2P_{1/2}$	33.1	29.7	113.9		
782.37	Mg VIII	$2s^2\,2p\ ^2P_{3/2} - 2s\,2p^2\ ^4P_{3/2}$	1.2	3.9	3.3		
782.98	S XI	$2s^2\,2p^2\ ^3P_1 - 2s^2\,2p^2\ ^1S_0$	1.0		2.4		
786.03	Fe XXI	$2s^2\,2p^2\ ^3P_2 - 2s^2\,2p^2\ ^1D_2$				1040	
787.43	S X	$2s^2\,2p^3\ ^4S_{3/2} - 2s^2\,2p^3\ ^2P_{1/2}$	1.5		2.4		
789.44	Mg VIII	$2s^2\,2p\ ^2P_{3/2} - 2s\,2p^2\ ^4P_{1/2}$	0.27	0.95	1.2		
789.78	Na VIII	$2s^2\ ^1S_0 - 2s\,2p^3\,P_1$	0.17	0.77	1.3		
792.79	Fe VII	$3d4p\ ^3F_2 - 3d4d\ ^3G_3$		0.038			
793.18	Cr XVIII	$2s^2\,2p^3\ ^4S_{3/2} - 2s^2\,2p^3\ ^2D_{3/2}$			0.071	6.2	
794.61	Ni XIX	$2p^5\,3s\ ^3P_1 - 2p^5\,3s\ ^3P_0$			0.13	11.5	
794.94					0.11		
797.90	(f)		0.72	0.065	1.0		I in CH
799.10	Fe VII	$3d4p\ ^3D_3 - 3d4d\ ^3D_3$		0.066			
800.64	Cl VII	$3s\ ^2S_{1/2} - 3p^2\,P_{3/2}$		0.10			
801.69	Fe VII	$3d4p\ ^3F_3 - 3d4d\ ^3G_3$		0.050			
803.23				0.060			
803.46	(e)		1.3	0.45	2.1		
804.16	S X	$2p^2\,3s\ ^4D_{7/2} - 2p^2\,3p\ ^4F_{9/2}$	0.21	0.093	0.45		
804.16	Fe VII	$3d4p\ ^3F_4 - 3d4d\ ^3G_4$					
804.42	(d)		0.18	0.25	0.48		
805.63	S VIII	$2p^4\,3s\ ^2D_{5/2} - 2p^4\,3p\ ^2D_{5/2}$	0.044	0.073			
806.92	(e)		0.036				F in CH, AR
812.95	Cl VII	$3s\ ^2S_{1/2} - 3p^2\,P_{1/2}$	0.033	0.064			F in CH, AR
812.95	S VIII	$2p^4\,3s\ ^2D_{3/2} - 2p^4\,3p\ ^2D_{3/2}$					F in CH, AR
814.52	Ar IX	$2p^5\,3s\ ^3P_2 - 2p^5\,3p\ ^3S_1$	0.054				F in AR
814.72	Si XIII	$1s2s\ ^3S_1 - 1s2p\ ^3P_2$				112	
815.21			0.012				F in CH, AR
818.97			0.046				
820.02	Co XIX	$2s^2\,2p^5\ ^2P_{3/2} - 2s^2\,2p^5\ ^2P_{1/2}$				3.8	
821.22	Ca IX	$3s3p\ ^1P_1 - 3p^2\ ^1D_2$	0.10	0.36	0.39		
821.71	Fe XX	$2s^2\,2p^3\ ^2D_{3/2} - 2s^2\,2p^3\ ^2P_{1/2}$				205	
830.15	(d)		0.15				F in CH, I in AR
830.47			0.064				
839.17	Si XI		0.093				
839.63	S X		0.034				
843.62					0.41		
844.00			0.025		0.72		
845.57	Fe XXII	$2s^2\,2p\ ^2P_{1/2} - 2s^2\,2p\ ^2P_{3/2}$				14000	
847.66	S VIII	$2p^4\,3s\ ^4P_{3/2} - 2p^4\,3p\ ^4D_{3/2}$	0.055				F in CH
847.91	Na VIII	$2sp\ ^1P_1 - 2p^2\,^1D_2$	0.053	0.16			F in AR
849.90	S VIII	$2p^4\,3s\ ^4P_{5/2} - 2p^4\,3p\ ^4D_{7/2}$	0.18	0.13			F in AR
850.78			0.036				
851.49			0.12				F in AR
852.85			0.044				F in AR

Table 3—Continued

λ_{obs} Å	Line	Transition	QS	CH	AR	flare	Notes
			line radiance L/ phot cm^{-2} s^{-1} arcsec^{-2}				
853.51	P IX	$2s^2\,2p^3\ ^4S_{3/2} - 2s^2\,2p^3\ ^2P_{3/2}$	0.069				F in CH, AR
854.64	Mg VII	$2s^2\,2p^2\ ^3P_1 - 2s\,2p^3\ ^5S_2$	0.14	0.98	0.86		
855.96			0.025				
856.77	(f)		1.6		4.1		F in CH
859.96	S VII	$2p^5\,3s\ ^3P_1 - 2p^5\,3p\ ^3P_2$	0.034				F in AR
860.68	Ar IX	–	0.0086				
861.09	P IX	$2s^2\,2p^3\ ^4S_{3/2} - 2s^2\,2p^3\ ^2P_{1/2}$	0.021				
861.78	Ti XVI	$2s^2\,2p^3\ ^4S_{3/2} - 2s^2\,2p^3\ ^2D_{3/2}$				15.0	
862.73	(d)		0.085	0.14			F in AR
864.75			0.017				
867.60	(g)		0.12				F in AR
868.08	Mg VII	$2s^2\,2p^2\ ^3P_2 - 2s\,2p^3\ ^5S_2$	0.25	0.20	1.9		
868.55	(g)		0.15				
869.01	(e)		0.014				F in AR
871.71	S IX	$2s^2\,2p^4\ ^3P_1 - 2s^2\,2p^4\ ^1S_0$	0.67	0.34	0.88		
871.71	S VIII	$2p^4\,3s\ ^4P_{3/2} - 2p^4\,3p\ ^2D_{5/2}$					
872.06	Na VII	$2s^2\,2p\ ^2P_{3/2} - 2s\,2p^2\ ^4P_{5/2}$	0.022	0.12			I in AR
873.33	(d)		0.052				
874.40	S VIII	$2p^4\,3s\ ^4P_{1/2} - 2p^4\,3p\ ^4D_{3/2}$	0.068				
877.08	S VII	$2p^5\,3s\ ^3P_0 - 2p^5\,3p\ ^1P_1$	0.049				
878.69	Si XIII	$1s2s\ ^3S_1 - 1s2p\ ^3P_0$				22.1	
878.77	S IX	$2p^3\,3s\ ^3D_3 - 2p^3\,3p\ ^3F_4$	0.19				F in CH, AR
879.10			0.064				F in CH
879.73			0.018				
880.34	Na VII	$2s^2\,2p\ ^2P_{3/2} - 2s\,2p^2\ ^4P_{3/2}$					
880.40	Ca XIV	$2s^2\,2p^3\ ^4S_{3/2} - 2s^2\,2p^3\ ^2D_{5/2}$			6.1	86.0	F in CH
882.45			0.037				
882.68	S IX	$2p^3\,3s\ ^3D_2 - 2p^3\,3p\ ^3F_3$	0.52				I in AR
882.68	S IX	$2p^3\,3s\ ^5S_2 - 2p^3\,3p\ ^5P_3$					
882.89				0.068			
883.30	Ni XII ?		0.18				
883.63	(c)		0.10	0.14			F in AR
886.23	(c)			0.086			F in QS, AR
887.24	Ne VII	$2s^2\ ^1S_0 - 2s2p^3\,P_2$		0.061			
887.74	S VII	$2p^5\,3s\ ^3P_2 - 2p^5\,3p\ ^3D_2$	0.041				F in CH, AR
889.13	S IX	$2p^3\,3s\ ^3D_1 - 2p^3\,3p\ ^3F_2$	0.026				F in CH
890.03	(c)		0.032				
892.27	S IX	$2p^3\,3s\ ^5S_2 - 2p^3\,3p\ ^5P_2$	0.22				F in CH
892.66			0.034				
894.33	S VII	$2p^5\,3s\ ^3P_1 - 2p^5\,3p\ ^3D_1$	0.016				F in CH, AR
895.16	Ne VII	$2s^2\ ^1S_0 - 2s2p^3\,P_1$	3.9	1.2	2.2		
897.35	S IX	$2p^3\,3s\ ^5S_2 - 2p^3\,3p\ ^5P_1$	0.13				F in CH, AR
897.81	S VII	$2p^5\,3s\ ^3P_2 - 2p^5\,3p\ ^3D_3$	0.046				F in AR
900.77	(d)		0.068				F in CH, AR
901.88	Si VII		0.069				
902.25	Si VII		0.029				
902.99	S VII	$2p^5\,3s\ ^1P_1 - 2p^5\,3p\ ^1D_2$	0.13				

Table 3—Continued

λ_{obs} Å	Line	Transition	QS	CH	AR	flare	Notes
			line radiance L/ phot cm^{-2} s^{-1} arcsec^{-2}				
904.93	S VII	$2p^5\,3p\ ^5P_2 - 2p^5\,3d\ ^5D_{3,2}$	0.078	0.15			F in AR
905.68	S VIII	$2p^4\,3s\ ^2D_{5/2} - 2p^4\,3p\ ^2F_{7/2}$	0.10				F in CH, AR
908.89	S IX	$2p^3\,3s\ ^3S_1 - 2p^3\,3p\ ^3P_2$	0.10				F in AR
909.11			0.030				
909.41	Si VII	$2p^3\,3p\ ^5P_3 - 2p^3\,3d\ ^5D_{4,5}$	0.071	0.24	0.31		
910.86	Ni XXIII	$2s^2\,2p^2\ ^3P_0 - 2s^2\,2p^2\ ^3P_1$				722	
911.88	S IX	$2p^3\,3s\ ^3S_1 - 2p^3\,3p\ ^3P_1$	0.090				I in AR
914.03			0.079				
915.07			0.038				
916.70	S VIII	$2p^4\,3s\ ^3P_{3/2} - 2p^4\,3p\ ^2D_{5/2}$	0.16	0.16			F in QS
918.80	Si VII	$2p^3\,3p\ ^3F_4 - 2p^3\,3d\ ^3G_5$	0.060	0.059	0.077		
919.73	Ti XV	$2s^2\,2p^4\ ^3P_2 - 2s^2\,2p^4\ ^1D_2$			0.21	8.3	
919.83	S VIII	$2p^4\,3s\ ^2D_{3/2} - 2p^4\,3p\ ^2F_{5/2}$	0.066	0.034			
920.68			0.048		0.067		
921.56	(c)		0.0084				
922.27	(c)		0.065	0.11	0.058		
924.93			0.044				
926.91	(f)		0.037				
931.78	Si VII	$2p^3\,3p\ ^1F_3 - 2p^3\,3d\ ^1G_4$		0.048			
932.16			0.040				
932.95			0.035				
933.41	S VI	$3s\ ^2S_{1/2} - 3p\ ^2P_{3/2}$		1.0	2.0		
934.43	(f)		0.040		0.069		
934.72			0.0066	0.020	0.055		
935.28					0.025		I in QS
935.94	(d)		0.012	0.0093			
938.70	S X	$2p^2\,3s\ ^4P_{1/2} - 2p^2\,3p\ ^4D_{3/2}$	0.070		0.16		
939.18	(b)				0.056		F in CH, QS
940.13	(e)		0.065		0.10		I in CH
940.87	S X	$2p^2\,3s\ ^4P_{3/2} - 2p^2\,3p\ ^4D_{5/2}$	0.091		0.095		
941.37	S VII	$2p^5\,3s\ ^3P_0 - 2p^5\,3p\ ^3D_1$	0.0053				
941.76			0.0036				
942.11					0.023		
943.63	Ca XIV	$2s^2\,2p^3\ ^4S_{3/2} - 2s^2\,2p^3\ ^2D_{3/2}$	0.024		7.0	478.0	
944.35	Si VIII	$2s^2\,2p^3\ ^4S_{3/2} - 2s^2\,2p^3\ ^2P_{3/2}$	4.9	7.7	11.3		
944.57	S VI	$3s\ ^2S_{1/2} - 3p\ ^2P_{1/2}$					
944.63	S VIII	$2p^4\,3s\ ^4P_{5/2} - 2p^4\,3p\ ^4P_{3/2}$			0.96		
945.90	K XIII	$2s^2\,2p^3\ ^4S_{3/2} - 2s^2\,2p^3\ ^2D_{5/2}$			0.43	2.3	
946.32	S X	$2p^2\,3s\ ^4P_{5/2} - 2p^2\,3p\ ^4D_{7/2}$	0.46	0.036	0.54	56.8	
949.24	Si VIII	$2s^2\,2p^3\ ^4S_{3/2} - 2s^2\,2p^3\ ^2P_{1/2}$	1.7	3.2	5.0		
950.16	Si IX	$2s^2\,2p^2\ ^3P_1 - 2s^2\,2p^2\ ^1S_0$	2.6	1.3	5.2		
951.45			0.034		0.049		
951.88	S IX	$2p^3\,3s\ ^3D_3 - 2p^3\,3p\ ^3D_3$	0.076	0.016	0.11		
951.92	P VIII	$2s^2\,2p^4\ ^3P_1 - 2s^2\,2p^4\ ^1S_0$					
953.64	(d)		0.024	0.040	0.073		
955.89	(d)		0.033	0.049	0.094		
956.59			0.0051		0.028		

Table 3—Continued

λ_{obs} Å	Line	Transition	QS	CH	AR	flare	Notes
			line radiance L/ phot cm^{-2} s^{-1} arcsec^{-2}				
957.04	(b)		0.020	0.014	0.071		
958.03			0.031		0.035		
958.34	S IX	$2p^3\,3s\ ^1D_2 - 2p^3\,3p\ ^1F_3$	0.074		0.083		
959.53	(d)		0.11	0.078	0.14		
960.08	S VII	$2p^5\,3s\ ^1P_1 - 2p^5\,3p\ ^3P_2$		0.015			
960.62	S X	$2p^2\,3s\ ^4P_{1/2} - 2p^2\,3p\ ^4D_{1/2}$	0.023		0.042		
961.44			0.0082		0.019		
961.80	S IX	$2p^3\,3s\ ^3D_2 - 2p^3\,3p\ ^3D_2$	0.030		0.029		
963.94	Si VII	$2p^3\,3s\ ^3F_4 - 2p^3\,3p\ ^3F_4$	0.0055				I in AR
964.61	(f)		0.050		0.067		
965.20	(d)		0.15	0.19	0.31		
965.64			0.021	0.018	0.045		
967.19	Si VII	$2p^3\,3p\ ^3F_3 - 2p^3\,3d\ ^3F_3$		0.0078			
968.44	Si VII	$2p^3\,3s\ ^1P_1 - 2p^3\,3p\ ^1D_2$	0.025	0.021	0.033		
968.44	Si VII	$2p^3\,3p\ ^3F_2 - 2p^3\,3d\ ^3F_2$					
968.84	Ti XVI	$2s^2\,2p^3\ ^2D_{3/2} - 2s^2\,2p^3\ ^2P_{3/2}$			0.40	2.0	
970.54	(c)		0.020	0.018			
973.33	Ne VII	$2s2p\ ^1P_1 - 2p^2\ ^1D_2$		0.26			
974.60	Si VIII	$2p^2\,3p\ ^2F_{7/2} - 2p^2\,3d\ ^2G_{9/2}$	0.077	0.080			
974.84	Fe XVIII	$2s^2\,2p^5\ ^2P_{3/2} - 2s^2\,2p^5\ ^2P_{1/2}$			15.3	8370	
975.83	(d)		0.052	0.035	0.079		
979.17	(c)		0.061				
981.75	(e)		0.039				
982.16	Si VIII	$2p^2\,3p\ ^4D_{1/2} - 2p^2\,3d\ ^4F_{3/2}$	0.033	0.026	0.047		
983.56	Si VIII	$2p^2\,3p\ ^4D_{3/2} - 2p^2\,3d\ ^4F_{5/2}$	0.069	0.038	0.095		
986.28	Si IX	$2s^2\,2p^2\ ^3P_2 - 2s^2\,2p^2\ ^1S_0$	0.083		0.31		
986.54					0.071		
988.22	Si VIII	$2p^2\,3p\ ^4D_{5/2} - 2p^2\,3d\ ^4F_{7/2}$	0.081	0.055	0.14		
992.03	(e)		0.050				I in AR
994.44	K XIII	$2s^2\,2p^3\ ^4S_{3/2} - 2s^2\,2p^3\ ^2D_{3/2}$				24.9	
994.58	Si VIII	$2p^2\,3p\ ^4D_{7/2} - 2p^2\,3d\ ^4F_{9/2}$	0.21	0.20	1.1		
996.54	(c)		0.022	0.023			
997.44	Mg XI	$1s2s\ ^3S_1 - 1s2p\ ^3P_2$			0.36	147	
997.69			0.034		0.26		
1000.84	(c)		0.042	0.095	0.099		
1005.00	Si VIII	$2p^2\,3p\ ^4D_{5/2} - 2p^2\,3d\ ^4F_{5/2}$	0.017				I in AR
1005.86	Mn XXI	$2s^2\,2p^3\ ^2P_{3/2} - 2s^2\,2p^3\ ^2P_{1/2}$				54.8	
1009.91	Si VII	$2p^3\,3s\ ^3P_2 - 2p^3\,3p\ ^3P_2$					
1013.05	(d)		0.0055		0.026		
1015.79	(e)		0.32		0.44		
1016.01	(e)		0.056				
1018.75	Ar XII	$2s^2\,2p^3\ ^4S_{3/2} - 2s^2\,2p^3\ ^2D_{5/2}$	0.11		1.7	7.8	
1018.93			0.40	0.040			
1020.10	(d)		0.030				
1020.66			0.0044				
1023.31	(e)						
1023.50	(d)		0.045		0.035		F in CH

Table 3—Continued

λ_{obs} Å	Line	Transition	QS	CH	AR	flare	Notes
			line radiance L/ phot cm^{-2} s^{-1} arcsec^{-2}				
1028.04	Fe X	$3p^4\,3d\ ^4D_{7/2} - 3p^4\,3d\ ^4F_{7/2}$	2.6	1.2	4.2		
1028.97	(e)		2.2	2.2	2.9		
1031.93	O VI	$2s\ ^2S_{1/2} - 2p\ ^2P_{3/2}$	124	74	260		
1033.01	Ni XV	$3s^2\,3p^2\ ^3P_1 - 3s^2\,3p^2\ ^1S_0$	0.046		2.2	474	
1034.40	Ni XIV	$3s^2\,3p^3\ ^4S_{3/2} - 3s^2\,3p^3\ ^2P_{3/2}$	0.19	0.78	2.3		
1035.08			0.029	0.039	0.093		
1037.63	O VI	$2s\ ^2S_{1/2} - 2p\ ^2P_{1/2}$	50.6	33.9	124		
1042.53	Fe X	$3p^4\,3d\ ^4D_{3/2} - 3p^4\,3d\ ^2F_{7/2}$	0.034		0.069		
1043.28	Mg XI	$1s2s\ ^3S_1 - 1s2p\ ^3P_0$			0.13	26.6	
1049.26	Si VII	$2s^2\,2p^4\ ^3P_1 - 2s^2\,2p^4\ ^1S_0$	0.21	0.84	0.97		
1051.63	S VII	$2p^5\,3s\ ^3P_2 - 2p^5\,3p\ ^3S_1$	0.027	0.086			
1052.09			0.0037				
1053.88	Al VII	$2s^2\,2p^3\ ^4S_{3/2} - 2s^2\,2p^3\ ^2P_{3/2}$	0.093	0.40	0.42		
1054.59	Ar XII	$2s^2\,2p^3\ ^4S_{3/2} - 2s^2\,2p^3\ ^2D_{3/2}$	0.19	0.024	2.2	146	
1056.79	Al VII	$2s^2\,2p^3\ ^4S_{3/2} - 2s^2\,2p^3\ ^2P_{1/2}$	0.032	0.18	0.21		
1057.26	Si VIII	$2p^2\,3s\ ^2S_{1/2} - 2p^2\,3p\ ^2P_{3/2}$	0.015		0.028		
1057.86	Al VIII	$2s^2\,2p^2\ ^3P_1 - 2s^2\,2p^2\ ^1S_0$	0.088	0.21	0.27		
1062.44	Fe VIII	$3p^6\,4s^2\,S_{1/2} - 3p^6\,4p^2\,P_{3/2}$	0.018				I in CH
1062.44						x	
1072.35			0.0076				
1077.17						x	
1079.42	Fe XXIII	$2s2p\ ^3P_2 - 2s2p\ ^3P_2$				1180	
1098.48	Ca XV	$2s^2\,2p^2\ ^3P_1 - 2s^2\,2p^2\ ^1D_2$			1.4	155	
1101.26	Cl XI	$2s^2\,2p^3\ ^4S_{3/2} - 2s^2\,2p^3\ ^2D_{5/2}$	0.042				
1102.93	S VII	$2p^5\,3s\ ^3P_1 - 2p^5\,3p\ ^3S_1$			0.043		
1111.76	Na X	$1s2s\ ^3S_1 - 1s2p\ ^3P_2$			0.14	8.6	
1116.03	Si VIII	$2p^2\,3s\ ^4P_{3/2} - 2p^2\,3p\ ^4P_{1/2}$	0.032		0.10		
1118.07	Fe XIX	$2s^2\,2p^4\ ^3P_2 - 2s^2\,2p^4\ ^3P_1$			0.69	4690	
1119.66			0.0097				
1121.74			0.042				
1124.39			0.065		0.28		
1126.56	Cl XI	$2s^2\,2p^3\ ^4S_{3/2} - 2s^2\,2p^3\ ^2D_{3/2}$	0.047				F in AR
1130.42	(e)		0.75		0.87		F in CH
1131.05				0.11			
1132.80	Si VII	$2p^3\,3s\ ^3D_3 - 2p^3\,3p\ ^3F_4$	0.12	0.23	0.21		
1133.76	Ca XIII	$2s^2\,2p^4\ ^3P_2 - 2s^2\,2p^4\ ^1D_2$	0.25	15.0	260		
1134.10	Co XIII	$3s^2\,3p^3\ ^4S_{3/2} - 3s^2\,3p^3\ ^2P_{3/2}$	0.081				
1135.02					0.031		
1135.39	Si VII	$2p^3\,3s\ ^5S_2 - 2p^3\,3p\ ^5P_3$	0.49	0.69	0.96		
1137.24	Si VII	$2p^3\,3s\ ^3D_2 - 2p^3\,3p\ ^3F_3$	0.073	0.12			I in AR
1137.99			0.023		0.081		
1138.48	(e)		0.089				
1141.47	Fe VII	$3d4s\ ^3D_3 - 3d4p\ ^3F_4$		0.044			
1142.50	Si VII	$2p^3\,3s\ ^5S_2 - 2p^3\,3p\ ^5P_2$	0.19	0.44			I in AR
1143.58	Si VII	$2p^3\,3s\ ^3P_2 - 2p^3\,3p\ ^3D_3$	0.15	0.134			I in AR
1146.57	Si VII	$2p^3\,3s\ ^5S_2 - 2p^3\,3p\ ^5P_1$	0.077	0.19			I in AR
1146.88	(c)		0.13	0.20			I in AR

Table 3—Continued

λ_{obs} Å	Line	Transition	QS	CH	AR	flare	Notes
			line radiance L/ phot cm^{-2} s^{-1} arcsec^{-2}				
1148.70	Si VI	$2p^4\,3s\ ^4P_{3/2} - 2p^4\,3p\ ^4D_{5/2}$	0.12	0.13			
1153.16	Fe XVII	$2p^5\,3s\ ^3P_1 - 2p^5\,3s\ ^3P_0$			5.2	111	
1157.55	(d)		0.082				
1164.82					0.086	x	
1166.17	Fe VII	$3d4s\ ^3D_1 - 3d4p\ ^3F_2$		0.028			
[1167.70	Si VII	$2p^3\,3s\ ^3S_1 - 2p^3\,3p\ ^3P_2$	0.086	0.16	0.58		
[1167.73	Mn XVII	$2s^2\,2p^5\ ^2P_{3/2} - 2s^2\,2p^5\ ^2P_{1/2}$				15.8	
1169.35	Si VII	$2p^3\,3s\ ^3S_1 - 2p^3\,3p\ ^3P_1$	0.046	0.079			
1174.64	Ni XIV	$3s^2\,3p^3\ ^4S_{3/2} - 3s^2\,3p^3\ ^2P_{1/2}$			2.6	x	
1182.48	Si VIII	$2p^2\,3s\ ^4P_{1/2} - 2p^2\,3p\ ^4D_{3/2}$	0.11		0.18		I in CH
1184.04	Si VIII	$2p^2\,3s\ ^4P_{3/2} - 2p^2\,3p\ ^4D_{5/2}$	0.25	0.16	0.45		I in AR
1187.53			0.014				
1188.10					0.22	x	1^{st} or 2^{nd}?
1189.52	Si VIII	$2p^2\,3s\ ^4P_{5/2} - 2p^2\,3p\ ^4D_{7/2}$	0.67	0.45			AR short slit
1189.84	Mg VII	$2s^2\,2p^2\ ^3P_1 - 2s^2\,2p^2\ ^1S_0$	0.28	1.4			AR short slit
1190.09	Mg VI	$2s^2\,2p^3\ ^4S_{3/2} - 2s^2\,2p^3\ ^2P_{3/2}$	0.13	0.90			
1191.64	Mg VI	$2s^2\,2p^3\ ^4S_{3/2} - 2s^2\,2p^3\ ^2P_{1/2}$	0.063	0.38			
1192.98	(f)					x	
1196.21	S X	$2s^2\,2p^3\ ^4S_{3/2} - 2s^2\,2p^3\ ^2D_{5/2}$	4.2	0.26	2.2		
1200.67			0.056				
1201.23					1.8	x	
1205.73	Cr XX	$2s^2\,2p\ ^2P_{1/2} - 2s^2\,2p\ ^2P_{3/2}$				118	
1212.97	S X	$2s^2\,2p^3\ ^4S_{3/2} - 2s^2\,2p^3\ ^2D_{3/2}$	9.6	0.38	15.5	⋆	
1224.97	Ni XII ?		0.28		0.11	⋆	
[1227.46							1^{st} or 2^{nd}?
[1227.65	(e)		0.032				1^{st} or 2^{nd}?
1230.31			0.039				1^{st} or 2^{nd}?
1231.46	Si VIII		0.57		0.69		F in CH
1232.09	(d)		0.11		0.51		1^{st} or 2^{nd}?
1232.65	Si VIII	$2p^2\,3s\ ^4P_{5/2} - 2p^2\,3p\ ^4D_{5/2}$	0.36		0.73		1^{st} or 2^{nd}?
1232.98	(e)		0.13				
1233.30					1.8		
1233.65					0.27		1^{st} or 2^{nd}?
1233.94					1.9		1^{st} or 2^{nd}?
1234.11			0.064				1^{st} or 2^{nd}?
1234.60	Si IX	$2s^2\,2p3s\ ^3P_1 - 2s^2\,2p3p\ ^3D_2$	0.15		0.47		1^{st} or 2^{nd}?
1236.00	Si VII	$2p^3\,3s\ ^1D_2 - 2p^3\,3p\ ^1F_3$	0.061	0.11			
1236.15					0.11		1^{st} or 2^{nd}?
1236.38			0.010				
1237.05			0.050				1^{st} or 2^{nd}?
1237.99			0.042		0.73		
1238.82	N V	$2s\ ^2S_{1/2} - 2p\ ^2P_{3/2}$	7.6	3.5			
1242.00	Fe XII	$3s^2\,3p^3\ ^4S_{3/2} - 3s^2\,3p^3\ ^2P_{3/2}$	30.9	0.81	47.8		
1242.81	N V	$2s\ ^2S_{1/2} - 2p\ ^2P_{1/2}$	3.9	1.9			
[1244.94	K XIII /2				0.080		cf., 622.47 Å
[1245.18	(s)						
1248.08	Ne IX	$1s2s\ ^3S_1 - 1s2p\ ^3P_2$			2.7	141	F in CH, QS

Table 3—Continued

λ_{obs} Å	Line	Transition	QS	CH	AR	flare	Notes
			line radiance L/ phot cm^{-2} s^{-1} arcsec^{-2}				
1253.39	(e)		0.37				I in AR
1256.49	K XII	$2s^2\,2p^4\ ^3P_2 - 2s^2\,2p^4\ ^1D_2$	0.38		1.4	19.6	
1258.06	Co XIII	$3s^2\,3p^3\ ^4S_{3/2} - 3s^2\,3p^3\ ^2P_{1/2}$			0.16		1^{st} or 2^{nd}?
1271.61	(f)		0.19		0.79		F in CH
1277.22	Ni XIII	$3s^2\,3p^4\ ^3P_1 - 3s^2\,3p^4\ ^1S_0$	0.47		1.7	133	F in CH
[1277.79	Ne IX	$1s2s\ ^3S_1 - 1s2p\ ^3P_0$			5.4	25.6	
[1277.84	Si X /2						cf., 638.92 Å
1291.61	Ca XIV	$2s^2\,2p^3\ ^2D_{3/2} - 2s^2\,2p^3\ ^2P_{3/2}$			1.6	69.9	
1307.52	P IX	$2s^2\,2p^3\ ^4S_{3/2} - 2s^2\,2p^3\ ^2D_{5/2}$	0.026				F in AR
1311.91					0.015		1^{st} or 2^{nd}?
1317.62	P IX	$2s^2\,2p^3\ ^4S_{3/2} - 2s^2\,2p^3\ ^2D_{3/2}$	0.17				F in AR
1320.79					0.077		1^{st} or 2^{nd}?
1322.20	Mn XII	$3s^2\,3p^2\ ^3P_1 - 3s^2\,3p^2\ ^1S_0$	0.22		0.24		
1322.58			0.16				1^{st} or 2^{nd}?
1328.79	Fe XIX	$2s^2\,2p^4\ ^3P_2 - 2s^2\,2p^4\ ^3P_0$				7.7	
1330.53	Ar XIII	$2s^2\,2p^2\ ^3P_1 - 2s^2\,2p^2\ ^1D_2$			0.97	43.8	
1331.50	(f)		0.28		0.46		
1349.37	Fe XII	$3s^2\,3p^3\ ^4S_{3/2} - 3s^2\,3p^3\ ^2P_{1/2}$	18.1	0.41	28.5		
1354.06	Fe XXI	$2s^2\,2p^2\ ^3P_0 - 2s^2\,2p^2\ ^3P_1$				14100	
1354.89	Mn XVIII	$2s^2\,2p^4\ ^3P_2 - 2s^2\,2p^4\ ^3P_1$			0.57	24.0	
1368.80	Co XII	$3s^2\,3p^4\ ^3P_1 - 3s^2\,3p^4\ ^1S_0$	0.25				
1370.51	Ni XII ?		0.11				
1375.95	Ca XV	$2s^2\,2p^2\ ^3P_2 - 2s^2\,2p^2\ ^1D_2$	0.12		2.9	183	
1392.10	Ar XI	$2s^2\,2p^4\ ^3P_2 - 2s^2\,2p^4\ ^1D_2$	0.53		1.8	223	
1408.65	(f)		0.41		0.65		
1409.44	(e)		1.0		1.6		
1410.60	Cr XVI	$2s^2\,2p^5\ ^2P_{3/2} - 2s^2\,2p^5\ ^2P_{1/2}$			2.1	29.0	1^{st} or 2^{nd}?
1411.12			2.1		3.9		
1428.75	(f)		4.5	0.48	6.1		
1432.23	Ca XIV	$2s^2\,2p^3\ ^2D_{5/2} - 2s^2\,2p^3\ ^2P_{3/2}$				27.6	
1439.99	Cr XI	$3s^2\,3p^2\ ^3P_1 - 3s^2\,3p^2\ ^1S_0$	0.18		0.28		
1440.51	Si VIII	$2s^2\,2p^3\ ^4S_{3/2} - 2s^2\,2p^3\ ^2D_{5/2}$	0.91	1.5	1.1		
1445.76	Si VIII	$2s^2\,2p^3\ ^4S_{3/2} - 2s^2\,2p^3\ ^2D_{3/2}$	11.1	15.6	13.1		
1452.66					0.77	x	1^{st} or 2^{nd}?
1453.36	(c)				11.0		1^{st} or 2^{nd}?
1463.50	Fe X	$3p^4\,3d\ ^4F_{9/2} - 3p^4\,3d\ ^2F_{7/2}$	3.1	1.4	4.9		
1464.44	Cl XII	$2s^2\,2p^2\ ^3P_1 - 2s^2\,2p^2\ ^1D_2$			0.21		
1467.07	Fe XI	$3s^2\,3p^4\ ^3P_1 - 3s^2\,3p^4\ ^1S_0$	12.5	1.5	15.5		
1477.16	K XIV	$2s^2\,2p^2\ ^3P_1 - 2s^2\,2p^2\ ^1D_2$			0.47		1^{st} or 2^{nd}?
1489.02	Cr X	$3s^2\,3p^3\ ^4S_{3/2} - 3s^2\,3p^3\ ^2P_{3/2}$	0.23				
[1504.27	Ca XIV	$2s^2\,2p^3\ ^4S_{3/2} - 2s^2\,2p^3\ ^2P_{1/2}$			1.4	23.0	F in QS
1515.19						x	
1544.18				1.1			1^{st} or 2^{nd}?
1586.36	Fe XX	$2s^2\,2p^3\ ^2P_{1/2} - 2s^2\,2p^3\ ^2P_{3/2}$				6.2	

Fig. 3. The SUMER spectral atlas of solar coronal features includes profiles of the quiescent corona (black), the corona above a coronal hole (blue), the corona above an active region (red) and during a flare (green). For comparison we also present the average on-disk spectrum of the quiet Sun. Resolved emission lines are indicated by a mark, the measured wavelength in angstrøm (Å), and the identification, if available. Marks and colours are coded and give a rough temperature estimate. Circles (○) indicate chromospheric emission seen as scattered light from the disk, blue squares (□) indicate transition region lines, red triangles (△) indicate true coronal emission. Green diamonds (◇) denote flare lines which are normally not observed in the solar atmosphere. Filled symbols denote lines observed in first order of diffraction, open symbols are second-order or third-order lines. Only the three least-significant digits of the wavelength values are given. If available, unidentified lines are characterized by the temperature classification of Feldman *et al.* (1997) (a: $T_e < 3\ 10^5$; b: $T_e \approx 3\ 10^5$; c: $T_e \approx 4\ 10^5$; d: $6\ 10^5 < T_e < 9\ 10^5$; e: $T_e \approx 1.4\ 10^6$; f: $T_e \approx 1.8\ 10^6$. The profiles have been radiometrically calibrated assuming first order of diffraction and the radiance axis is scaled to mW sr^{-1} m^{-2} $Å^{-1}$. We have taken care of the type of photocathode (bare or KBr) when applying the radiometric calibration to different sections of the spectrum. For lines observed in second order, the right vertical axis is applicable. Note, that the sensitivity ratio between both orders, which is wavelength dependent, has been chosen for (and is only correct for) the central wavelength. Also note, that second order lines are always superimposed on a first order background.

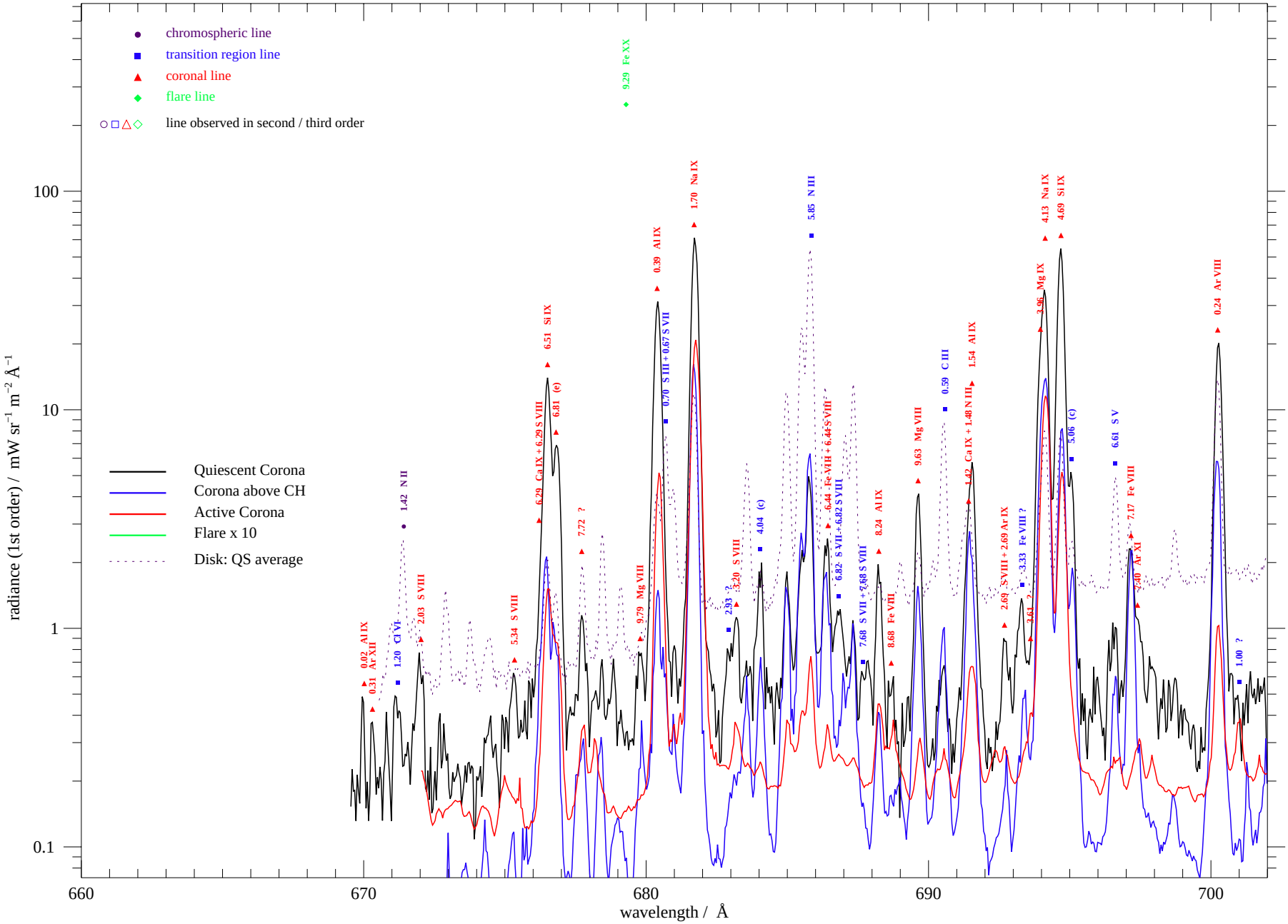
chromospheric line
transition region line
coronal line
flare line
line observed in second / third order
Quiescent Corona
Corona above CH
Active Corona
Flare x 10
Disk: QS average
radiance (1st order) / mW sr^{-1} m^{-2} Å^{-1}
wavelength / Å
100
10
1
0.1
660
670
680
690
700
0.02 Al IX
Ar XII
0.31
1.20 Cl VI
1.42 N II
2.03 S VIII
5.34 S VIII
6.29 Ca IX + 6.29 S VIII
6.51 Si IX
6.81 (e)
7.72 ?
9.29 Fe XX
9.79 Mg VIII
0.39 Al IX
0.70 S III + 0.67 S VII
1.70 Na IX
2.93 ?
3.20 S VIII
4.04 (e)
5.85 N III
6.44 Fe VIII + 6.44 S VIII
6.82 S VII + 6.82 S VIII
7.68 S VII + 7.68 S VIII
8.24 Al IX
8.68 Fe VIII
9.63 Mg VIII
0.59 C III
1.42 Ca IX + 1.40 N III
1.54 Al IX
2.69 S VIII + 2.69 Ar IX
3.33 Fe VIII ?
3.61 ?
3.96 Mg IX
4.13 Na IX
4.69 Si IX
5.06 (e)
6.61 S V
7.17 Fe VIII
7.40 Ar XI
0.24 Ar VIII
1.00 ?

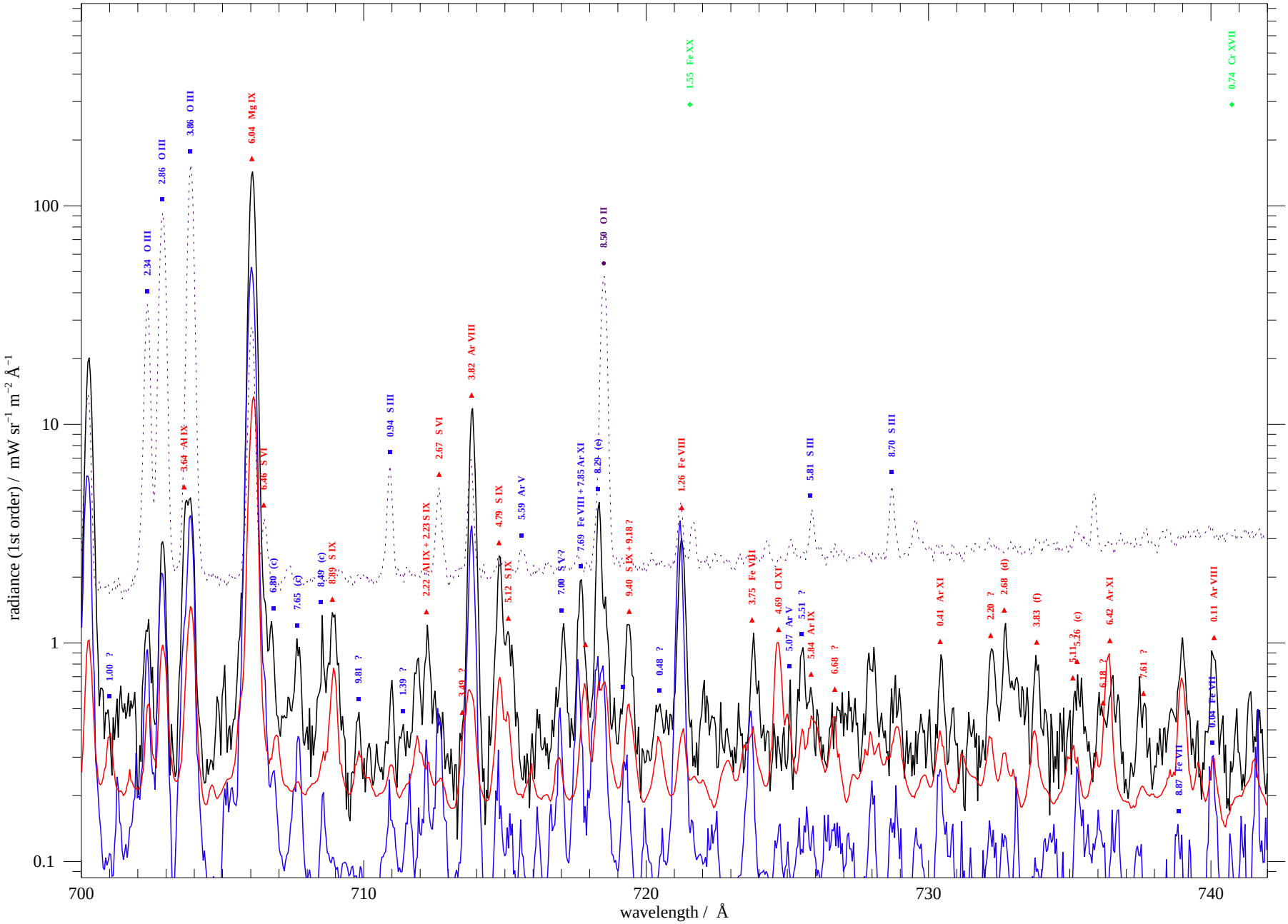
radiance (1st order) / mW sr^{-1} m^{-2} Å^{-1}
wavelength / Å
100
10
1
0.1
700
710
720
730
740
1.00 ?
2.34 O III
2.86 O III
3.64 Al IX
3.86 O III
6.04 Mg IX
6.46 S VI
6.80 (c)
7.65 (c)
8.49 (c)
8.89 S IX
0.94 S III
1.39 ?
2.22 Al IX + 2.23 S IX
2.67 S VI
3.49 ?
3.82 Ar VIII
4.79 S IX
5.12 S IX
5.59 Ar V
7.00 S V ?
7.69 Fe VIII + 7.85 Ar XI
8.29 (e)
8.50 O II
9.40 S IX + 9.18 ?
0.48 ?
1.26 Fe VIII
3.75 Fe VIII
4.69 Cl XI
5.07 Ar V
5.51 ?
5.81 S III
5.84 Ar IX
6.68 ?
8.70 S III
0.41 Ar XI
2.20 ?
2.68 (d)
3.83 (f)
5.11, 5.26 (c)
6.18 ?
6.42 Ar XI
7.61 ?
8.87 Fe VII
0.04 Fe VII
0.11 Ar VIII
1.55 Fe XX
0.74 Cr XVII

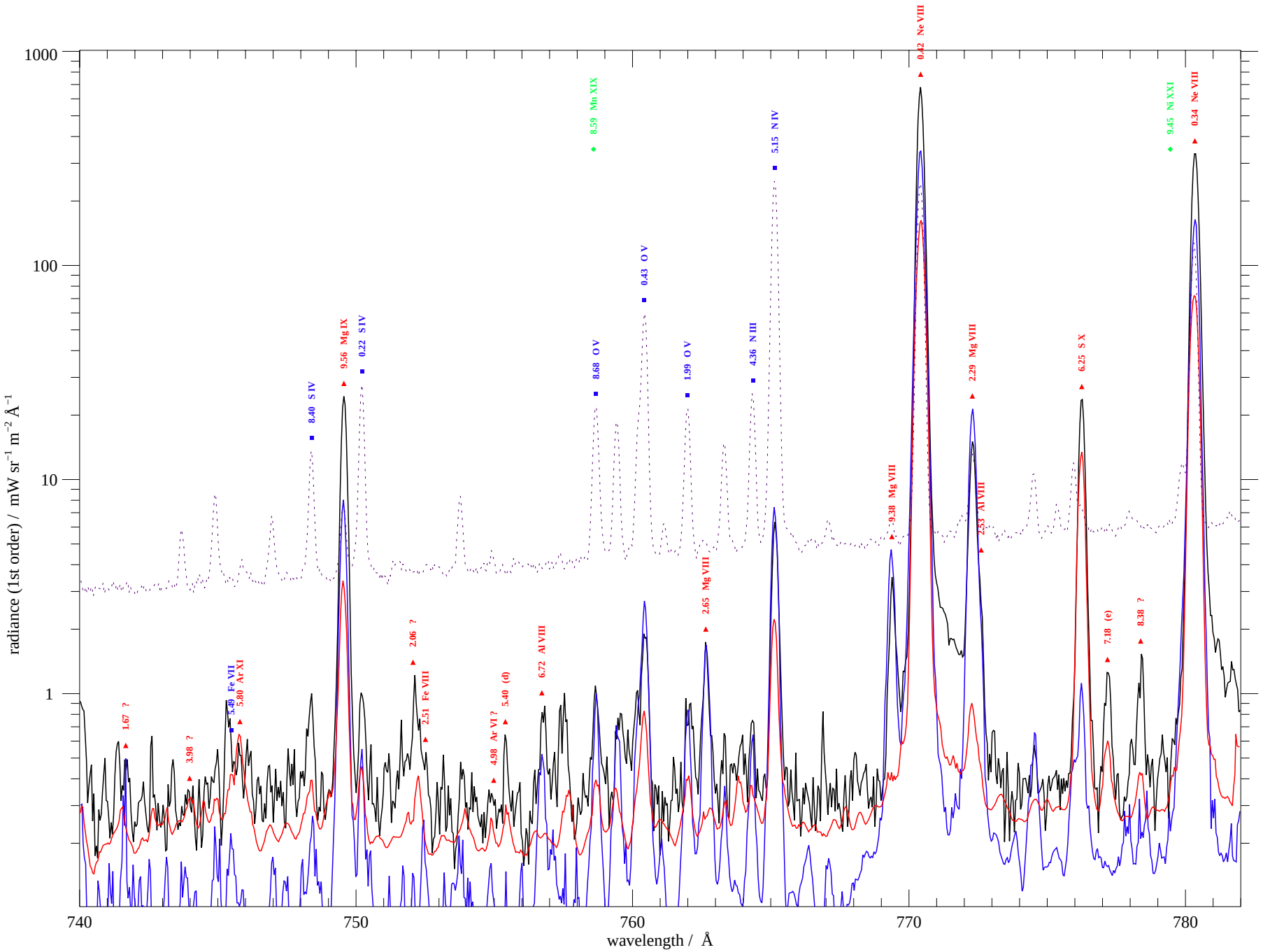
1000
100
10
1
radiance (1st order) / mW sr^{-1} m^{-2} Å^{-1}
740
750
760
770
780
wavelength / Å
1.67 ?
3.98 ?
5.49 Fe VII
5.80 Ar XI
8.40 S IV
9.56 Mg IX
0.22 S IV
2.06 ?
2.51 Fe VIII
4.98 Ar VI ?
5.40 (d)
6.72 Al VIII
8.59 Mn XIX
8.68 O V
0.43 O V
1.99 O V
2.65 Mg VIII
4.36 N III
5.15 N IV
9.38 Mg VIII
0.42 Ne VIII
2.53 Al VIII
2.29 Mg VIII
6.25 S X
7.18 (e)
8.38 ?
9.45 Ni XXI
0.34 Ne VIII

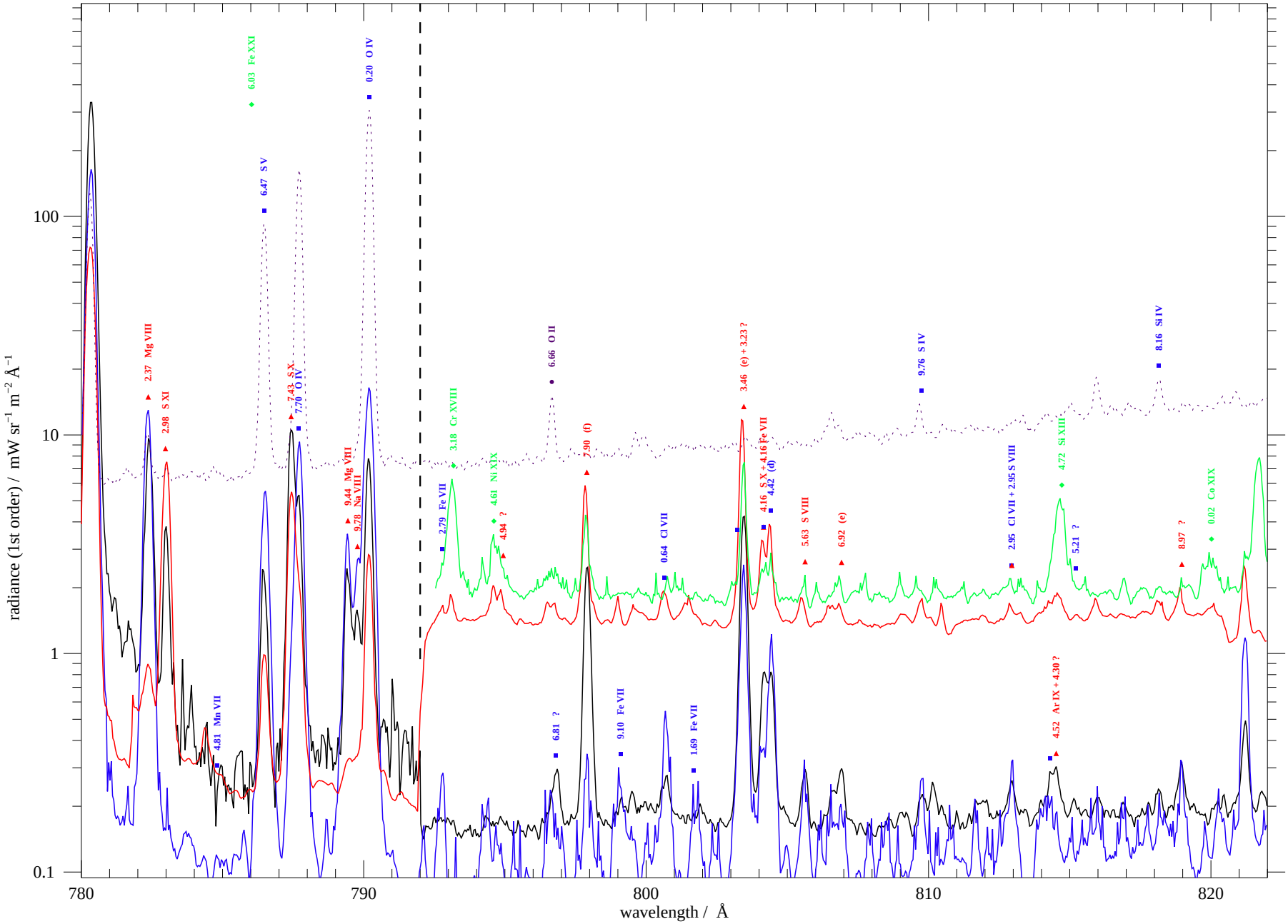
radiance (1st order) / mW sr^{-1} m^{-2} Å^{-1}
wavelength / Å
100
10
1
0.1
780
790
800
810
820
6.03 Fe XXI
6.47 S V
0.20 O IV
2.37 Mg VIII
2.98 S XI
7.43 S X
7.70 O IV
9.44 Mg VIII
9.78 Na VIII
4.81 Mn VII
3.18 Cr XVIII
2.79 Fe VII
4.61 Ni XIX
4.94 ?
6.66 O II
7.90 (f)
0.64 Cl VII
6.81 ?
9.10 Fe VII
1.69 Fe VII
3.46 (e) + 3.23 ?
4.16 S X + 4.16 Fe VII
4.42 (d)
5.63 S VIII
6.92 (e)
9.76 S IV
2.95 Cl VII + 2.95 S VIII
4.72 Si XIII
5.21 ?
4.52 Ar IX + 4.30 ?
8.16 Si IV
8.97 ?
0.02 Co XIX

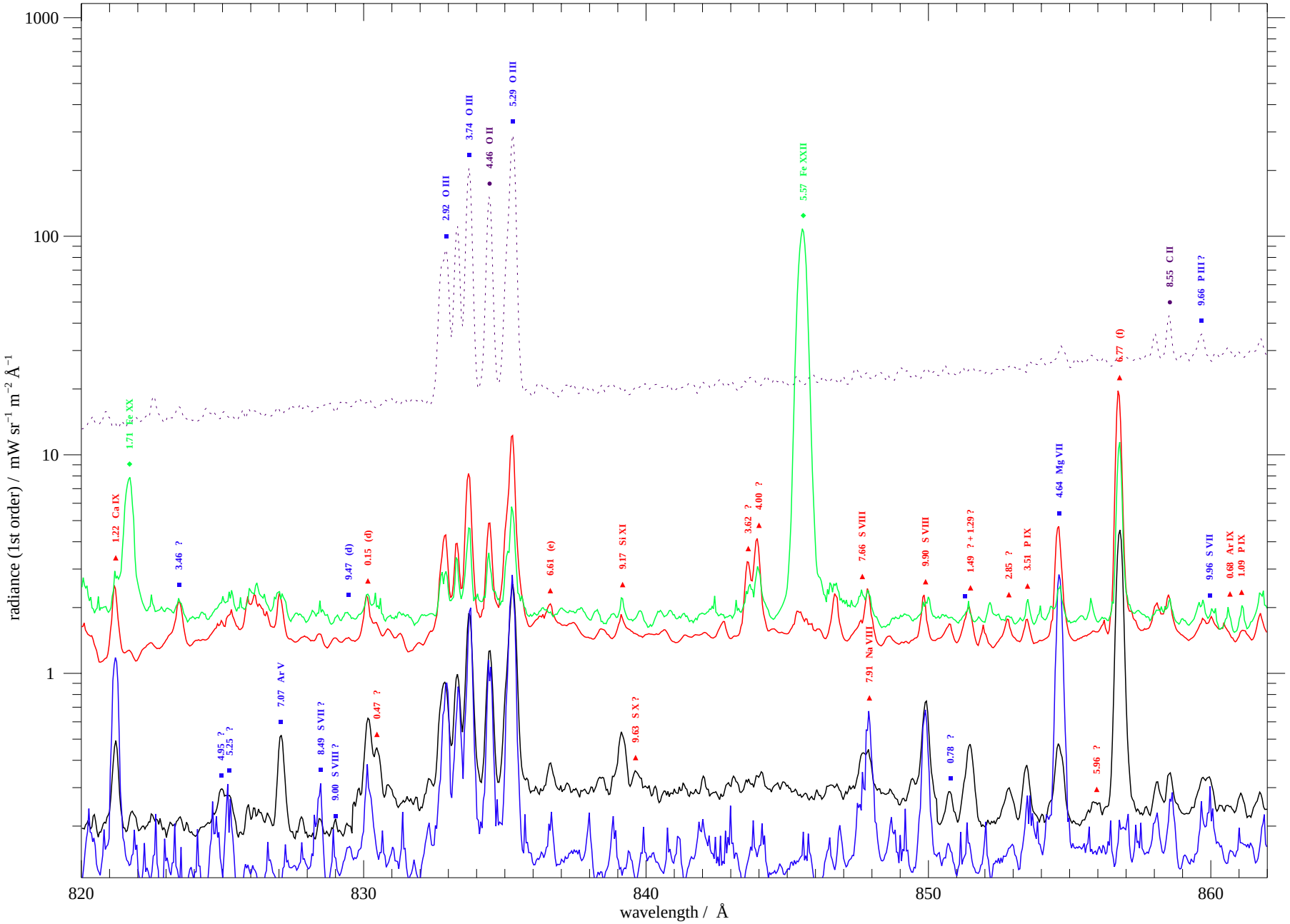
1000
100
10
1
radiance (1st order) / mW sr^{-1} m^{-2} Å^{-1}
820
830
840
850
860
wavelength / Å
1.71 Fe XX
1.22 Ca IX
3.46 ?
9.47 (d)
0.15 (d)
6.61 (e)
9.17 Si XI
3.62 ?
4.00 ?
2.92 O III
3.74 O III
4.46 O II
5.29 O III
5.57 Fe XXII
7.66 S VIII
9.90 S VIII
1.49 ? + 1.29 ?
2.85 ?
3.51 P IX
4.64 Mg VII
6.77 (f)
8.55 C II
9.66 P III ?
9.96 S VII
0.68 Ar IX
1.09 P IX
7.91 Na VIII
4.95 ?
5.25 ?
7.07 Ar V
8.49 S VII ?
9.00 S VIII ?
0.47 ?
9.63 S X ?
0.78 ?
5.96 ?

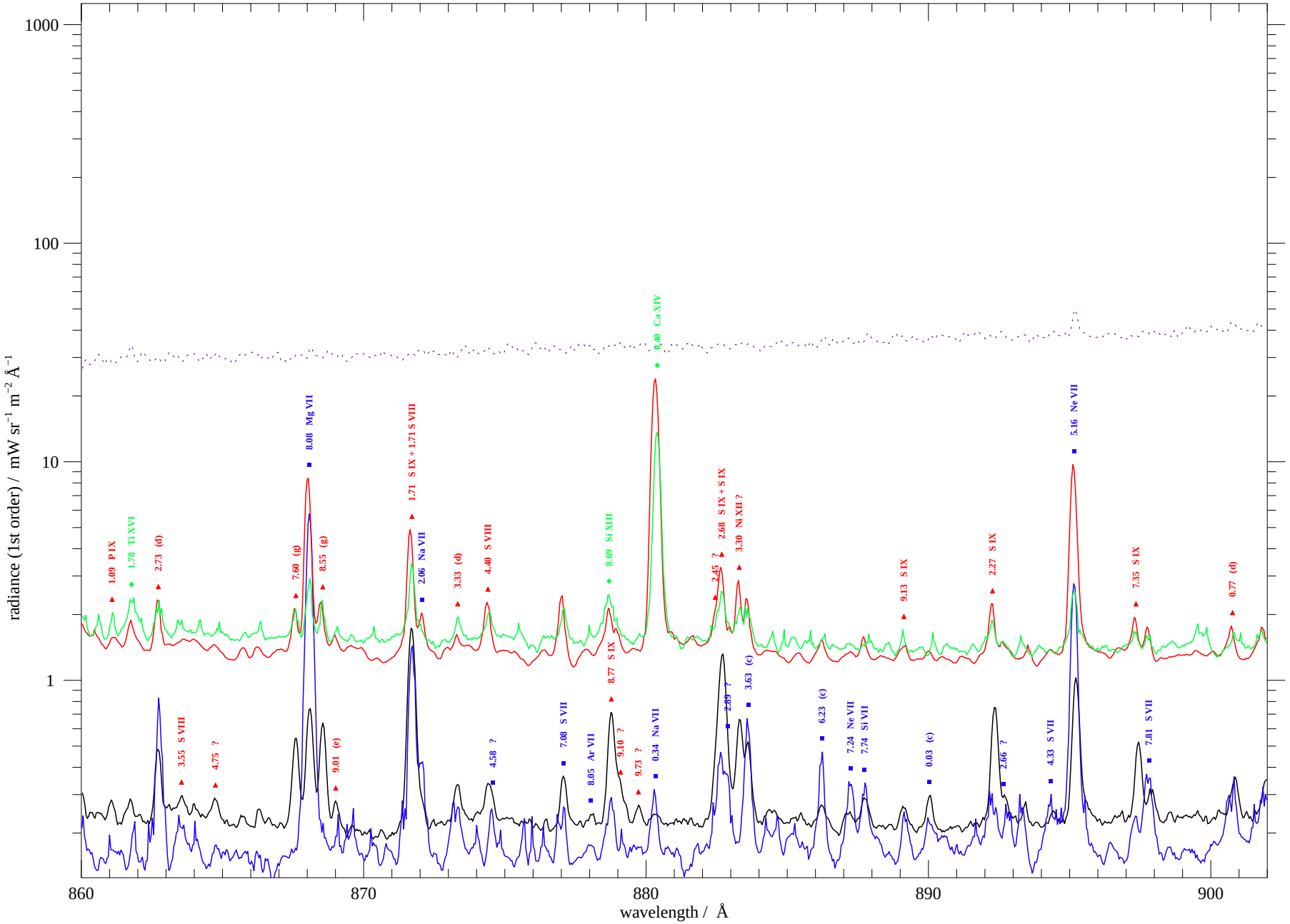
1000
100
10
1
radiance (1st order) / mW sr^{-1} m^{-2} Å^{-1}
860
870
880
890
900
wavelength / Å
1.09 P IX
1.78 Ti XVI
2.73 (d)
7.60 (g)
8.08 Mg VII
8.55 (g)
1.71 S IX + 1.71 S VIII
2.06 Na VII
3.33 (d)
4.40 S VIII
8.69 Si XIII
0.40 Ca XIV
2.45 ?
2.68 S IX + S IX
3.30 Ni XII ?
9.13 S IX
2.27 S IX
5.16 Ne VII
7.35 S IX
0.77 (d)
3.55 S VIII
4.75 ?
9.01 (e)
4.58 ?
7.08 S VII
8.05 Ar VII
8.77 S IX
9.10 ?
9.73 ?
0.34 Na VII
2.89 ?
3.63 (e)
6.23 (e)
7.24 Ne VII
7.74 Si VII
0.03 (e)
2.66 ?
4.33 S VII
7.81 S VII

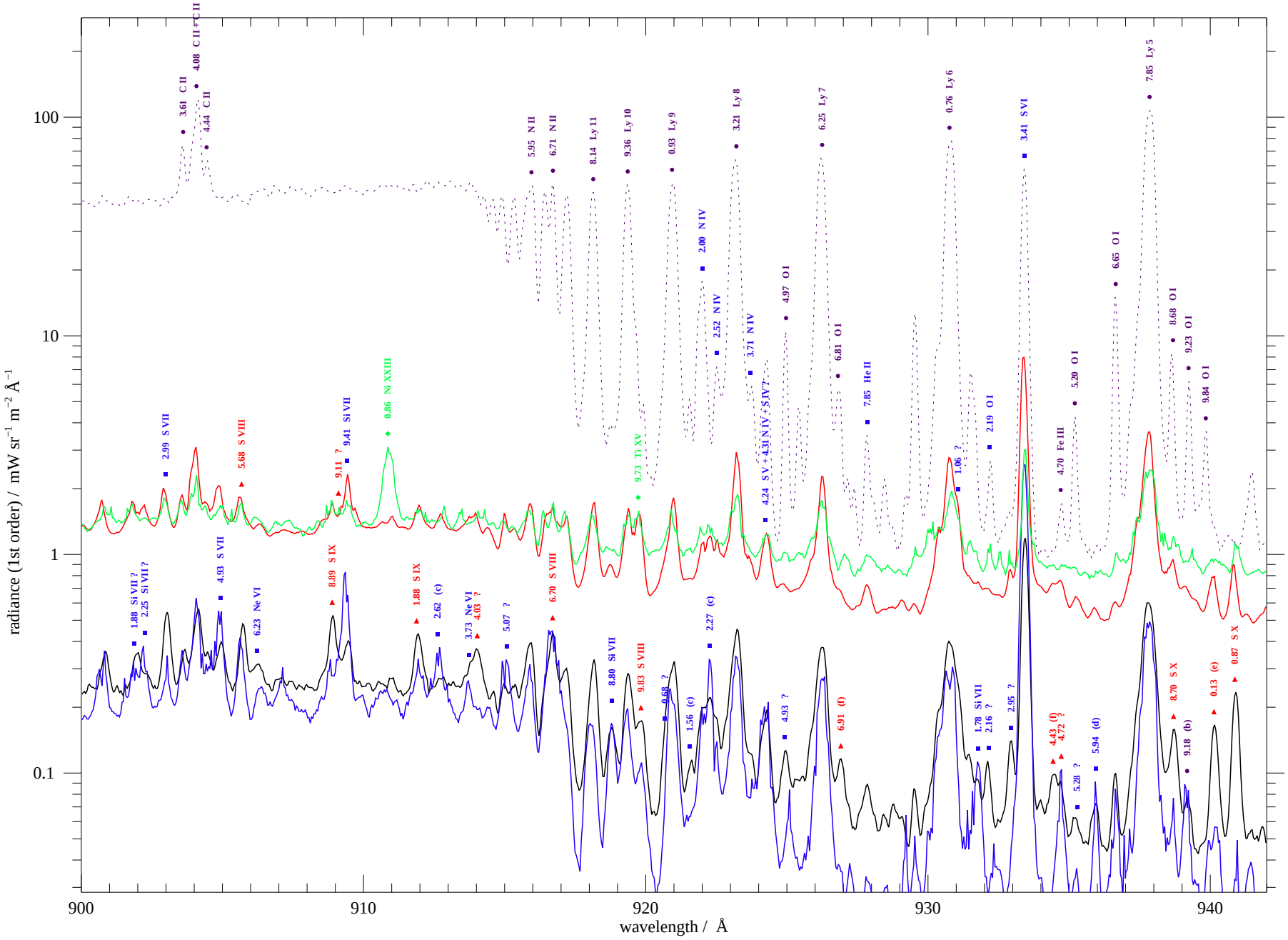
radiance (1st order) / mW sr^{-1} m^{-2} Å^{-1}
wavelength / Å
100
10
1
0.1
900
910
920
930
940
3.61 C II
4.08 C II + C II
4.44 C II
5.95 N II
6.71 N II
8.14 Ly 11
9.36 Ly 10
0.93 Ly 9
2.00 N IV
2.52 N IV
3.21 Ly 8
3.71 N IV
4.24 S V + 4.31 N IV + S IV ?
4.97 O I
6.25 Ly 7
6.81 O I
7.85 He II
0.76 Ly 6
1.06 ?
2.19 O I
3.41 S VI
4.70 Fe III
5.20 O I
6.65 O I
7.85 Ly 5
8.68 O I
9.23 O I
9.84 O I
2.99 S VII
5.68 S VIII
9.11 ?
9.41 Si VII
0.86 Ni XXIII
9.73 Ti XV
1.88 Si VII ?
2.25 Si VII ?
4.93 S VII
6.23 Ne VI
8.89 S IX
1.88 S IX
2.62 (c)
3.73 Ne VI
4.03 ?
5.07 ?
6.70 S VIII
8.80 Si VII
9.83 S VIII
0.68 ?
1.56 (c)
2.27 (c)
4.93 ?
6.91 (f)
1.78 Si VII ?
2.16 ?
2.95 ?
4.43 (f)
4.72 ?
5.28 ?
5.94 (d)
8.70 S X
9.18 (b)
0.13 (e)
0.87 S X

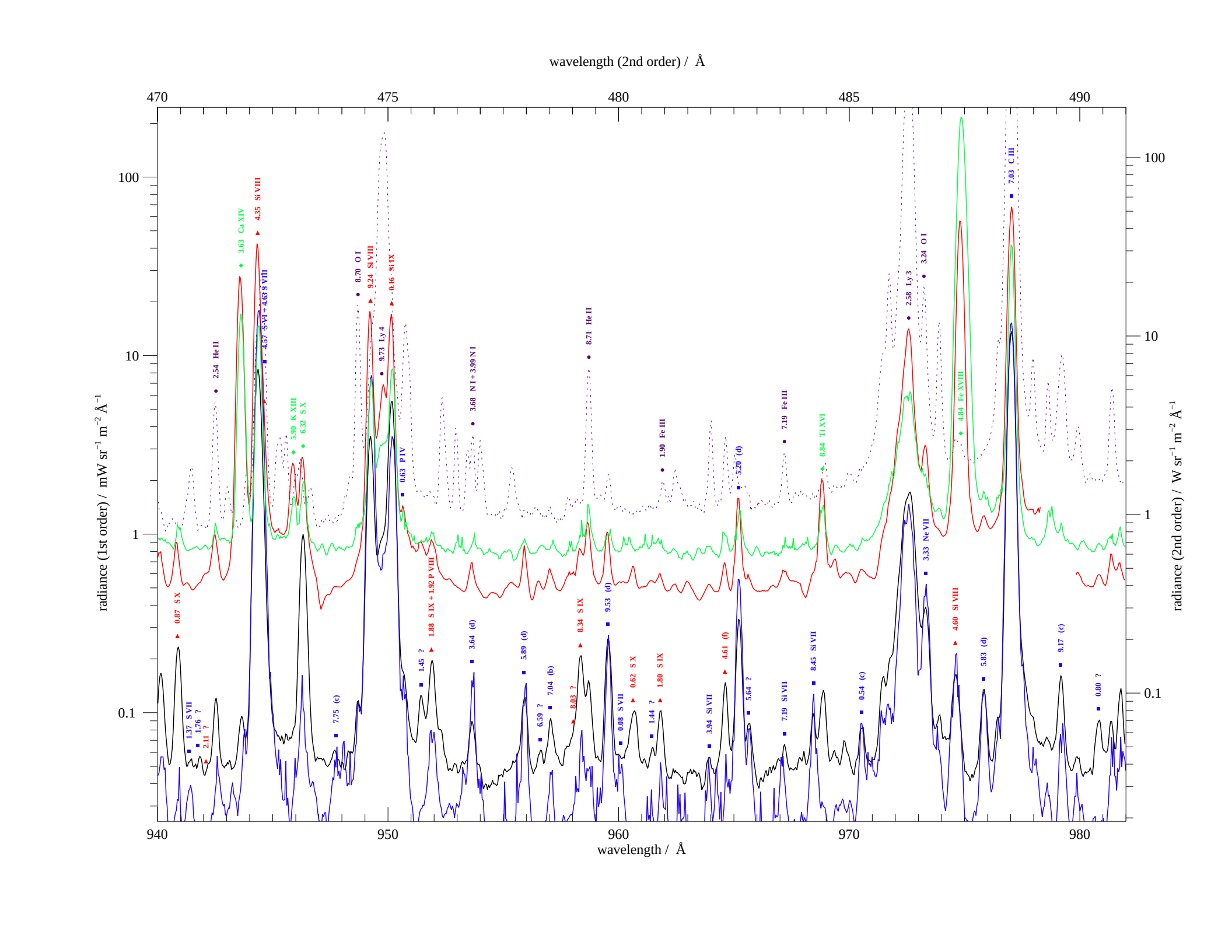
wavelength (2nd order) / Å
470
475
480
485
490
940
950
960
970
980
wavelength / Å
radiance (1st order) / mW sr^{-1} m^{-2} Å^{-1}
radiance (2nd order) / W sr^{-1} m^{-2} Å^{-1}
100
10
1
0.1
2.54 He II
3.63 Ca XIV
4.35 Si VIII
4.57 S VI + 4.63 S VIII
5.90 K XIII
6.32 S X
8.70 O I
9.24 Si VIII
9.73 Ly 4
10.16 Si IX
0.63 P IV
3.68 N I + 3.99 N I
8.71 He II
1.90 Fe III
5.20 (d)
7.19 Fe III
8.84 Ti XVI
2.58 Ly 3
3.24 O I
4.84 Fe XVIII
7.03 C III
0.87 S X
1.37 S VII
1.76 ?
2.11 ?
7.75 (c)
1.45 ?
1.88 S IX + 1.92 P VIII
3.64 (d)
5.89 (d)
6.59 ?
7.04 (b)
8.03 ?
8.34 S IX
9.53 (d)
0.08 S VII
0.62 S X
1.44 ?
1.80 S IX
3.94 Si VII
4.61 (f)
5.64 ?
7.19 Si VII
8.45 Si VII
0.54 (c)
3.33 Ne VII
4.60 Si VIII
5.83 (d)
9.17 (c)
0.80 ?

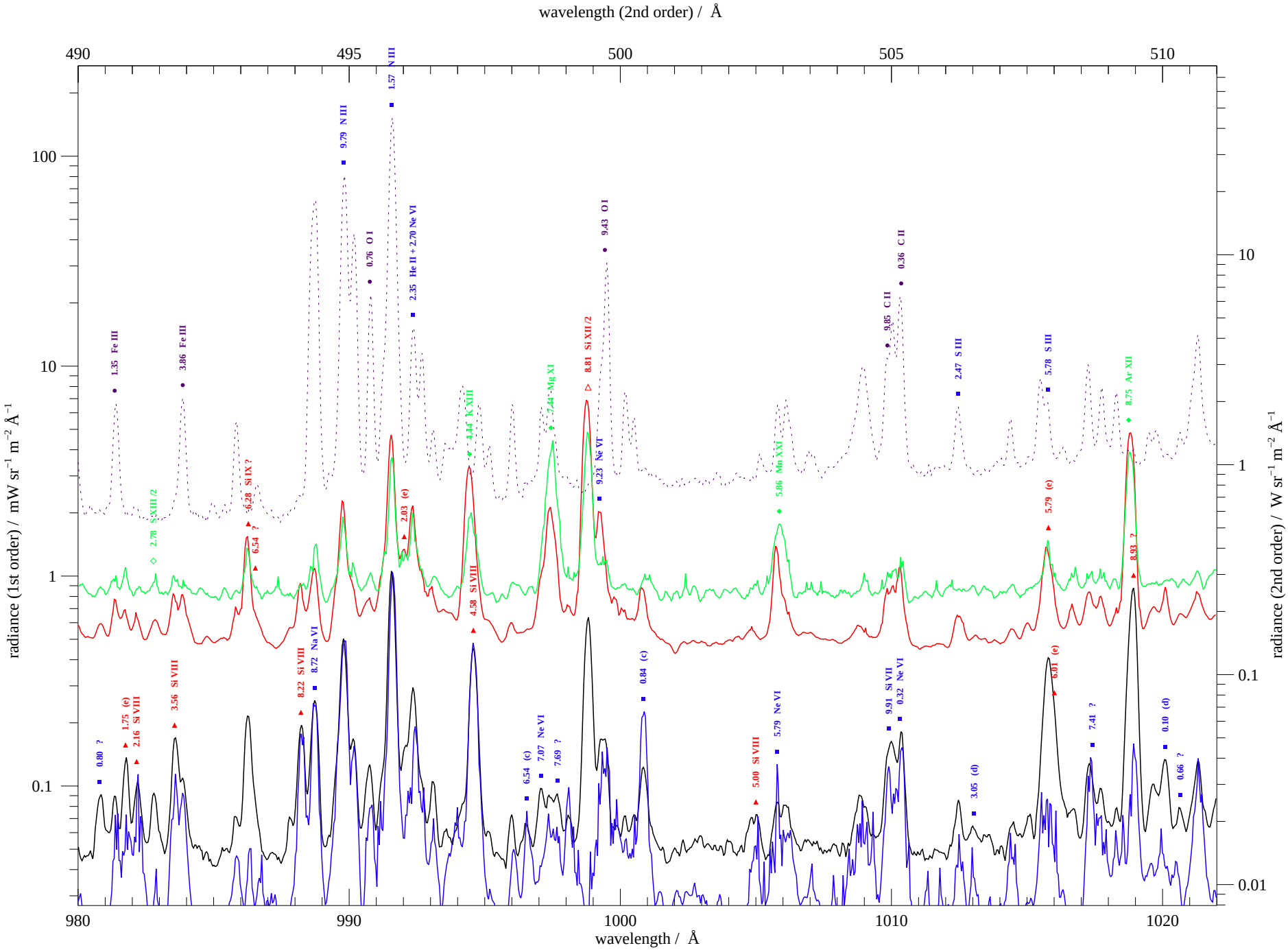
wavelength (2nd order) / Å
490
495
500
505
510
1.57 N III
9.79 N III
0.76 O I
2.35 He II + 2.70 Ne VI
9.43 O I
8.81 Si XII /2
9.23 Ne VI
0.36 C II
9.85 C II
2.47 S III
5.78 S III
8.75 Ar XII
1.35 Fe III
3.86 Fe III
2.78 S XIII /2
6.28 Si IX ?
6.54 ?
4.44 K XIII
7.44 Mg XI
5.86 Mn XXI
2.03 (e)
4.58 Si VIII
5.79 (e)
8.93 ?
radiance (1st order) / mW sr^{-1} m^{-2} Å^{-1}
radiance (2nd order) / W sr^{-1} m^{-2} Å^{-1}
100
10
1
0.1
10
1
0.1
0.01
0.80 ?
1.75 (e)
2.16 Si VIII
3.56 Si VIII
8.22 Si VIII
8.72 Na VI
6.54 (e)
7.07 Ne VI
7.69 ?
0.84 (c)
5.00 Si VIII
5.79 Ne VI
9.91 Si VII
0.32 Ne VI
3.05 (d)
6.01 (e)
7.41 ?
0.10 (d)
0.66 ?
980
990
1000
1010
1020
wavelength / Å

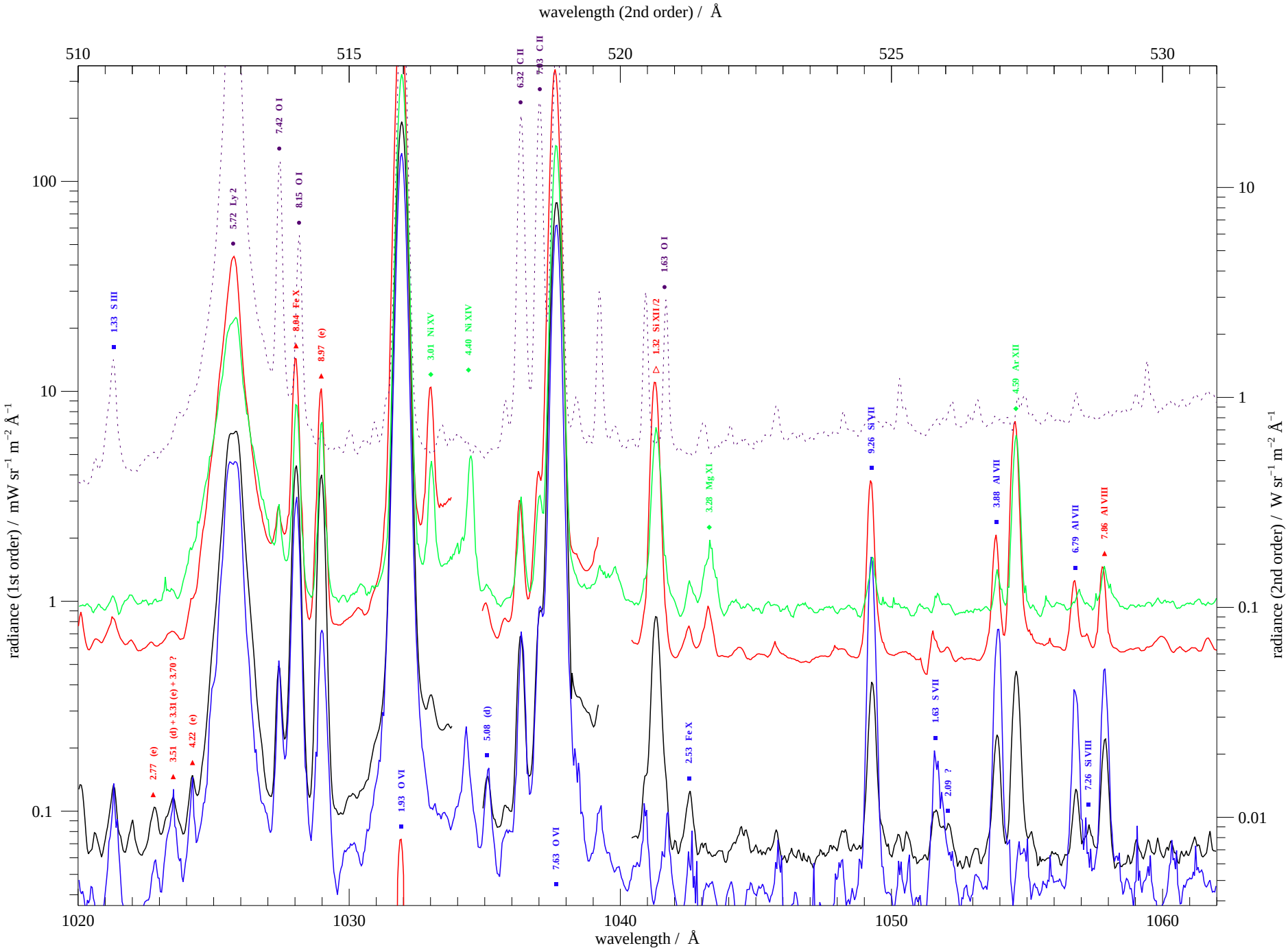
wavelength (2nd order) / Å
510
515
520
525
530
1.33 S III
5.72 Ly 2
7.42 O I
8.15 O I
8.04 Fe X
8.97 (e)
6.32 C II
7.43 C II
3.01 Ni XV
4.40 Ni XIV
1.32 Si XII / 2
1.63 O I
3.28 Mg XI
9.26 Si VII
4.59 Ar+ XII
3.88 Al VII
6.79 Al VII
7.86 Al VIII
2.77 (e)
3.51 (d) + 3.31 (e) + 3.70 ?
4.22 (e)
1.93 O VI
5.08 (d)
7.63 O VI
2.53 Fe X
1.63 S VII
2.09 ?
7.26 Si VIII
radiance (1st order) / mW sr^{-1} m^{-2} Å^{-1}
radiance (2nd order) / W sr^{-1} m^{-2} Å^{-1}
100
10
1
0.1
10
1
0.1
0.01
1020
1030
1040
1050
1060
wavelength / Å

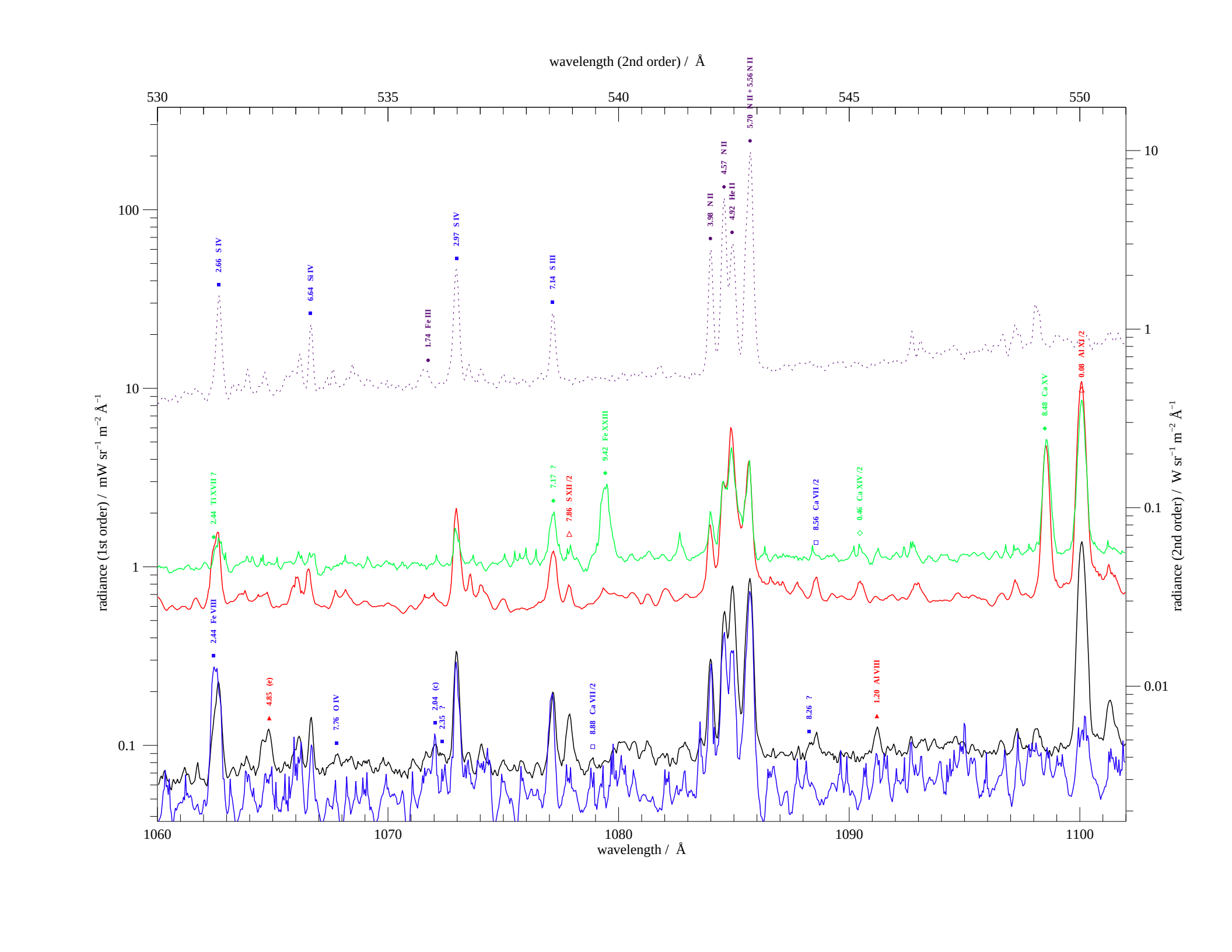
wavelength (2nd order) / Å
530
535
540
545
550
5.70 N II + 5.56 N II
4.57 N II
4.92 He II
3.98 N II
2.97 S IV
1.74 Fe III
6.64 Si IV
2.66 S IV
7.14 S III
Al XI /2
0.08
8.48 Ca XV
9.42 Fe XXIII
7.17 ?
7.86 S XII /2
2.44 Ti XVII ?
8.56 Ca VII /2
0.46 Ca XIV /2
2.44 Fe VIII
4.85 (e)
7.76 O IV
2.04 (e)
2.35 ?
8.88 Ca VII /2
8.26 ?
1.20 Al VIII
radiance (1st order) / mW sr^{-1} m^{-2} Å^{-1}
radiance (2nd order) / W sr^{-1} m^{-2} Å^{-1}
100
10
1
0.1
10
1
0.1
0.01
1060
1070
1080
1090
1100
wavelength / Å

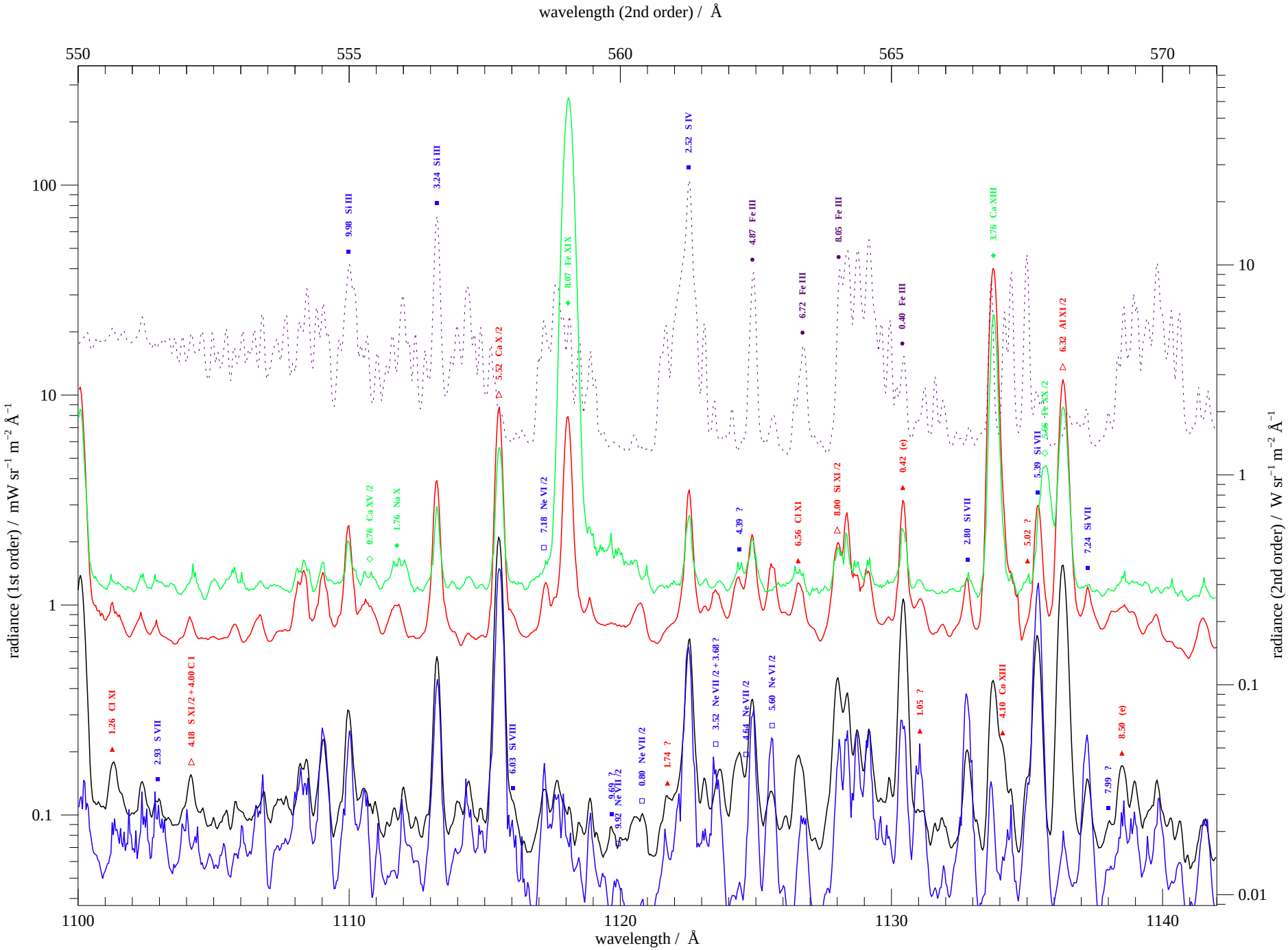
wavelength (2nd order) / Å
550
555
560
565
570
radiance (1st order) / mW sr^{-1} m^{-2} Å^{-1}
radiance (2nd order) / W sr^{-1} m^{-2} Å^{-1}
100
10
1
0.1
10
1
0.1
0.01
9.98 Si III
3.24 Si III
2.52 S IV
5.52 Ca X /2
8.07 Fe XIX
4.87 Fe III
6.72 Fe III
8.05 Fe III
0.40 Fe III
3.76 Ca XIII
6.32 Al XI /2
0.76 Ca XV /2
1.76 Na X
7.18 Ne VI /2
4.39 ?
6.56 Cl XI
8.00 Si XI /2
0.42 (e)
2.80 Si VII
5.02 ?
5.39 Si VII
7.24 Si VII
1.26 Cl XI
2.93 S VII
4.18 S XI /2 + 4.00 C I
6.03 Si VIII
9.69 ?
9.92 Ne VII /2
0.80 Ne VII /2
1.74 ?
3.52 Ne VII /2 + 3.68 ?
4.64 Ne VII /2
5.60 Ne VI /2
1.05 ?
4.10 Co XIII
7.99 ?
8.50 (e)
1100
1110
1120
1130
1140
wavelength / Å

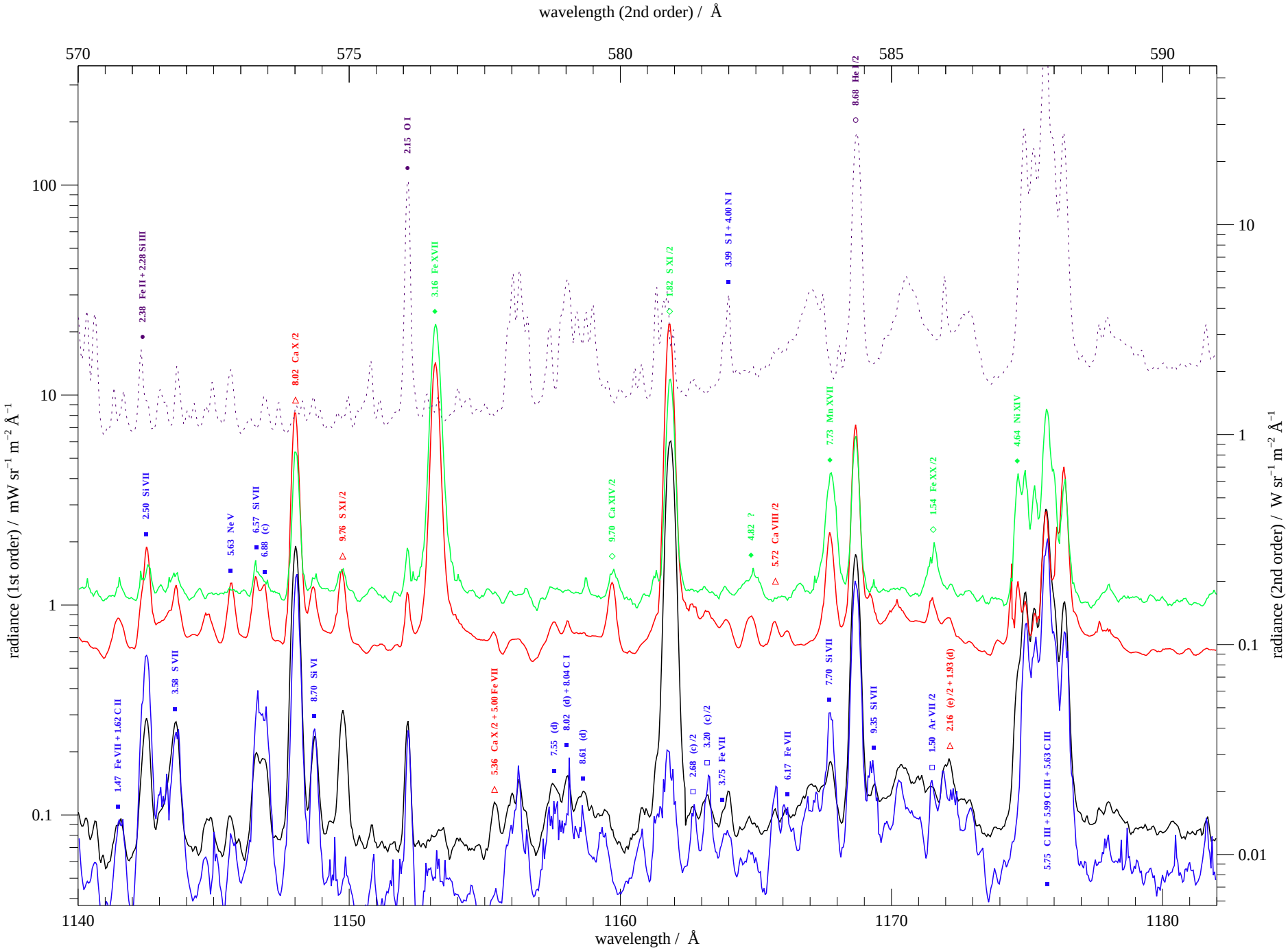
wavelength (2nd order) / Å
570
575
580
585
590
radiance (1st order) / mW sr^{-1} m^{-2} Å^{-1}
radiance (2nd order) / W sr^{-1} m^{-2} Å^{-1}
100
10
1
0.1
10
1
0.1
0.01
2.38 Fe II + 2.28 Si III
2.15 O I
3.16 Fe XVII
8.02 Ca X /2
1.82 S XI /2
3.99 S I + 4.00 N I
8.68 He I /2
2.50 Si VII
5.63 Ne V
6.57 Si VII
6.88 (c)
9.76 S XI /2
9.70 Ca XIV /2
4.82 ?
5.72 Ca VIII /2
7.73 Mn XVII
1.54 Fe XX /2
4.64 Ni XIV
1.47 Fe VII + 1.62 C II
3.58 S VII
8.70 Si VI
5.36 Ca X /2 + 5.00 Fe VII
7.55 (d)
8.02 (d) + 8.04 C I
8.61 (d)
2.68 (c) /2
3.20 (c) /2
3.75 Fe VII
6.17 Fe VII
7.70 Si VII
9.35 Si VII
1.50 Ar VII /2
2.16 (e) /2 + 1.93 (d)
5.75 C III + 5.99 C III + 5.63 C III
1140
1150
1160
1170
1180
wavelength / Å

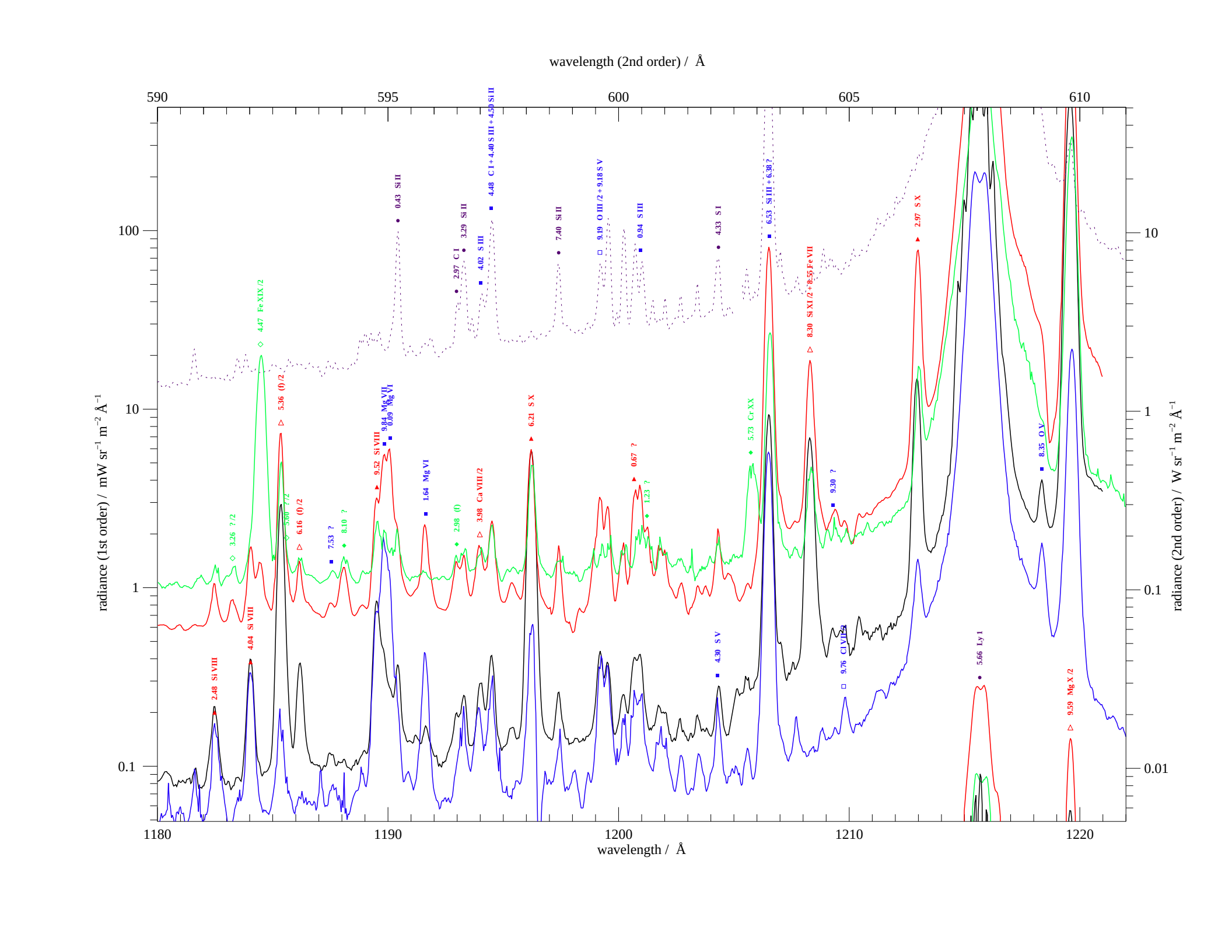
wavelength (2nd order) / Å
590
595
600
605
610
radiance (1st order) / mW sr^{-1} m^{-2} Å^{-1}
radiance (2nd order) / W sr^{-1} m^{-2} Å^{-1}
100
10
1
0.1
10
1
0.1
0.01
1180
1190
1200
1210
1220
wavelength / Å
2.48 Si VIII
3.26 ? /2
4.04 Si VIII
4.47 Fe XIX /2
5.36 (f) /2
5.60 ? /2
6.16 (f) /2
7.53 ?
8.10 ?
9.52 Si VIII
9.84 Mg VII
10.00 Mg VI
0.43 Si II
1.64 Mg VI
2.97 C I
2.98 (f)
3.29 Si II
3.98 Ca VIII /2
4.02 S III
4.48 C I + 4.40 S III + 4.50 Si II
6.21 S X
7.40 Si II
9.19 O III /2 + 9.18 S V
0.67 ?
1.23 ?
0.94 S III
4.30 S V
4.33 S I
5.73 Cr XX
6.53 Si III + 6.50 ?
8.30 Si XI /2 + 8.55 Fe VII
9.30 ?
9.76 Cl VIII /2
2.97 S X
5.66 Ly 1
8.35 O V
9.59 Mg X /2

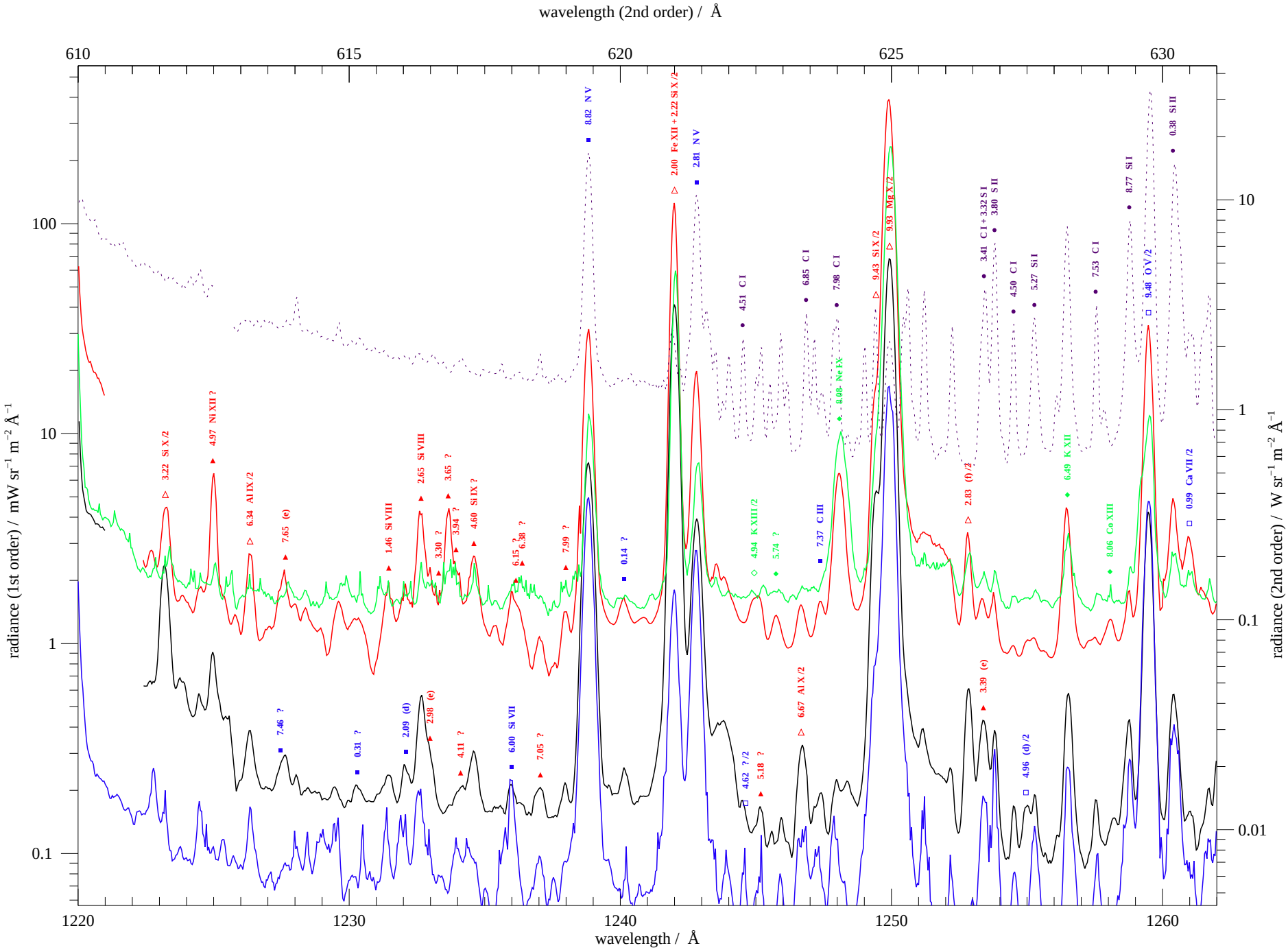
wavelength (2nd order) / Å
610
615
620
625
630
radiance (1st order) / mW sr^{-1} m^{-2} Å^{-1}
radiance (2nd order) / W sr^{-1} m^{-2} Å^{-1}
100
10
1
0.1
10
1
0.1
0.01
3.22 Si X /2
4.97 Ni XII ?
6.34 Al IX /2
7.65 (e)
1.46 Si VIII
2.65 Si VIII
3.30 ?
3.65 ?
3.94 ?
4.60 Si IX ?
6.15 ?
6.38 ?
7.99 ?
8.82 N V
0.14 ?
2.00 Fe XII + 2.22 Si X /2
2.81 N V
4.51 C I
4.94 K XIII /2
5.74 ?
6.85 C I
7.37 C III
7.98 C I
8.00 Ne IX
9.43 Si X /2
9.93 Mg X /2
2.83 (f) /2
3.41 C I + 3.32 S I
3.80 S II
4.50 C I
5.27 Si I
6.49 K XII
7.53 C I
8.06 Ca XIII
8.77 Si I
9.40 O V /2
0.38 Si II
0.99 Ca VII /2
7.46 ?
0.31 ?
2.09 (d)
2.98 (e)
4.11 ?
6.00 Si VII
7.05 ?
4.62 ? /2
5.18 ?
6.67 Al X /2
3.39 (e)
4.96 (d) /2
1220
1230
1240
1250
1260
wavelength / Å

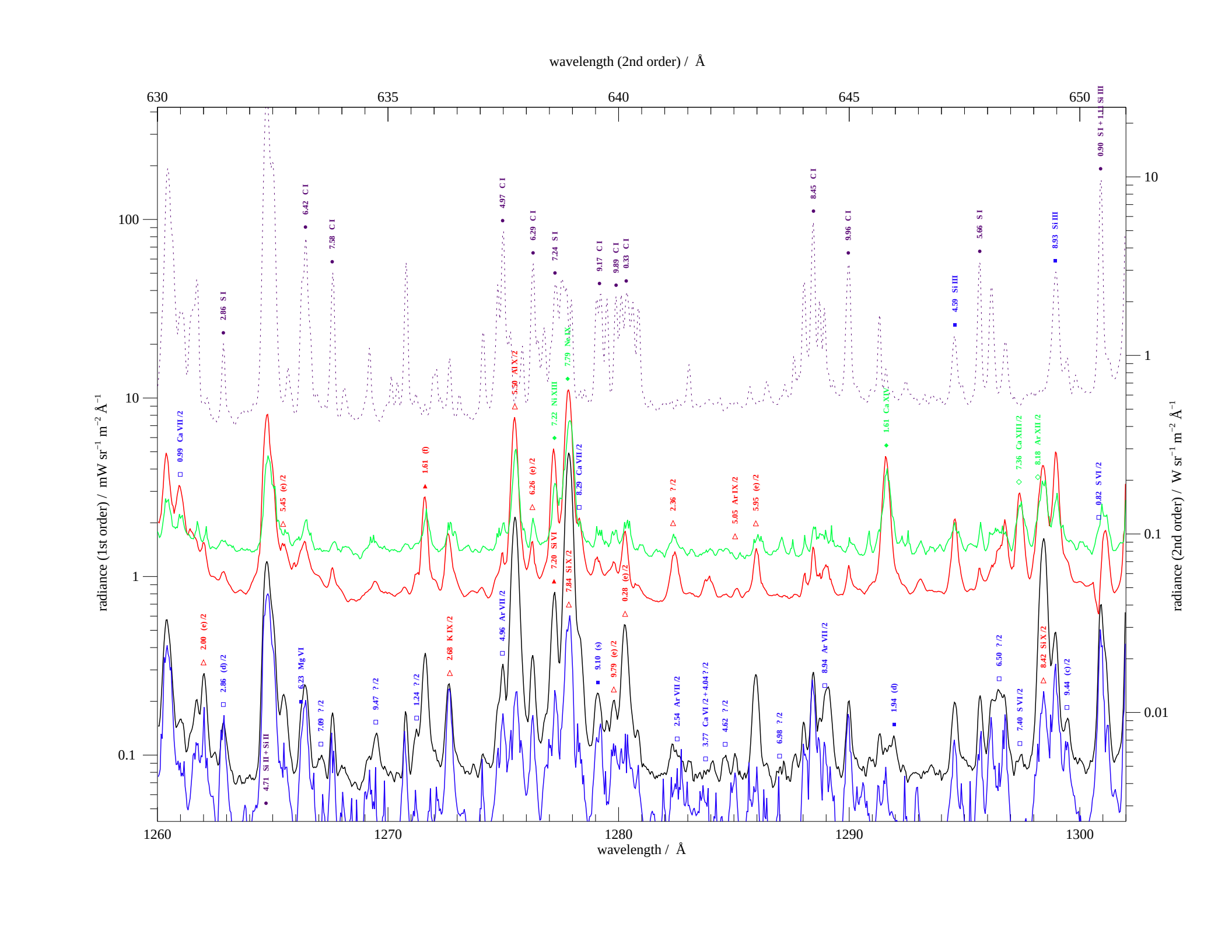
wavelength (2nd order) / Å
630
635
640
645
650
0.90 Si III + 1.11 Si III
8.45 C I
9.96 C I
5.66 S I
4.59 Si III
8.93 Si III
6.42 C I
7.58 C I
4.97 C I
6.29 C I
7.24 S I
9.17 C I
9.89 C I
0.33 C I
2.86 S I
5.50 Al X /2
7.79 Ne IX
7.22 Ni XIII
1.61 Ca XIV
7.36 Ca XIII /2
8.18 Ar XII /2
0.99 Ca VII /2
5.45 (e) /2
1.61 (f)
6.26 (e) /2
8.29 Ca VII /2
2.36 ? /2
5.05 Ar IX /2
5.95 (e) /2
0.82 S VI /2
7.20 Si VI
7.84 Si X /2
0.28 (e) /2
2.00 (e) /2
2.86 (d) /2
4.71 Si II + Si II
6.23 Mg VI
7.09 ? /2
4.96 Ar VII /2
2.68 K IX /2
9.47 ? /2
1.24 ? /2
9.10 (s)
9.79 (e) /2
2.54 Ar VII /2
3.77 Ca VI /2 + 4.04 ? /2
4.62 ? /2
6.98 ? /2
8.94 Ar VII /2
1.94 (d)
6.50 ? /2
7.40 S VI /2
8.42 Si X /2
9.44 (c) /2
radiance (1st order) / mW sr^{-1} m^{-2} Å^{-1}
100
10
1
0.1
radiance (2nd order) / W sr^{-1} m^{-2} Å^{-1}
10
1
0.1
0.01
1260
1270
1280
1290
1300
wavelength / Å

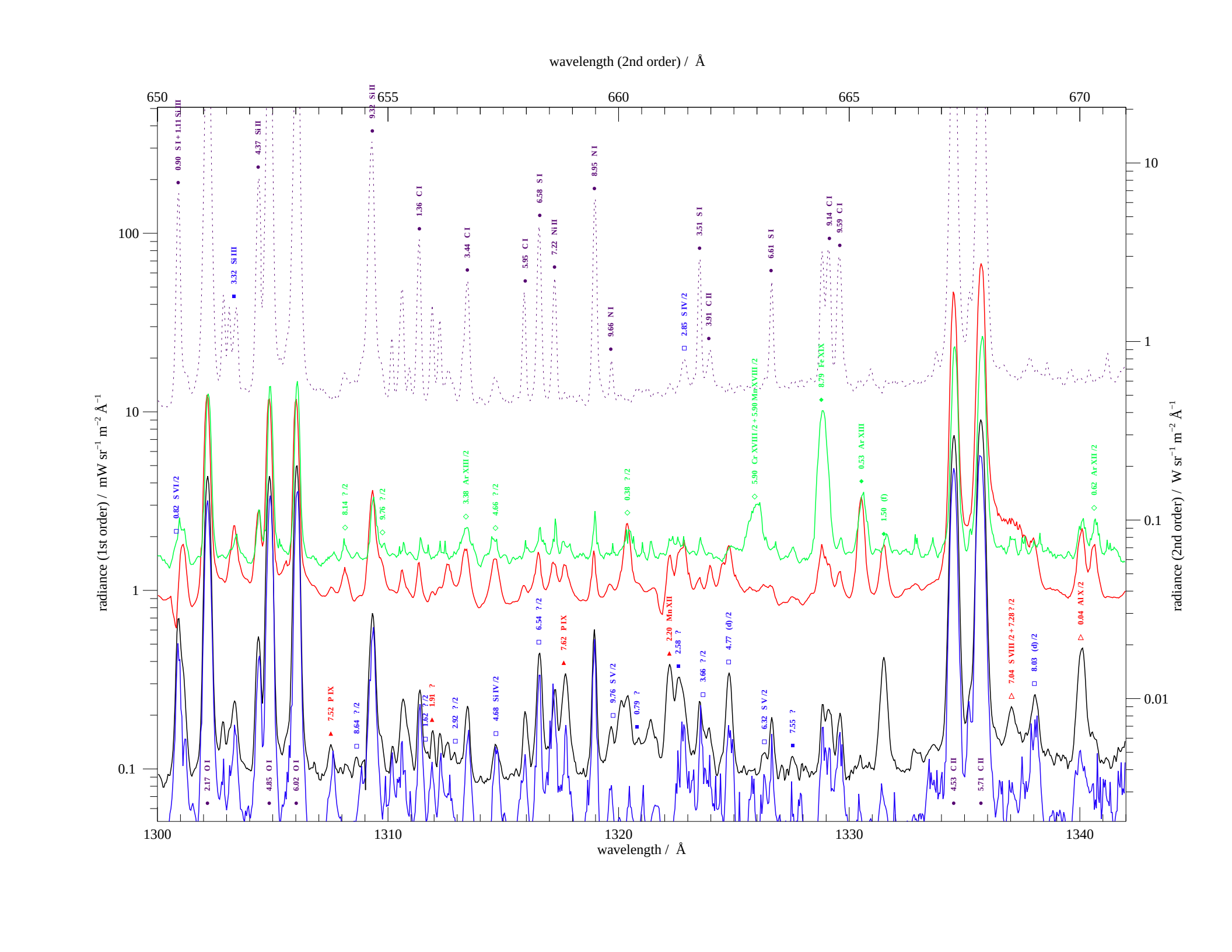
wavelength (2nd order) / Å
650
655
660
665
670
0.90 S I + 1.11 Si III
9.37 Si II
4.37 Si II
3.32 Si III
1.36 C I
3.44 C I
5.95 C I
6.58 S I
7.22 Ni II
8.95 N I
9.66 N I
2.85 S IV /2
3.51 S I
3.91 C II
6.61 S I
8.79 Fe XIX
9.14 C I
9.59 C I
0.82 S VI /2
8.14 ? /2
9.76 ? /2
3.38 Ar XIII /2
4.66 ? /2
0.38 ? /2
5.90 Cr XVIII /2 + 5.90 Mn XVIII /2
0.53 Ar XIII
1.50 (f)
0.62 Ar XII /2
2.17 O I
4.85 O I
6.02 O I
7.52 P IX
8.64 ? /2
1.62 ? /2
1.91 ?
2.92 ? /2
4.68 Si IV /2
6.54 ? /2
7.62 P IX
9.76 S V /2
0.79 ?
2.20 Mn XII
2.58 ?
3.66 ? /2
4.77 (d) /2
6.32 S V /2
7.55 ?
4.53 C II
5.71 C II
7.04 S VIII /2 + 7.28 ? /2
8.03 (d) /2
0.04 Al X /2
radiance (1st order) / mW sr^{-1} m^{-2} Å^{-1}
radiance (2nd order) / W sr^{-1} m^{-2} Å^{-1}
100
10
1
0.1
10
1
0.1
0.01
1300
1310
1320
1330
1340
wavelength / Å

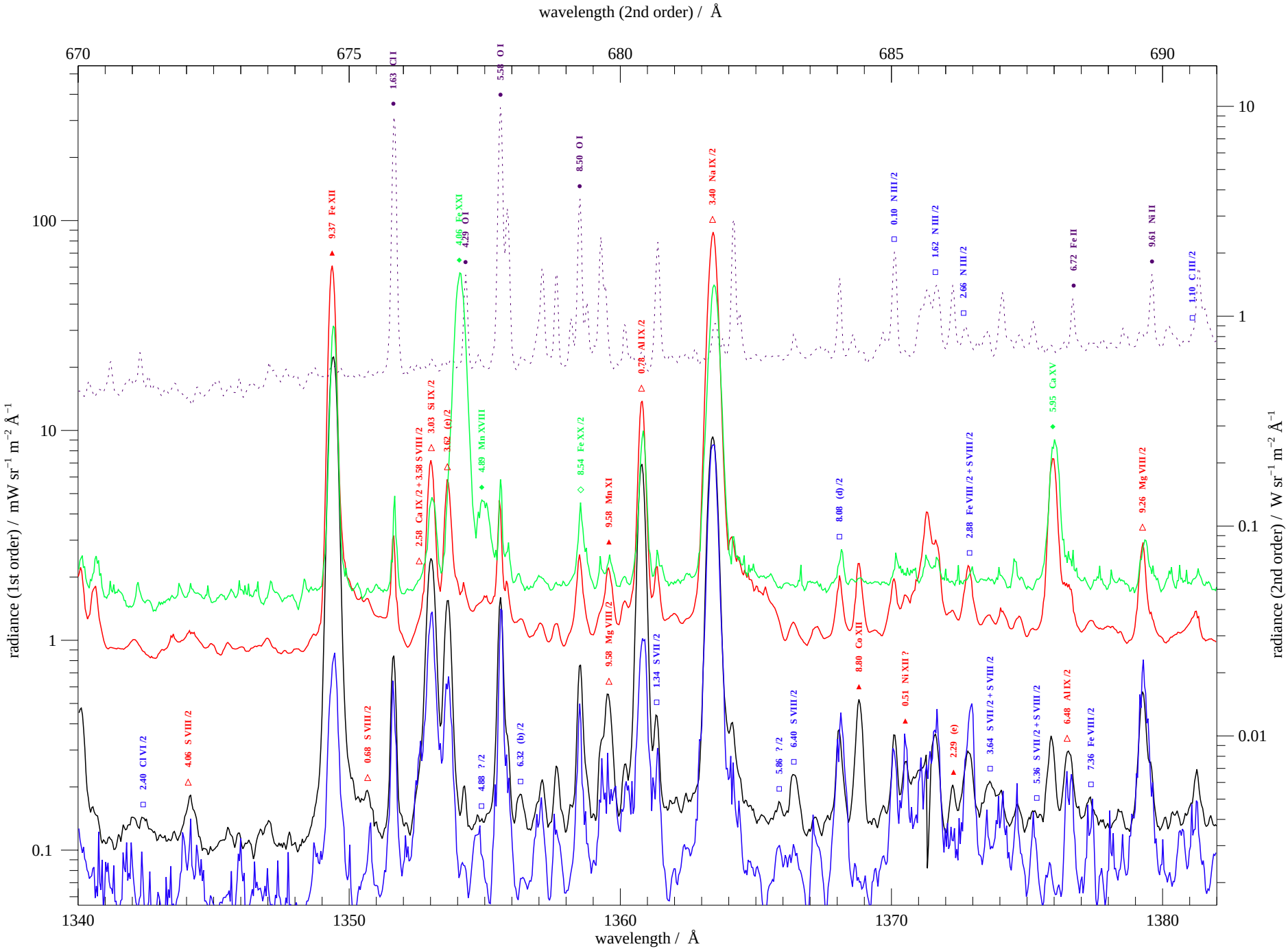
wavelength (2nd order) / Å
670
675
680
685
690
1.63 Cl I
5.58 O I
8.50 O I
3.40 Na IX /2
0.10 N III /2
1.62 N III /2
2.66 N III /2
6.72 Fe II
9.61 Ni II
1.10 C III /2
9.37 Fe XII
4.06 Fe XXI
4.29 O I
0.70 Al IX /2
5.95 Ca XV
2.58 Ca IX /2 + 3.58 S VIII /2
3.03 Si IX /2
3.62 (e) /2
4.89 Mn XVIII
8.54 Fe XX /2
9.58 Mn XI
8.08 (d) /2
2.88 Fe VIII /2 + S VIII /2
9.26 Mg VIII /2
9.58 Mg VIII /2
1.34 S VII /2
8.80 Co XII
0.51 Ni XII ?
2.29 (e)
3.64 S VII /2 + S VIII /2
5.36 S VII /2 + S VIII /2
6.48 Al IX /2
7.36 Fe VIII /2
2.40 Cl VI /2
4.06 S VIII /2
0.68 S VIII /2
4.88 ? /2
6.32 (b) /2
5.86 ? /2
6.40 S VIII /2
100
10
1
0.1
10
1
0.1
0.01
radiance (1st order) / mW sr^{-1} m^{-2} Å^{-1}
radiance (2nd order) / W sr^{-1} m^{-2} Å^{-1}
1340
1350
1360
1370
1380
wavelength / Å

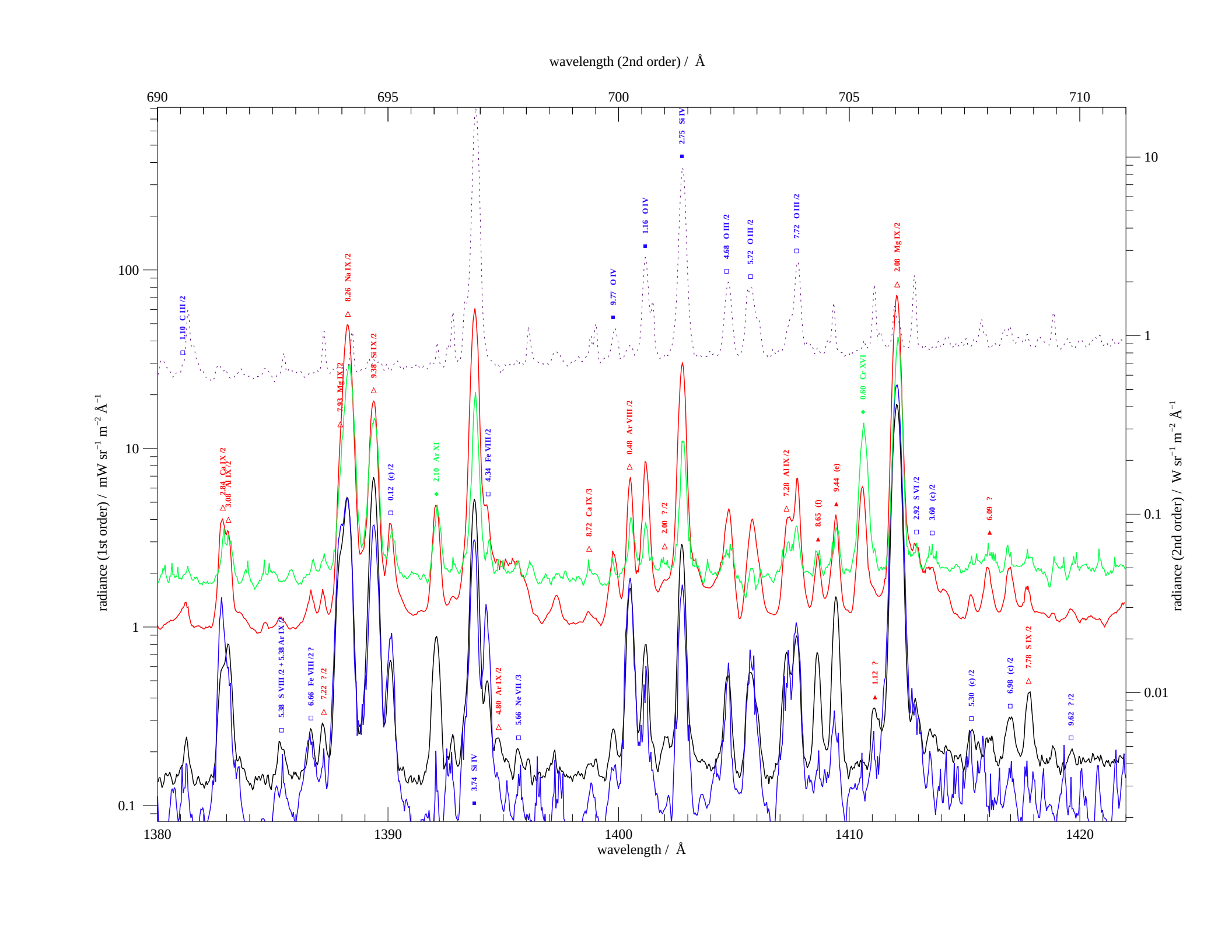
wavelength (2nd order) / Å
690
695
700
705
710
1.10 C III /2
8.26 Na IX /2
7.93 Mg IX /2
9.38 Si IX /2
9.77 O IV
1.16 O IV
2.75 Si IV
4.68 O III /2
5.72 O III /2
7.72 O III /2
2.08 Mg IX /2
3.08 Al IX /2
2.84 Ca IX /2
0.12 (e) /2
2.10 Ar XI
4.34 Fe VIII /2
8.72 Ca IX /3
0.48 Ar VIII /2
2.00 ? /2
7.28 Al IX /2
8.65 (f)
9.44 (e)
0.60 Cr XVI
2.92 S VI /2
3.60 (e) /2
6.09 ?
5.38 S VIII /2 + 5.38 Ar IX /2
6.66 Fe VIII /2 ?
7.22 ? /2
3.74 Si IV
4.80 Ar IX /2
5.66 Ne VII /3
1.12 ?
5.30 (e) /2
6.98 (e) /2
7.78 S IX /2
9.62 ? /2
radiance (1st order) / mW sr^{-1} m^{-2} Å^{-1}
radiance (2nd order) / W sr^{-1} m^{-2} Å^{-1}
100
10
1
0.1
10
1
0.1
0.01
1380
1390
1400
1410
1420
wavelength / Å

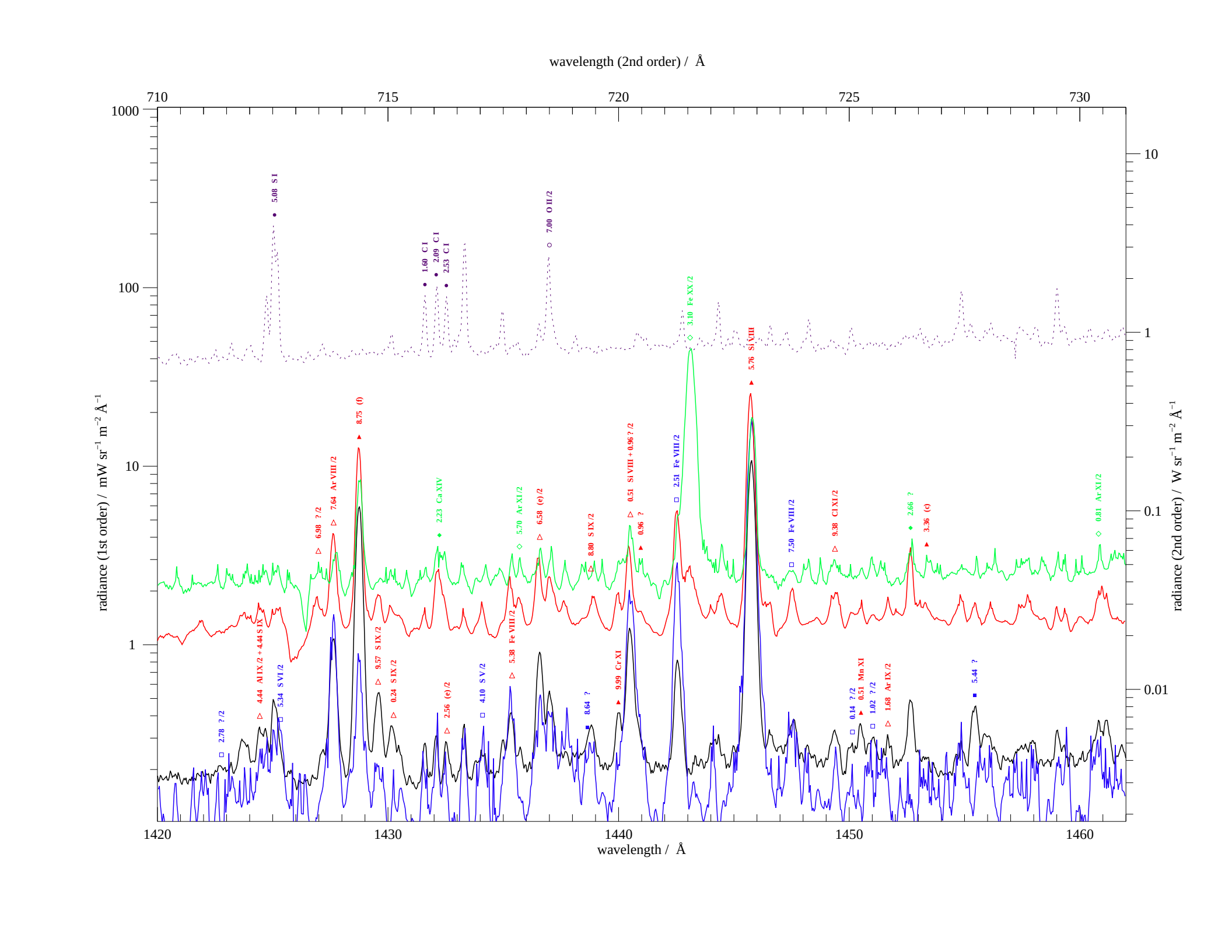
wavelength (2nd order) / Å
710
715
720
725
730
1000
100
10
1
5.08 S I
1.60 C I
2.09 C I
2.53 C I
7.00 O II /2
3.10 Fe XX /2
5.76 Si VIII
6.98 ? /2
7.64 Ar VIII /2
8.75 (f)
2.23 Ca XIV
5.70 Ar XI /2
6.58 (e) /2
8.80 S IX /2
0.51 Si VIII + 0.96 ? /2
0.96 ?
2.51 Fe VIII /2
7.50 Fe VIII /2
9.38 Cl XI /2
2.66 ?
3.36 (e)
0.81 Ar XI /2
2.78 ? /2
4.44 Al IX /2 + 4.44 S IX
5.34 S VI /2
9.57 S IX /2
0.24 S IX /2
2.56 (e) /2
4.10 S V /2
5.38 Fe VIII /2
8.64 ?
9.99 Cr XI
0.14 ? /2
0.51 Mn XI
1.02 ? /2
1.68 Ar IX /2
5.44 ?
radiance (1st order) / mW sr^{-1} m^{-2} Å^{-1}
radiance (2nd order) / W sr^{-1} m^{-2} Å^{-1}
10
1
0.1
0.01
1420
1430
1440
1450
1460
wavelength / Å

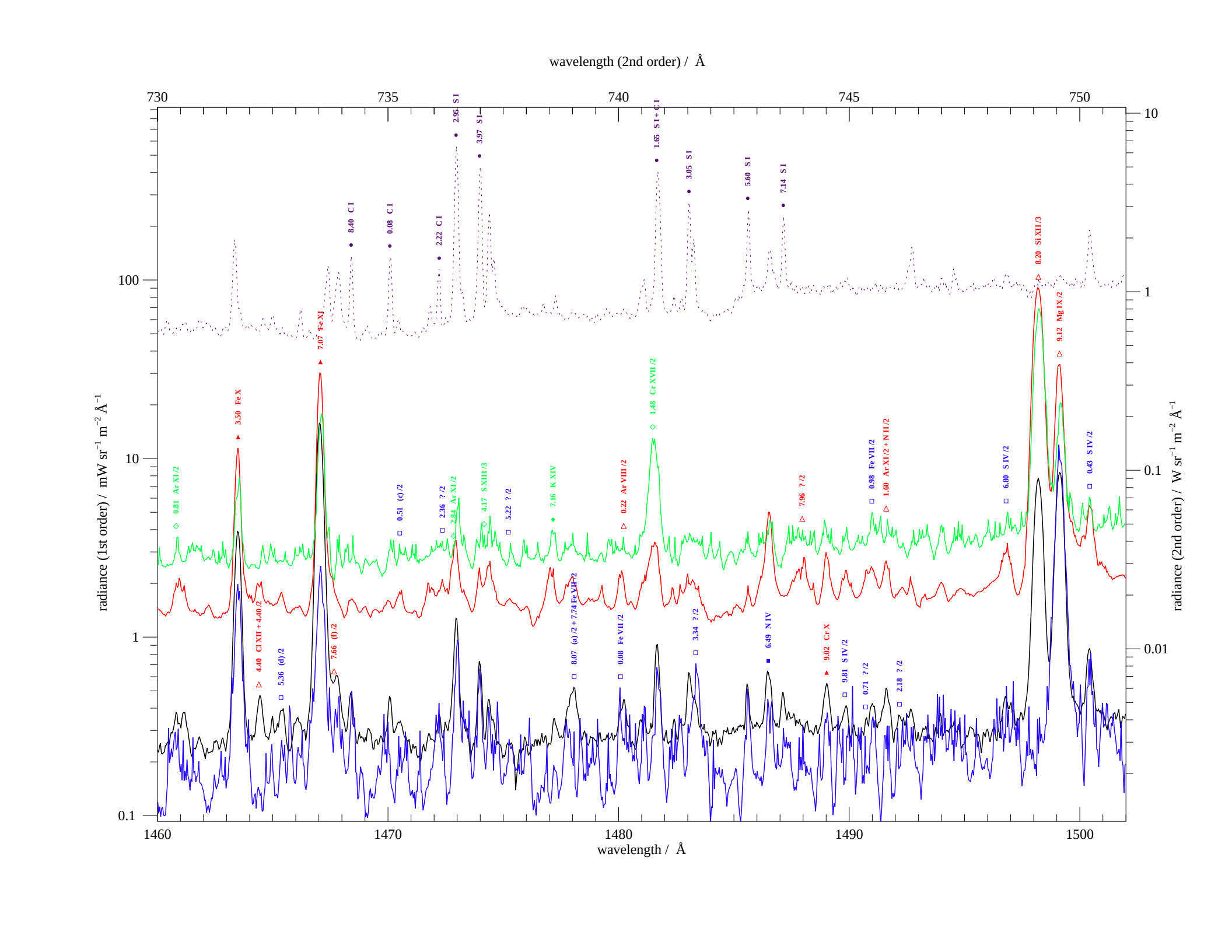
wavelength (2nd order) / Å
730
735
740
745
750
2.95 S I
3.97 S I
1.65 S I + C I
3.05 S I
5.60 S I
7.14 S I
8.40 C I
0.08 C I
2.22 C I
8.20 Si XII /3
7.07 Fe XI
9.12 Mg IX /2
3.50 Fe X
1.48 Cr XVII /2
0.81 Ar XI /2
0.51 (e) /2
2.36 ? /2
2.84 Ar XI /2
4.17 S XIII /3
5.22 ? /2
7.16 K XIV
0.22 Ar VIII /2
7.96 ? /2
0.98 Fe VII /2
1.60 Ar XI /2 + N II /2
6.80 S IV /2
0.43 S IV /2
4.40 Cl XII + 4.40 /2
5.36 (d) /2
7.66 (f) /2
8.07 (a) /2 + 7.74 Fe VII /2
0.08 Fe VII /2
3.34 ? /2
6.49 N IV
9.02 Cr X
9.81 S IV /2
0.71 ? /2
2.18 ? /2
radiance (1st order) / mW sr^{-1} m^{-2} Å^{-1}
radiance (2nd order) / W sr^{-1} m^{-2} Å^{-1}
100
10
1
0.1
10
1
0.1
0.01
1460
1470
1480
1490
1500
wavelength / Å

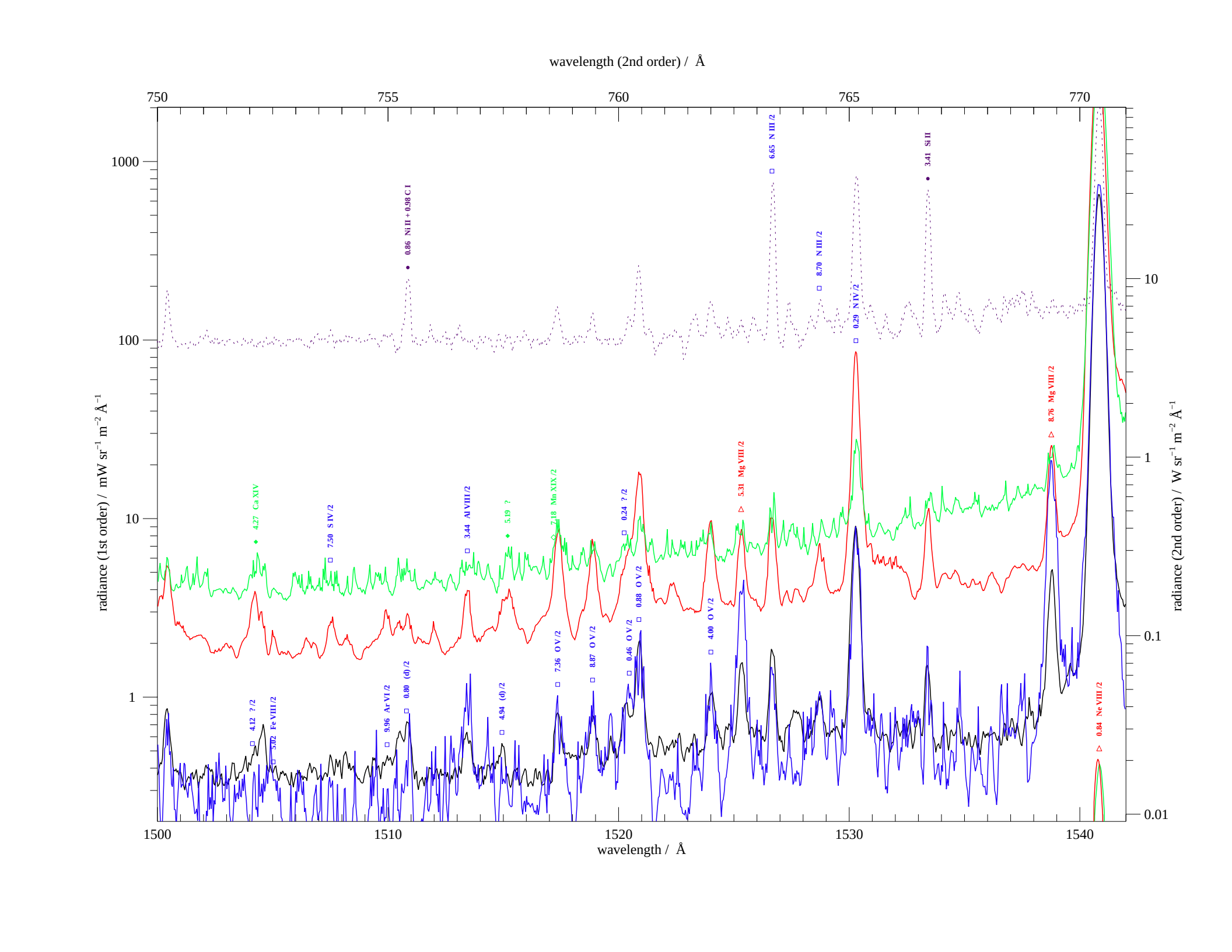
wavelength (2nd order) / Å
750
755
760
765
770
1000
100
10
1
0.86 Ni II + 0.98 C I
6.65 N III /2
8.70 N III /2
0.29 N IV /2
3.41 Si II
4.27 Ca XIV
7.50 S IV /2
3.44 Al VIII /2
5.19 ?
7.18 Mn XIX /2
0.24 ? /2
5.31 Mg VIII /2
8.76 Mg VIII /2
4.12 ? /2
3.72 Fe VIII /2
9.96 Ar VI /2
0.80 (d) /2
4.94 (d) /2
7.36 O V /2
8.87 O V /2
0.46 O V /2
0.88 O V /2
4.00 O V /2
0.84 Ne VIII /2
radiance (1st order) / mW sr^{-1} m^{-2} Å^{-1}
radiance (2nd order) / W sr^{-1} m^{-2} Å^{-1}
10
1
0.1
0.01
1500
1510
1520
1530
1540
wavelength / Å

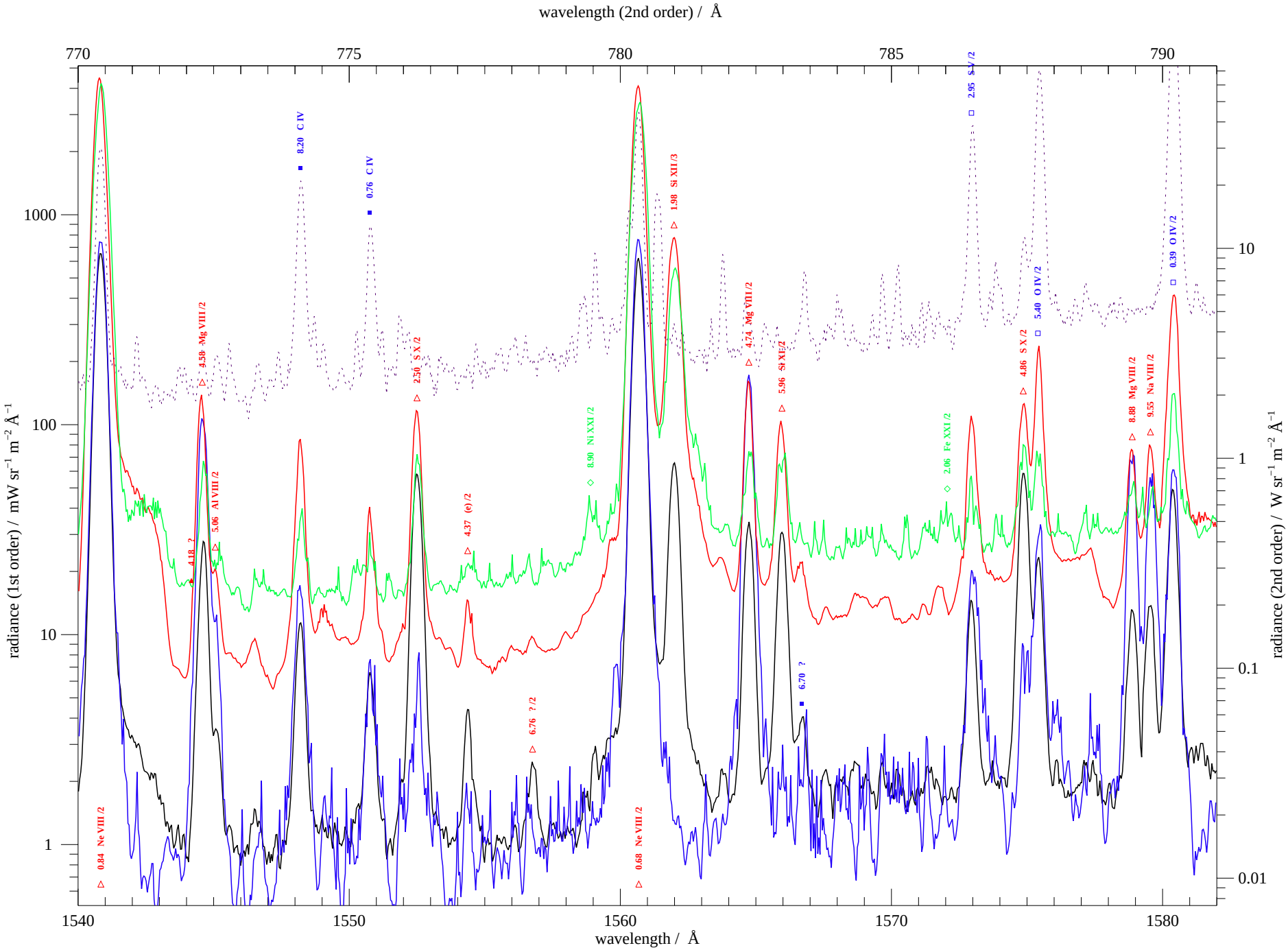
wavelength (2nd order) / Å
770
775
780
785
790
8.20 C IV
0.76 C IV
2.95 S V /2
1.98 Si XII /3
9.58 Mg VIII /2
2.50 S X /2
4.74 Mg VIII /2
5.96 Si XII /2
5.40 O IV /2
0.39 O IV /2
4.86 S X /2
8.88 Mg VIII /2
9.55 Na VIII /2
8.90 Ni XXI /2
2.06 Fe XXI /2
5.06 Al VIII /2
4.37 (e) /2
6.76 ? /2
6.70 ?
0.84 Ne VIII /2
0.68 Ne VIII /2
1000
100
10
1
10
1
0.1
0.01
radiance (1st order) / mW sr^{-1} m^{-2} Å^{-1}
radiance (2nd order) / W sr^{-1} m^{-2} Å^{-1}
1540
1550
1560
1570
1580
wavelength / Å

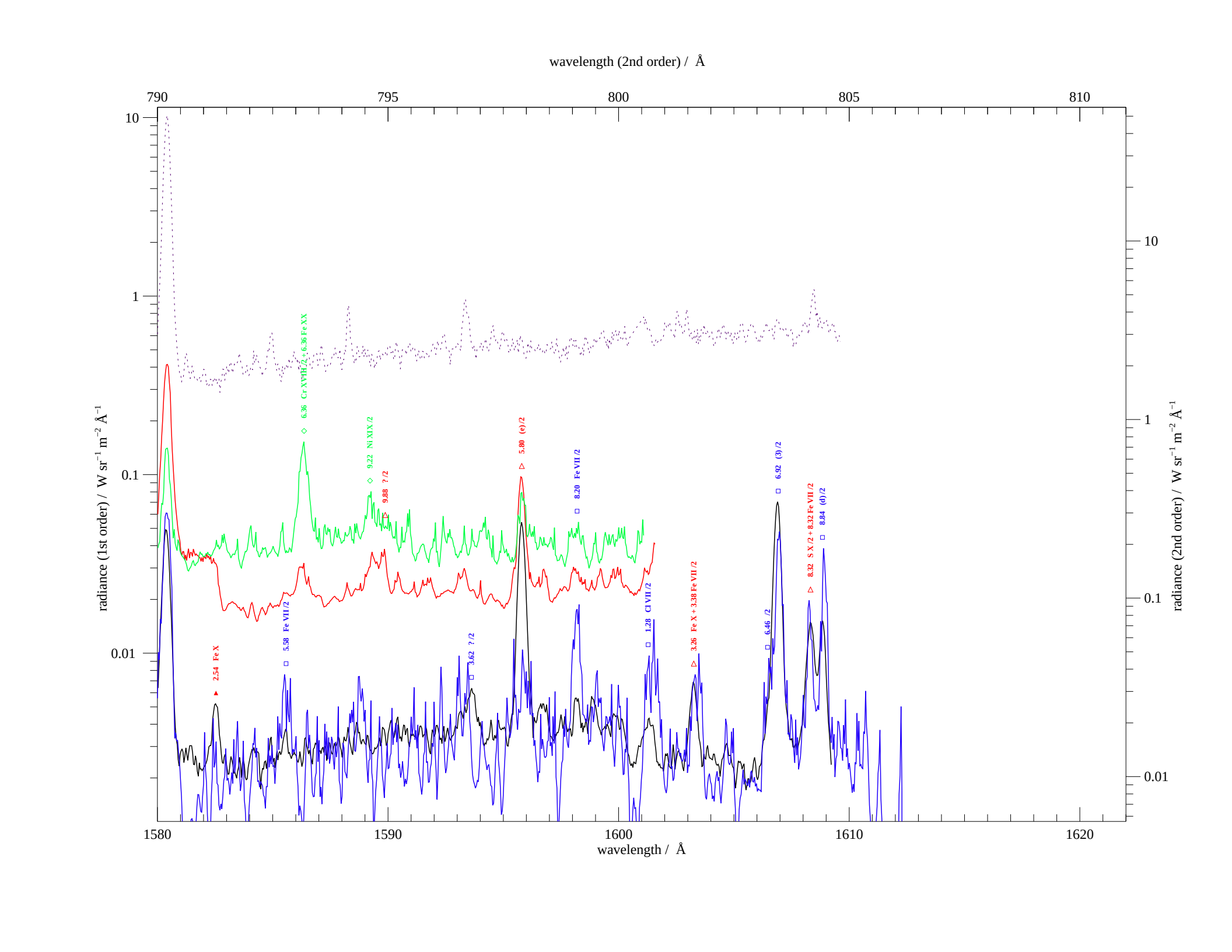
wavelength (2nd order) / Å
790
795
800
805
810
10
1
0.1
0.01
radiance (1st order) / W sr^{-1} m^{-2} Å^{-1}
6.36 Cr XVIII /2 + 6.36 Fe XX
9.22 Ni XIX /2
9.88 ? /2
5.80 (e) /2
8.20 Fe VII /2
6.92 (3) /2
8.32 S X /2 + 8.32 Fe VII /2
8.84 (d) /2
2.54 Fe X
5.58 Fe VII /2
3.62 ? /2
1.28 Cl VII /2
3.26 Fe X + 3.38 Fe VII /2
6.46 /2
1580
1590
1600
1610
1620
wavelength / Å